Improved Modelling of Induction and Transduction Heaters

Lisiate Takau

A thesis presented for the degree of
Doctor of Philosophy
in
Electrical and Computer Engineering
at the
University of Canterbury,
Christchurch, New Zealand.

2015

ABSTRACT

This thesis starts by describing research on the design of low frequency induction heaters using a series equivalent circuit model. Limitations associated with this design method are explained. An alternative called the transformer equivalent circuit (TEC) model is then presented. This models the induction heater as a single turn secondary transformer. Its advantage is that the currents and voltages associated with components of the induction heater are what you would expect to measure on components of an actual induction heater. Finite element analysis (FEA) is also used to predict the performance of induction heaters. The performances of these models are compared, with experimental verification on a small induction heater unit.

The research is then extended to transduction heaters, a combination of transformer and induction heaters, which include a secondary winding to boost performance. The transformer equivalent circuit method is used to predict the performance of transduction heaters as they cannot be modelled using the series equivalent circuit model. The performances of the transformer equivalent circuit and finite element analysis models are compared with results from a set of experimental transduction heaters.

Modifications are then made to the components of the TEC model to improve its performance predictions. The accuracy of TEC modelling is confirmed with a second design and verified with experimental results. This forms the basis for the final design and implementation of an industrial unit.

The improved TEC model is then used to predict the performance of a 40kW transduction fluid heater that was designed, built and tested. Comparisons are made between the TEC and FEA models calculated results and test results. The TEC calculated results yielded much closer values to those measured.

ACKNOWLEDGEMENTS

First of all, I would like to express my sincere gratitude to my supervisor, Professor Pat Bodger and my co-supervisor Associate Professor Paul Gaynor for all the encouragement and support that they have provided throughout the course of this study. I would like to thank Pat for guidance and advice even after he retired from the University. The benefit of his experience has contributed significantly to all stages of this work.

I would like to express my gratitude to my postgraduate comrades, Dr Bhaba Das, Dr Michael Huang, Dr Senthuran Sivasubramaniam, Ming Zhong, Yanosh Irani, and Diwakar Bhujel for the never-ending discussions on research we shared together. I would also like to mention my colleagues at UL, Vinesh Chand, Christopher Bennetts, Neil Mallare, and Michael Passe, for all our whiteboard-discussions about transformer equivalent circuits. The quote that summed up these discussions was: "It's all about the magnetizing reactance".

I would like to acknowledge the technical staff at the Electrical and Computer Engineering Department, Ken Smart in the Electrical Machines Lab, Edsel Villa in the Power Electronics Lab, Florin Predan in the Computer Lab, David Healey in the Mechanical Workshop, and Paul Agger in the High Voltage Lab for their support over the past years.

Finally, I would like to express my most sincere appreciation to my family for their love, patience, and support.

CONTENTS

ABSTRACT iii

ACKNOWLEDGEMENTS v

LIST OF FIGURES xii

LIST OF TABLES xiv

GLOSSARY xv

CHAPTER 1 INTRODUCTION 1
- 1.1 General Overview 1
- 1.2 Thesis Objectives 2
- 1.3 Thesis Contribution 2
- 1.4 Thesis Outline 3

CHAPTER 2 HISTORICAL DEVELOPMENT 5
- 2.1 Introduction 5
- 2.2 Background 5
- 2.3 Induction Heating 6
  - 2.3.1 Electromagnetic Induction 7
  - 2.3.2 Basic Induction Heating 8
- 2.4 SEC Model of Induction Heater 11
  - 2.4.1 SEC Performance 15
  - 2.4.2 Equivalent Circuit Performance for an Experimental Induction Heater 16
  - 2.4.3 Material Properties 17
- 2.5 Calculated Performance Using SEC Model 17
- 2.6 Summary 18

CHAPTER 3 TRANSFORMER MODEL OF INDUCTION HEATER 21
- 3.1 Introduction 21
- 3.2 Transformer Fundamentals 21
  - 3.2.1 Ideal Transformers 21
  - 3.2.2 Non-Ideal Transformers 24
- 3.3 Transformer Equivalent Circuit of Induction Heater 26

3.4 Calculation of Equivalent Circuit Parameters 27
3.4.1 Coil Resistance 28
3.4.2 Workpiece Magnetizing Reactance 30
3.4.3 Coil/Workpiece Leakage Reactance 33
3.4.4 Workpiece Eddy Current Resistance 35
3.5 Equivalent Circuit Performance 36
3.5.1 Equivalent Circuit Performance for an Experimental Induction Heater 36
3.5.2 Equivalent Circuit Parameters 36
3.5.3 TEC Calculated Performance 37
3.6 Summary 39

CHAPTER 4 FINITE ELEMENT ANALYSIS AND MEASURED PERFORMANCE OF EXPERIMETAL INDUCTION HEATER 41
4.1 Introduction 41
4.2 Finite Element Method 41
4.2.1 FEA Study of the Experimental Induction Heater 42
4.2.2 Flux Plot of the Experimental Induction Heater 44
4.2.3 FEA Performance Calculation 45
4.3 Measured Performance of Experimental Induction Heater 46
4.3.1 Analysis 48
4.4 Summary 49

CHAPTER 5 TRANSFORMER AND TRANSDUCTION HEATING 51
5.1 Introduction 51
5.2 Transformer Heater 51
5.3 Equivalent Circuit of Transformer Heater 52
5.3.1 Winding Resistances 53
5.3.2 Magnetizing Reactance 54
5.3.3 Leakage Reactance 55
5.4 Transduction Heating 55
5.4.1 Basic Heating Concepts 55
5.5 Transduction Heater 57
5.6 Measured Performance of Experimental Transduction Heater 59
5.7 Equivalent Circuit of Transduction Heater 60
5.7.1 Winding Resistance 62
5.7.2 Magnetizing Reactance 63
5.7.3 Core Tube Eddy Current Resistance 63
5.7.4 Leakage Reactance 63
5.8 Equivalent Circuit Performance 64
5.9 FEA Performance Calculation 65
5.10 Design of a 6kW Transduction Heater 68
5.11 Summary 70

CHAPTER 6 DESIGN OF AN INDUSTRIAL TRANSDUCTION FLUID HEATER 73
6.1 Introduction 73
6.2 Transformers 73
6.3 Induction Heaters 74
6.4 Transduction Heater Design 74
6.5 Design Description 75
6.5.1 Design Consideration 75
6.6 Construction Details 76
6.6.1 Core Tube 77
6.6.2 Secondary Tube 77
6.6.3 Thermal Insulation 79
6.6.4 Primary Winding 80
6.6.5 Inter-Layer Insulation 80
6.6.6 Baffle 81
6.6.7 Transduction Heater Cooling 82
6.6.8 Transduction Heater Housing 83
6.7 Equivalent Circuit 84
6.7.1 Equivalent Circuit Performance 84
6.7.2 Calculated Performance 84
6.8 FEA Results 86
6.9 Summary 88

CHAPTER 7 EXPERIMENTAL RESULTS 89
7.1 Introduction 89
7.2 Experimental Setup 89
7.2.1 Test Equipment 89
7.2.2 Taking Measurements 90
7.3 Transduction Heater Performance 91
7.3.1 Winding Resistance and Insulation Resistance Tests 91
7.3.2 Power Input Test 92
7.3.3 Heating Test 92
7.4 Other Experimental Results 96
7.4.1 AC Withstand Voltage Test 96
7.4.2 Glow-wire Test 97
7.5 Comparison with TEC and FEA Models 98
7.5.1 Winding Resistance Test Results 98
7.5.2 Electrical Performance 99
7.6 Summary 99

CHAPTER 8 CONCLUSIONS AND FUTURE WORK 101
8.1 Conclusions 101
8.2 Future Work 103
8.2.1 Heater Design 103
8.2.2 Improve Performance 104

REFERENCES **107**

APPENDIX A GLOW-WIRE FLAMMABILITY TEST RESULTS **113**

APPENDIX B LIST OF PUBLICATIONS **115**
B.1 Conference Papers 115
B.2 Journal Papers 115

LIST OF FIGURES

2.1 Induction heating. 7
2.2 Magnetic flux plot of steel bar workpiece. 8
2.3 Induction heating coil around a billet. 9
2.4 Series equivalent circuit of induction heater. 11
2.5 Short coil equivalent circuit which includes an external reactance. 14

3.1 An ideal full-core transformer. 22
3.2 Equivalent circuit of a non-ideal transformer. 24
3.3 Transformer equivalent circuit of an induction heater. 27
3.4 Cross-section of a multi-layer coil induction heater with a tube workpiece. 28
3.5 Flux distribution for induction heaters with different winding thicknesses. 29
3.6 Axial view of the flux flow from a cylindrical workpiece. 31
3.7 Magnetic circuit of induction heater. 32
3.8 Dimensions for representing the leakage flux for an induction heater. 34

4.1 Cross-section of workpiece 1. 43
4.2 Finite element mesh of experimental induction heater of workpiece 1. 44
4.3 Flux plot of experimental induction heater of workpiece 1. 46

5.1 Transformer heater physical arrangement. 52
5.2 Coupled circuit representation. 52
5.3 Transformer heater equivalent circuit. 53
5.4 Cross-section of a multi-layer winding transformer heater with a full core. 54
5.5 Conceptual arrangement of induction fluid heater. 56
5.6 Conceptual arrangement of transformer fluid heater. 56
5.7 Conceptual arrangement of combined transformer heater and induction fluid heater. 57
5.8 Conceptual arrangement of transduction fluid heater. 58

5.9 Cut-away image of transduction fluid heater. 59
5.10 Transduction heater with combination of tubes (2+5). 61
5.11 Equivalent circuit of transduction heater. 62
5.12 Flux plot of workpiece combination (1+4). 66
5.13 Flux plot of workpiece combination (2+5). 67
5.14 6kW transduction fluid heater. 69

6.1 Cross-section details of transduction fluid heater. 76
6.2 The core and secondary tubes over the workpiece. 78
6.3 Thermal insulation composite tube. 79
6.4 Inter-layer insulation. 81
6.5 Winding layout of 40kW transduction heater. 81
6.6 Assembled winding without outside insulation baffle. 82
6.7 Transduction heater housing. 83
6.8 Equivalent circuit of transduction heater. 84
6.9 Flux plot of designed heater. 87

7.1 Test setup (front view). 90
7.2 Test setup (rear view). 91
7.3 Temperatures over time during heating test. 94
7.4 Temperatures over time during heating test. 96
7.5 Glow-wire test setup. 98

8.1 Transduction heater with baffle. 104
8.2 Non-metallic cover piece with four slots. 105

LIST OF TABLES

2.1 Coil dimensions 16
2.2 Workpiece dimensions 17
2.3 Physical properties of copper and mild steel 17
2.4 Component values for the SEC long coil model 18
2.5 Calculated performance of experimental heater using SEC long coil model 18

3.1 Component values for the TEC model 36
3.2 Calculated performance using TEC model 37
3.3 Calculated performance using TEC model below the saturation point 40

4.1 Physical properties of copper and mild steel 45
4.2 Calculated performance using FEA model 45
4.3 Measured performance of experimental induction heater 47
4.4 Ratio of coil and workpiece loss 48

5.1 Coil dimensions 60
5.2 Workpiece and secondary tube dimensions 60
5.3 Measured performance at 100V supply 61
5.4 Physical properties 64
5.5 Calculated performance using TEC model for a 100V supply 64
5.6 Calculated performance using TEC model at 100V supply with scale factor applied 65
5.7 Calculated performance using FEA at a 100V supply 67
5.8 Coil dimensions 68
5.9 Workpiece dimensions 68
5.10 Component values for the TEC model 69
5.11 Calculated and measured results of the designed transduction heater 69
5.12 TEC calculated performance 70

6.1 Core tube dimensions 77
6.2 Secondary tube dimensions 78
6.3 Thermal insulation dimensions 79
6.4 Primary winding dimensions 80
6.5 Stainless steel baffle dimensions 82
6.6 Equivalent circuit parameters 85
6.7 Equivalent circuit performance 85
6.8 TEC calculated performance 86
6.9 FEA transduction heater performance 87

7.1 Measured winding resistance 92
7.2 Insulation resistance test 92
7.3 Measured power input at rated voltage(horizontal mounting) 93
7.4 Measured power input at rated voltage(vertical mounting) 93
7.5 Heating test 94
7.6 Heating test 95
7.7 AC Withstand voltage test 97
7.8 Measured winding resistance results 98
7.9 Measured and calculated performance 99

GLOSSARY

NOMENCLATURE

δ_c	Skin depth of coil in meters
δ_w	Skin depth of workpiece in meters
η	Efficiency
μ	Magnetic permeability in henries per meter
μ_0	Magnetic permeability of free space equal to $(4\pi \times 10^{-7})$
μ_r	Relative permeability
ω	Angular frequency in radians per second
ϕ	Magnetic flux in webers
σ	Conductivity in siemens per meter
a	Nominal turns ratio
A_g	Cross-section air-gap area in square meters
A_w	Cross-section area of workpiece in square meters
B	Magnetic field density in tesla
D_w	Diameter of workpiece in meters
e, E_c	Induced emf of coil in volts
f	Frequency in hertz
I_c	Coil current in amperes
J	Current density in ampere per square meter
k	Hysteresis loss constant
K_r	Dimensionless workpiece correction factor
k_r	Dimensionless coil space correction factor

N, N_c	Number of coil turns
p	Dimensionless flux factor
P_c	Coil power loss in watts
p_c	Inside perimeter of coil in meters
P_w	Total power input to workpiece in watts
P_e	Eddy current loss in watts
P_h	Hysteresis loss in watts
q	Dimensionless flux factor
R_c	Coil resistance in ohms
R_e	Reluctance of external flux path in centimeter-gram-second units
R_w	Workpiece resistance in ohms
V_c	Applied coil voltage in volts
W_c	Diameter of coil wire in meters
x	Steinmetz factor
X_c	Coil reactance in ohms
X_e	End-effect reactance in ohms
X_g	Air gap reactance in ohms
X_{mc}	Core tube magnetising reactance in ohms
X_{mw}	Workpiece magnetising reactance in ohms
X_w	Workpiece reactance in ohms
Z	Total impedance in ohms

ABBREVIATIONS

ac	Alternating current
emf	Electromotive force
FEA	Finite element analysis
mmf	Magnetomotive force
RMS	Root mean squared
SEC	Series equivalent circuit
TEC	Transformer equivalent circuit

Chapter 1

INTRODUCTION

1.1 GENERAL OVERVIEW

New high efficiency technology in the heating industry is prompting a demand for safe, efficient, and less energy consuming products. Induction heating has been widely used for different applications such as heating of metals to heating of dairy fluids [Jang *et al.* 2003], [Egan and Furlani 1991], [Tham *et al.* 2009], because of its preciseness of application which satisfy these consumer demands. Electric water heaters have been the focus of several previous studies because of their pervasiveness in power systems and their consequential potential importance when considering conservation of energy through more efficient design and operation [Laurent and Malhame 1994].

A transformer heater can be combined with an induction heater to improve performance. The concept was initially developed as a new technology [Bodger *et al.* 1996] and is further developed in this thesis under the term transduction heater. Transduction heating is normally used for fluid heating. The typical arrangement is to have a primary winding that does not produce much heat, a core tube that produces some heat, and a shorted secondary winding that produces most of the heat. By making the secondary conductor hollow, or by adding a fluid channel outside the conductor, the real power losses in the secondary tube can be transferred by convection to the fluid, thus heating it up. A transduction heater converts electrical energy into hot fluids as a continuous process.

The concept of transduction heating is new compared to induction heating. The existing models used to calculate the performance of induction heaters cannot be used to model the performance of transduction heaters. Therefore a new design method is needed that will accurately model the performance of transduction heaters.

This thesis starts by introducing a transformer equivalent circuit (TEC) model as an alternative to the existing series equivalent circuit (SEC) model and finite element analysis (FEA) for designing induction heaters. These three models are used to model the performance of a set of

experimental units. The performance testing of the real heaters is then used to ascertain which model gives the best prediction of real performance.

The research is then extended to transduction heating. The TEC model is then modified to calculate their performance as they cannot be modelled using a SEC model. The modified TEC model is then used to predict the performances of a set of transduction heating experiments. The calculated results from the TEC and FEA models are compared with the measured results and the TEC model is then improved by applying an empirical correction factor to three of its circuit parameters.

This model has been used to design a 40kW transduction fluid heater. The calculated results from the TEC and FEA models are compared with those measured from the actual heater.

1.2 THESIS OBJECTIVES

The main objectives of this thesis are:

- to improve the modelling of transduction heaters using finite element analysis.
- to develop and improve the transformer equivalent circuit to model the performance of transduction heaters more accurately.
- to verify the performance prediction of the TEC model on a 40kW transduction heater.

The thesis entails both developing a computer model for modelling transduction heater performance as well as the design and production of physical models.

1.3 THESIS CONTRIBUTION

The work in this thesis has led to development of a computer model that will be used to model the performance of transduction heaters more accurately. This has been achieved through four significant steps:

- The development of TEC model to calculate the performance of induction heaters at mains frequency. The validity of this model was compared with the calculated results obtained from the SEC model and FEA and also experimental results.
- The TEC model was improved to model the performance of transduction heaters and verified on a 6kW design.

- The proof of the design through the construction and testing of 40kW transduction fluid heater. The validity of the modelling was tested through comparisons to measured data.

- The thermal properties of the winding and oil were validated through extensive testing of the 40kW prototype.

1.4 THESIS OUTLINE

To achieve the objectives above, the thesis is structured into eight chapters. The chapters are organized functionally from the modelling, design, simulation, construction and testing process through to conclusions and future work.

Chapter 2 gives an introduction to induction heating and electromagnetic induction. The basic theory of induction heating is covered. This is followed with an existing modelling technique which models the performance of induction heaters. This is called the series equivalent circuit model. This modelling technique is applied to a set of induction heaters.

Chapter 3 details the development of a transformer model of an induction heater. This is an alternative to the SEC model presented in Chapter 2. The equivalent circuits for ideal and non-ideal transformers are presented. These are transformed into a circuit to model the performance of an induction heater. The parameters of the equivalent circuit are calculated using the reverse design method. The TEC model is applied to the set of induction heaters presented in Chapter 2. The calculated results from the TEC model are compared with those from the SEC model.

Chapter 4 describes the work on finite element analysis and experimental induction heaters. A 2D model of the set of experimental induction heaters was created and used for FEA. The calculated results from the FEA are compared to those from TEC and SEC models. The calculated results from the three models are compared with the measured experimental results.

Chapter 5 extends the research on induction heating to transduction heating, an induction heater which includes a secondary winding to boost performance. The TEC model is used to model the performance of transduction heating experiments. The validation of the model is applied to a set of experimental transduction heaters. The calculated results from the TEC model are compared with the measured experimental results. Modifications are made to the parameters of the TEC model to improve its performance predictions. The improved TEC model is then validated on a 6kW transduction heater.

Chapter 6 discusses the design and construction of a 40kW transduction fluid heater using the improved TEC model. The details of the construction of the transduction fluid heater are given including the insulation design, cooling system and construction materials.

Chapter 7 presents the performance tests of the 40kW transduction fluid heater. The test results are compared to the calculated results from the TEC and FEA models.

Chapter 8 contains the conclusions and future work.

Chapter 2

HISTORICAL DEVELOPMENT

2.1 INTRODUCTION

Induction heating is a process where a varying magnetic field is used to heat a conductor or workpiece. When a piece of metal or conductor is placed near a magnetic field created by energising a coil of wire, the magnetic field transfers energy into the conductor, thus heating it up. This chapter presents the theory of induction heating and its applications. It includes a method for modelling induction heaters at mains frequency. This model is known as the series equivalent circuit (SEC) model. The performance of this model is applied for a set of demonstration induction heaters. The calculated results from the SEC model are discussed.

2.2 BACKGROUND

The discovery of electromagnetic induction by Michael Faraday in 1831 led to the understanding of the principles involved in induction heating. Faraday's experiments with two coils wound onto an iron ring showed that the induced electromotive force (emf) in any closed circuit is equal to the time rate of change of the magnetic flux through the circuit,

$$|e| = \left|\frac{d\phi}{dt}\right| \tag{2.1}$$

where e is the magnitude of the induced emf in volts and ϕ is the magnetic flux in webers. This principle was used in motors, generators, transformers, and radio communications for almost a decade [Zinn and Semiatin 1988].

The first major application of induction heating was melting of metals in the 19th century [Zinn and Semiatin 1988]. Initially, this was done using metal or electrically conducting crucibles. Later, Ferranti, Colby, and Kjellin [Zinn and Semiatin 1988] developed induction melting fur-

naces using non-conducting crucibles. In these designs, electric currents were induced directly into the charge or the workpiece, at simple line frequency, or 60Hz.

Ring melting furnaces were all superseded in the early 1900s by the work of Northrup, who designed and built equipment consisting of a cylindrical crucible and a high-frequency spark-gap power supply [Zinn and Semiatin 1988]. This equipment was first used by Baker and Company to melt platinum and by the American Brass Company to melt other non ferrous alloys [Zinn and Semiatin 1988].

Other applications were developed following the acceptance of induction heating for melting metal. These included induction surface hardening of steels introduced by Midvale Steel and the Ohio Crankshaft Company [Zinn and Semiatin 1988].

A great use of induction heating technology was during the World War II, particularly in heat treating of ordnance components such as armour-piercing projectiles and shot [Zinn and Semiatin 1988].

The application of induction heating and melting in recent years has increased to a point where most engineers in the metalworking industries are familiar with existing applications and have some ideas for potential uses. Induction heating is unique, as compared to other conventional heating process. It is a non-contact method of quickly heating metal by inducing current in the part to be heated. It does not rely on a heating element to touch the part to conduct heat.

2.3 INDUCTION HEATING

Induction heating is the heating of electrical conducting parts in a varying magnetic field. It involves electromagnetic induction, skin effect and heat transfer.

An induction heating system consists of a source of alternating current ac, an induction coil, and the workpiece to be heated [Zinn and Semiatin 1988]. The role of the power supply is taken into account only in terms of the frequency and magnitude of the ac voltage that it supplies to the coil.

Induction heating relies on two mechanisms of energy dissipation for the purpose of heating [Zinn and Semiatin 1988]. These are energy losses due to Joule heating and energy losses associated with magnetic hysteresis.

The first of these is the sole mechanism of heat generation in non-magnetic materials (e.g. aluminium, copper, stainless steel and carbon steels above the Curie temperature) and the primary mechanism in ferromagnetic materials (carbon steel below the Curie temperature) [Zinn and Semiatin 1988].

The second mechanism of heat generation by induction for ferromagnetic materials is hysteresis losses. This is where the magnetic dipoles turn around with each reversal of the magnetic field applied to the material. The losses are due to the rotational friction between the molecules. This loss is often ignored in design studies.

2.3.1 Electromagnetic Induction

Electromagnetic induction describes the generation of a voltage in a conductor. It can happen in two entirely different ways; motional induction, where a conductor moves in a magnetic field, or transformer induction, where the circuit is stationary and the field varies with time [Edwards 2004]. Faraday's law of electromagnetic induction, which relates the generated voltage to the rate of change of flux, can take account of both effects.

If a conductor is supplied with an alternating current, then a magnetic field is set up in the region surrounding the conductor [Barber 1983]. If a second electrical circuit is placed in this magnetic field, an electromotive force (emf) or voltage is induced in the circuit. If the circuit is closed, a current will flow in the circuit. The magnitude of this secondary current will depend on the strength of the magnetic field, the electrical impedance of the secondary circuit and the geometrical configuration of the two sets of conductors.

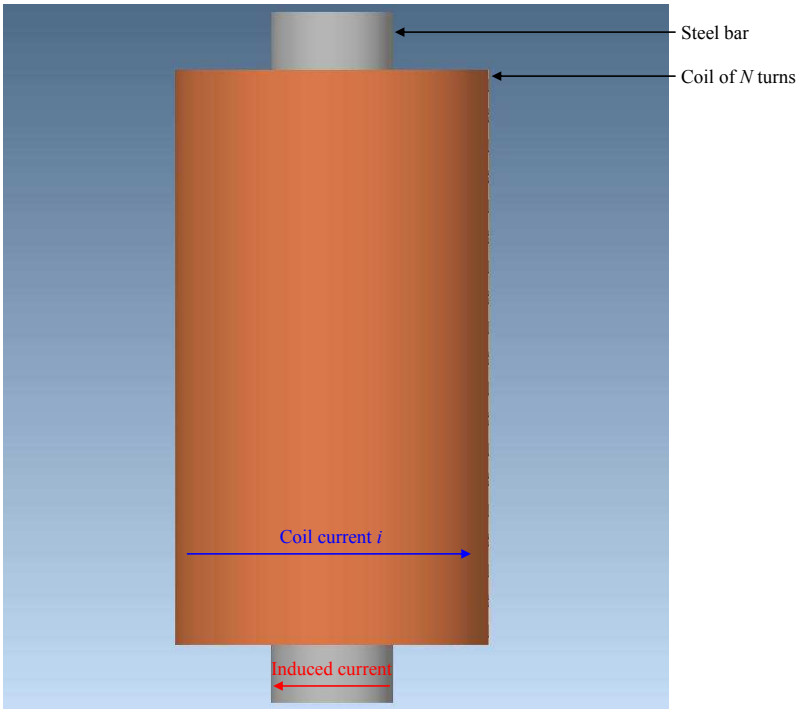

Figure 2.1: Induction heating.

Applied to induction heating, if the conductor is formed into a coil of N turns surrounds a steel

bar, as shown in Figure 2.1, the magnetic field will be normal to the direction of the coil current i. The flux will flow inside the coil in the longitudinal axis direction, as shown in Figure 2.2.

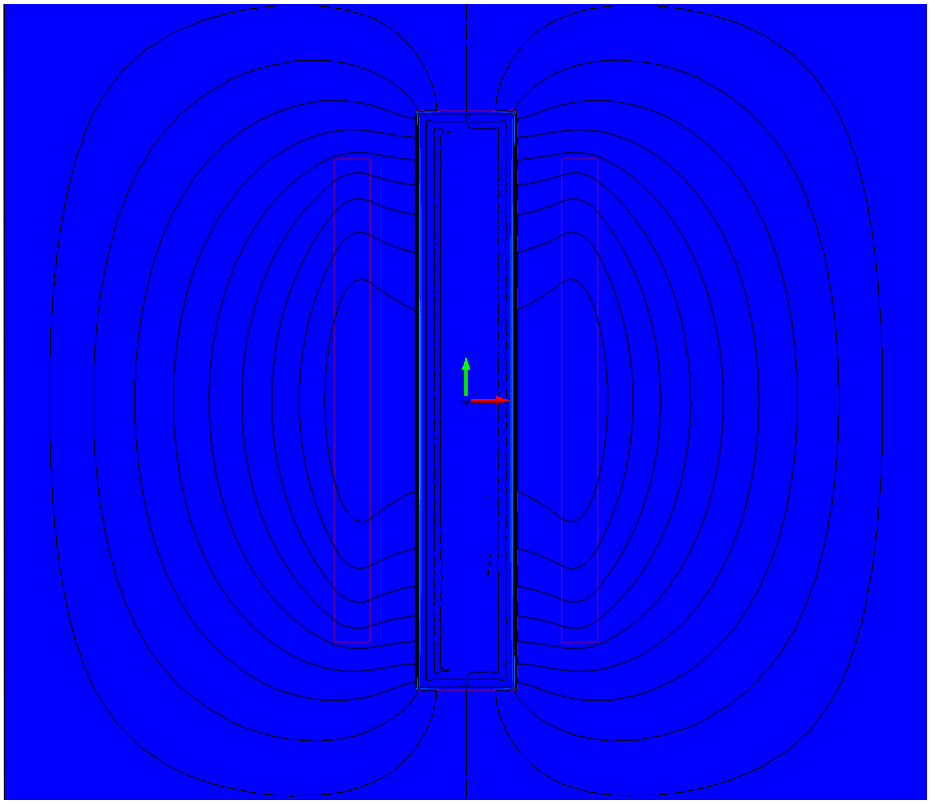

Figure 2.2: Magnetic flux plot of steel bar workpiece.

The direction of the current induced in the steel bar workpiece to be heated is also normal to the magnetic field [Stansel 1949]. Because of Lenz's law, it opposes the current in the coil but in the same circumferential direction. The shape of the workpiece or billet does not affect the principle involved [Stansel 1949]. Thus a workpiece of any shape can be heated by eddy currents.

2.3.2 Basic Induction Heating

In induction heating, a metal workpiece is heated by a passage of currents through a material which are induced from a separate source, as shown in Figure 2.3(a) [Davies and Simpson 1979]. The real power dissipated is equal to the current squared times the effective resistance of the workpiece. The metal workpiece heats due to the resistance to the flow of this current.

The metal to be heated, known as a billet in induction heating terminology, can also be regarded as the secondary winding of a transformer, as shown in Figure 2.3(b) [Davies and Simpson 1979]. In its normal cylindrical form, the transformer is a multi-turn, single layer primary winding and a single-turn short-circuited secondary winding, separated by a small air gap.

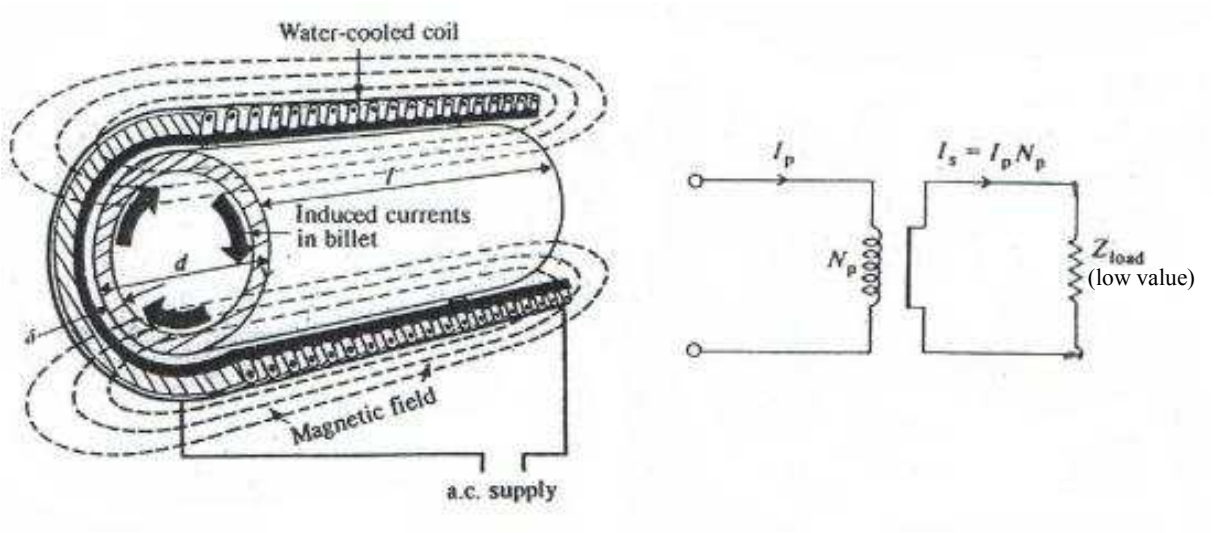

(a) (b)

Figure 2.3: Induction heating coil around a billet.

When alternating current flows in the primary, voltages are induced in the secondary which causes the current to flow in it. The current tends to cancel the flux that produces it, according to Lenz's Law. The current thus effectively flows in about a skin depth δ, where

$$\delta = \sqrt{\frac{2\rho}{\mu\omega}} \tag{2.2}$$

and ρ is the workpiece material resistivity, μ is the workpiece material permeability, ω is the supply angular frequency. The skin depth is a well known phenomena which describes the depth at which the magnitude of the current drops $e^{-1}(= 0.368)$ of its value at the surface. Its depth depends on the workpiece material resistivity, the frequency of the supply electromagnetic field, and the permeability of the workpiece. The skin depth can be derived from Maxwell's equations by first expressing them as two second order differential equations [Fisk 2008].

There are a number of models that have been used for calculating the impedance of the workpiece in induction heating.

The equivalent resistance of a solid bar is that which, if placed in series with the induction coil, would dissipate as much heat as all the eddy currents in the actual workpiece [Zinn and Semiatin 1988]. For a solid round bar of diameter d

$$R_{eq} = \frac{K_r \rho N^2 \pi d}{\delta l} \tag{2.3}$$

where K_r is a workpiece correction factor, N is the number of turns in the coil, and l is the length of the workpiece.

K_r accounts for the variation of the electrical path between the internal and external diameters of the equivalent sleeve. It has a non-linear dependence on the ratio of $\frac{d}{\delta}$ [Zinn and Semiatin 1988].

An analytical approximation for solid round bars is

$$\begin{aligned} K_r = &\quad 0.15\tfrac{d}{\delta} \quad \text{for } 0 < \frac{d}{\delta} < 5 \\ = &\quad 0.015\tfrac{d}{\delta} \quad \text{for } 5 < \frac{d}{\delta} < 15 \\ = &\quad 0.95 \quad \text{for } \frac{d}{\delta} > 15 \end{aligned}$$

For a round hollow tube, the value of K_r changes dramatically when the tube thickness t becomes less than the skin depth. Under these conditions a uniform flux density is assumed and the equivalent resistance becomes

$$R_{eq} = \frac{\rho N^2 \pi d}{tl} \tag{2.4}$$

For rectangular workpieces of width w and thickness t, the equivalent resistance is

$$R_{eq} = \frac{K_r \rho N^2 2w}{tl} \tag{2.5}$$

The factor K_r can be approximated to

$$\begin{aligned} K_r = &\quad 0.4\tfrac{t}{\delta} \quad \text{for } 0 < \frac{t}{\delta} < 2.5 \\ = &\quad 1.0 \quad \text{for } \frac{t}{\delta} > 2.5 \end{aligned}$$

For short, stubby round bars, a second multiplication correction factor K_r is used to account for the fringing of the magnetic field at the bar ends [Zinn and Semiatin 1988]. This is dependent on both the ratio of the workpiece diameter to the inside diameter of the coil, $\frac{d}{b_1}$, and the ratio of the latter to the coil length, $\frac{b_1}{l}$. It is a highly non-linear relationship as shown in [Zinn and Semiatin 1988].

2.4 SEC MODEL OF INDUCTION HEATER

Modelling an induction heater involves developing mathematical relationships of the physical process of electromagnetic induction. There are a number of models [Dodd and Deeds 1968], [Dodd *et al.* 1974], [Namjoshi *et al.* 2001], [Namjoshi and Biringer 1993], [Hussein and Biringer 1992] which are considered valid at high frequencies only. However, at mains frequency, the SEC model [Baker 1957], [Davies and Simpson 1979] is often used.

The SEC model looks at the parallel flow of magnetic flux through the coil, airgap and workpiece of an induction heater and converts these into an equivalent electrical circuit, where all components are in series. The circuit components are the coil and workpiece resistance, and the coil, airgap and workpiece reactances, which cannot be interpreted as being actual values that can be measured. It is their combined series impedance that yields appropriate terminal current, power and power factor for a given applied voltage.

This model of an induction heater is based on the series equivalent circuit depicted in Figure 2.4 [Baker 1957], [Davies and Simpson 1979]. This equivalent circuit has the resistance of the coil and workpiece (R_c, R_w) and the reactances of the workpiece, air gap and coil (X_w, X_g,andX_c) all in series.

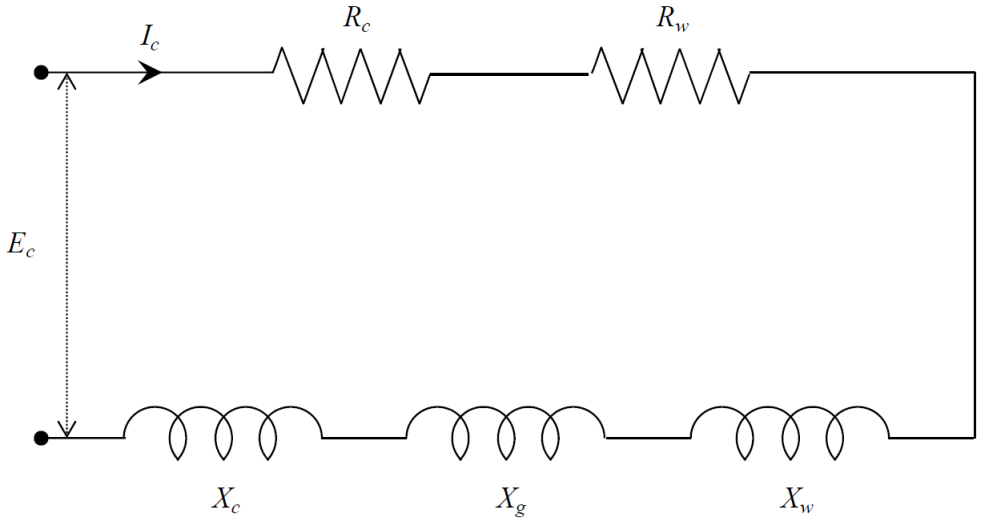

Figure 2.4: Series equivalent circuit of induction heater.

The SEC method requires the coil to be designed by obtaining the values of the resistances and reactances of the coil, workpiece and the air gap between them, and then solving the circuit.

The series impedance is

$$Z = (R_w + R_c) + j(X_g + X_w + X_c) \tag{2.6}$$

where the components are

workpiece resistance

$$R_w = K(\mu_r p A_w) \tag{2.7}$$

coil resistance

$$R_c = K\left(\frac{k_r \pi d_c \delta_c}{2}\right) \tag{2.8}$$

air gap reactance

$$X_g = K(A_g) \tag{2.9}$$

workpiece reactance

$$X_w = K(\mu_r q A_w) \tag{2.10}$$

coil reactance

$$X_c = K\left(\frac{k_r \pi d_c \delta_c}{2}\right) = R_c \tag{2.11}$$

and

$$K = \left(\frac{2\pi f \mu_0 N_c^2}{l_c}\right) \tag{2.12}$$

In these equations, μ_r is the relative permeability of the workpiece, A_w is the cross-section of the workpiece, d_c is the coil inner diameter, δ_c is the skin depth of the coil, A_g is the air gap between the coil and the workpiece, μ_0 is the magnetic permeability of free space ($4\pi \times 10^{-7}$), N_c is the coil turns, and l_c is the coil length.

In the equation for the coil resistance and reactance, k_r is a correction factor, allowing for the spacing between the turns (k_r lies between 1 and 1.5, with 1.15 being a typical value). The expression (2.8) for the coil resistance is dependent on relative permeability and does not appear dimensionally correct. However, this is an expression of the model that allows terminal conditions

to be calculated. The individual component value calculated should not be interpreted as what you would measure in practice.

The p and q factors in the equation for the workpiece resistance and reactance can be estimated from graphs or calculated from analytical expressions [Davies and Simpson 1979]. The dimensionless flux factors p and q depend on geometry, frequency, resistivity, and also the permeability of the material.

In the equation for the workpiece resistance and reactance, the effective cross-sectional area of the current flow in the workpiece should be used. This is dependent on the skin depth.

For $\frac{d_w}{\delta_w}$ ratios greater than 8, then [Davies 1990]

$$p = \frac{2}{\left(1.23 + \frac{d_w}{\delta_w}\right)} \tag{2.13}$$

$$q = \frac{2}{\left(\frac{d_w}{\delta_w}\right)} \tag{2.14}$$

Alternatively, for $\frac{d_w}{t_w} \geq 10$ and $\frac{t_w}{\delta_w} \leq 0.2$, the p and q factors can be calculated from analytical expressions.

$$p = \frac{\gamma}{(1+\gamma^2)} \tag{2.15}$$

$$q = \frac{1}{(1+\gamma^2)} \tag{2.16}$$

where

$$\gamma = \frac{d_w t_w}{(2\gamma^2)} \tag{2.17}$$

If the thickness ratios lie outside the limit, then p and q can be estimated from the graph of p and q versus $\frac{2b}{\delta_w}$ for a slap of thickness $2b$, or $\frac{d_w}{\delta_w}$ for a solid cylinder of diameter d_w. These graphs have been derived from complex expressions involving hyperbolic and Bessel functions respectively [Davies 1990].

This set of equations is most relevant for long coils [Baker 1957]. However, for short coils, a modification is suggested [Baker 1957] whereby an external reluctance X_e is placed in parallel with the series combination of R_w, X_w, X_g, and X_c. This is to accommodate the likely significant

leakage and distortion of flux flow about the end regions if the length to diameter ratio of the workpiece and coil is small (i.e. approaching unity). It is suggested that to accommodate this distortion, the equivalent circuit is modified, as shown in Figure 2.5.

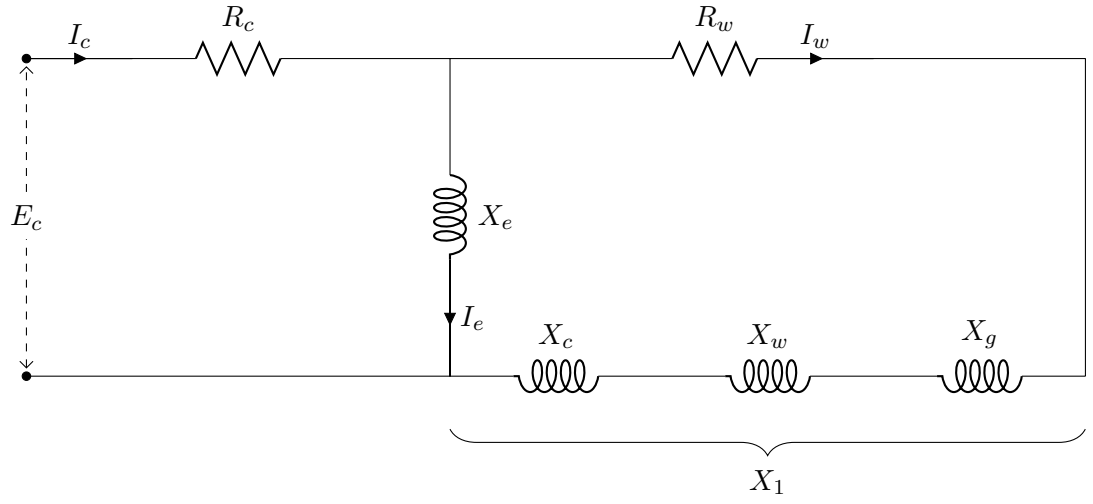

Figure 2.5: Short coil equivalent circuit which includes an external reactance.

This reactance represents the impedance of the end effects of the external flux path. It can be calculated from

$$X_e = K\left(\frac{l_c}{R_e}\right) \tag{2.18}$$

where R_e is the external reluctance given in [Baker 1957] as

$$R_e = k_c \frac{1.80}{p_c} \tag{2.19}$$

and k_c is an empirical factor which is assumed to be 1, and p_c is the coil perimeter.

On the basis of the change in inductance of a cylindrical solenoid with length, it is possible to show that its external reluctance is practically independent of the length and equal approximately to $\frac{0.57}{d_c}$ where d_c is the coil diameter [Baker 1957].

For an unknown reason, the addition of the short coil external reactance has since been regarded as an "ill-defined quantity"and "manifestly wrong"[Davies and Simpson 1979]. Hence, the long coil model is used in this thesis. The addition of the short coil reactance would increase the current drawn from the supply and decrease the power factor.

2.4.1 SEC Performance

The component values of the SEC model in Figure 2.4 can be used to calculate the major coil properties such as efficiency, coil power factor, the number of volts per turn and the number of ampere-turns.

The applied coil voltage V_c which is equal to the emf E_c is

$$V_c = I_c Z \tag{2.20}$$

where I_c is the coil current.

The total impedance is

$$Z = R + jX \tag{2.21}$$

and

$$Z^2 = (R_w + R_c)^2 + (X_g + X_w + X_c)^2 \tag{2.22}$$

The electrical performance of the induction heater can now be calculated. The coil efficiency η is the ratio of workpiece resistance R_w to the total resistance.

$$\eta = \frac{R_w}{R_c + R_w} \tag{2.23}$$

It can be seen from (2.23) that to obtain high efficiencies, the coil resistance value R_c is required to be significantly less than R_w. This is usually obtained by choosing copper or aluminium as the coil material because they have the lowest resistivities of the commonly used metals.

The ratio of the total resistance to impedance Z is the coil power factor

$$\cos\theta = \frac{R_w + R_c}{|Z|} \tag{2.24}$$

The coil power is

$$P_c = \frac{P_w}{\eta} \tag{2.25}$$

where P_w is the total work power input to workpiece.

The coil volt-amperes

$$|S| = \frac{P}{\cos\theta} = I_c^2|Z| \tag{2.26}$$

The coil volts/turn

$$= \frac{E_c}{N_c} \tag{2.27}$$

The coil ampere-turns

$$= I_c N_c \tag{2.28}$$

where I_c and E_c from Equation 2.27 are RMS quantities.

2.4.2 Equivalent Circuit Performance for an Experimental Induction Heater

A coil of a small induction heater was constructed with the parameter dimensions shown in Table 2.1.

Table 2.1: Coil dimensions

Material	Copper	Units
Resistivity	1.72×10^{-8}	Ωm
Length	208	mm
Outside diameter	114	mm
Inside diameter	83	mm
Wire diameter	1.7	mm
Wire area	2.27	mm^2
Number of layers	9	-
Turns per layer	111	-
Number of turns	999	-
Length of wire	309	m
Calculated resistance	2.34	Ω
Measured resistance (50Hz)	2.15	Ω

A number of mild steel tubes of various diameters and thicknesses were cut to provide workpieces that fitted inside the coil former. The dimensions of the workpieces are listed in Table 2.2.

Table 2.2: Workpiece dimensions

Workpiece	Material	Length (mm)	Diameter (mm)	Thickness (mm)
1	Mild steel	250	44.3	solid
2	Mild steel	250	44.5	12.6
3	Mild steel	250	44.2	6.3
4	Mild steel	250	48.3	3.3
5	Mild steel	250	54.0	2.6
6	Mild steel	250	70.0	2.0
7	Mild steel	250	73.0	solid

2.4.3 Material Properties

For the sake of calculation, the physical characteristics of the copper coil and mild steel workpieces were taken as given in Table 2.3. These are generic values as the actual values were unknown. There may be differences due to the metallurgy of their manufacture.

Table 2.3: Physical properties of copper and mild steel

Material	Copper	Mild steel
Resistivity (Ωm $\times$ 10^{-8})	1.72	16
Relative permeability	1	750
Skin depth at 50Hz (mm)	9.3	1.0

Having obtained all the parameters of the equivalent circuits from the material characteristics and dimensions, the performance of the heater could be calculated by solving the equivalent circuit equations and determining the current, power and power factor for a given applied voltage. In addition, efficiencies, voltage gradients, voltages per turn and current densities could be calculated.

2.5 CALCULATED PERFORMANCE USING SEC MODEL

To check the performance of the induction heaters, a program was written in MATLAB [Recktenwald 2000] for the SEC long coil model to perform all the above calculations. The various components of the SEC model are given in Table 2.4.

The value of the coil resistance should not be taken too literally. Indeed, for the actual as-build induction heater of the dimensions listed in Table 2.1, the coil resistance was measured to be 2.15Ω. Rather, it is the total circuit that gives rise to terminal conditions that is of importance. The calculated value from the SEC model is significantly lower than that measured. The workpiece resistance and reactance are significantly higher than the coil resistance and reactance. The airgap reactance is about 10 times more than the coil resistance and reactance.

Table 2.4: Component values for the SEC long coil model

Circuit component	Value (Ω)
R_c	0.241
R_w	9.346
X_c	0.241
X_w	9.510
X_g	2.321

For the SEC model, the short coil reactance, as suggested by Baker [Baker 1957], was calculated to be 57.4Ω. This is much higher than any of the other components and therefore had little effect on the results, increasing the current by about 0.1A and insignificantly changing the power factor.

Having calculated the component values of the SEC model, the performance of the induction heater is obtained by solving the equivalent circuit equations. Table 2.5 shows the performances of the induction heaters for a 100V supply.

Table 2.5: Calculated performance of experimental heater using SEC long coil model

Workpiece	Voltage (V)	Current (A)	Flux density (T)	Coil loss (W)	Workpiece loss (W)	Apparent power (VA)	Power factor
1	100	6.9	3.2	7.6	438.6	692.1	0.6
2	100	6.9	3.2	7.6	438.3	691.7	0.6
3	100	6.9	3.2	7.6	438.8	692.3	0.6
4	100	6.9	2.9	7.9	431.7	685.1	0.6
5	100	6.8	2.6	8.5	422.2	675.8	0.6
6	100	6.5	2.0	9.9	397.6	652.7	0.6
7	100	6.5	1.9	10.2	393.3	648.7	0.6

The calculated performances from the SEC model show a maximum current of close to 7A and a flux density of 3.2T which is likely to be more than the saturation point for all the workpieces. The calculated flux density decreases to 1.9T as the diameter of the workpiece increases. In addition, the calculated coil losses increase from 7.6W to 10.2W as the diameter of the workpiece increases. The coil losses are all significantly lower compared to the workpiece losses. Both the workpiece losses and apparent power have decreased as the workpiece diameter increased. The power factors for the different workpieces are all the same.

2.6 SUMMARY

The theory of induction heating has been presented. Firstly, the background and applications of induction heating were introduced. This chapter also introduced electromagnetic induction

as a basis to understand the principle of operation of induction heating.

The conventional approach to induction heater design which has been widely used in research is the SEC model. It has been presented in this chapter. The SEC model was used to calculate the performance of a demonstration induction heater using a set of different workpieces. The calculated results from the SEC model were also discussed in terms of the coil losses, workpiece losses and power factors.

Chapter 3

TRANSFORMER MODEL OF INDUCTION HEATER

3.1 INTRODUCTION

An induction heater can be regarded as a special type of transformer with a single shorted turn secondary winding. The coil is the equivalent of a multiple turn primary winding, and the workpiece is the single turn secondary winding. The workpiece also performs the function of being the core, which the magnetic field generated by the coil passes through. Hence, a transformer equivalent circuit model can be used to calculate the performance of the induction heater.

In this chapter, the equivalent circuits model of ideal and non-ideal transformers are presented. These are then transformed into a circuit to model an induction heater. The performance calculations from this circuit are compared to the more conventional SEC model of Chapter 2.

3.2 TRANSFORMER FUNDAMENTALS

The basic concept of induction heating can be shown to be similar to the well known transformer theory. In order to develop the circuit to model the induction heater, it is useful to look at the operation of an ideal transformer, and also the deviations from the ideal.

3.2.1 Ideal Transformers

In an ideal transformer, it is assumed that the input power to the transformer is equal to the output power. Figure 3.1 [Lapthorn 2013] shows a schematic representation of a single phase transformer with two coils wound on a magnetic core. The magnetic coupling is assumed to be perfect, that is the same flux ϕ passes through each turn of each coil.

In Figure 3.1, V_1 is the primary voltage, V_2 is the secondary voltage, i_1 is the primary current, i_2 is the secondary current, N_1 is the number of turns on the primary, N_2 is the number of turns

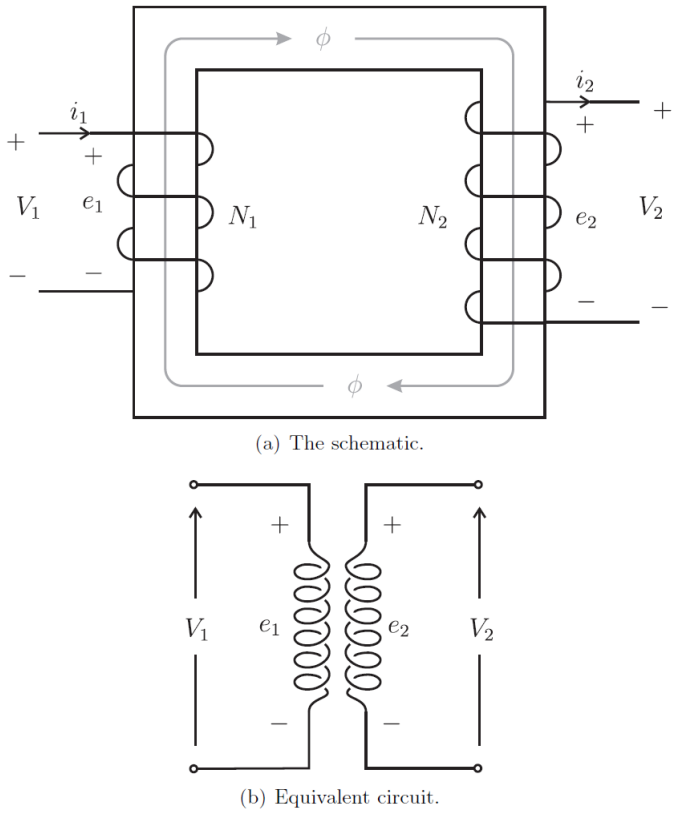

Figure 3.1: An ideal full-core transformer.

on the secondary, e_1 is the induced emf in the primary, e_2 is the induced emf in the secondary, and ϕ is the magnetic flux in the core.

Faraday's law of electromagnetic induction states that a changing magnetic flux ϕ induces electromotive forces (emf's) in the circuit, thus emf's e_1 and e_2 are induced in N_1 and N_2 owing to a finite rate of change of flux ϕ such that

$$e_1 = N_1 \frac{d\phi}{dt} \tag{3.1}$$

and

$$e_2 = N_2 \frac{d\phi}{dt} \tag{3.2}$$

With the transformer being ideal, $e_1 = V_1$ and $e_2 = V_2$. The direction of e_1 is such that it produces a current which opposes the flux change, according to Lenz's law. Using the dot convention, from Equations 3.1 and 3.2,

$$\frac{e_1}{e_2} = \frac{N_1}{N_2} \tag{3.3}$$

If E_1 and E_2 are the RMS values of e_1 and e_2 respectively, then

$$\frac{E_1}{E_2} = \frac{N_1}{N_2} = a \tag{3.4}$$

where a is the turns ratio.

Since $e_1 = V_1$ and $e_2 = V_2$ for an ideal transformer, the flux and voltage are related by

$$\phi = \frac{1}{N_1}\int V_1 dt = \frac{1}{N_2}\int V_2 dt \tag{3.5}$$

In general terms, if the flux varies sinusoidally such that

$$\phi = \phi_m \sin \omega t \tag{3.6}$$

then the corresponding induced voltage e linking an N-turn winding is given by Faraday's law as

$$e = \omega N \phi_m \cos \omega t \tag{3.7}$$

From Equation 3.7, the RMS value of the induced voltage is thus

$$V = \frac{\omega N \phi_m}{\sqrt{2}} = 4.44 f N \phi_m \tag{3.8}$$

where $\omega = 2\pi f$ (f is the frequency in Hertz). This is usually referred to the transformer equation.

For an ideal transformer, the magnetomotive force (mmf) required to produce the working flux is negligibly small. This mmf is the resultant of the mmf due to the primary current and that due to the secondary current such that

$$N_1 i_1 = N_2 i_2 \tag{3.9}$$

Therefore

$$\frac{i_1}{i_2} = \frac{N_2}{N_1} = \frac{1}{a} \tag{3.10}$$

Multiplying Equations 3.3 and 3.10

$$e_1 i_1 = e_2 i_2 \tag{3.11}$$

Thus, the apparent powers through both the primary and secondary windings are equal. The primary absorbs power from the sources, whereas the secondary delivers power. In the ideal transformer, no power is lost internally due to the windings and core so that the two quantities are equal.

3.2.2 Non-Ideal Transformers

In a practical transformer, the winding resistances and the core reluctance are not zero, and the magnetic coupling is not perfect. In addition, power will be lost in the core because the eddy currents and hysteresis in the magnetic material. All of these effects can be represented by the equivalent circuit shown in Figure 3.2 [Lapthorn *et al.* 2013a]. The equivalent circuit shows an ideal transformer coupled with other components to model the various non-ideal characteristics. This equivalent circuit is relevant for low frequency modeling of power transformers.

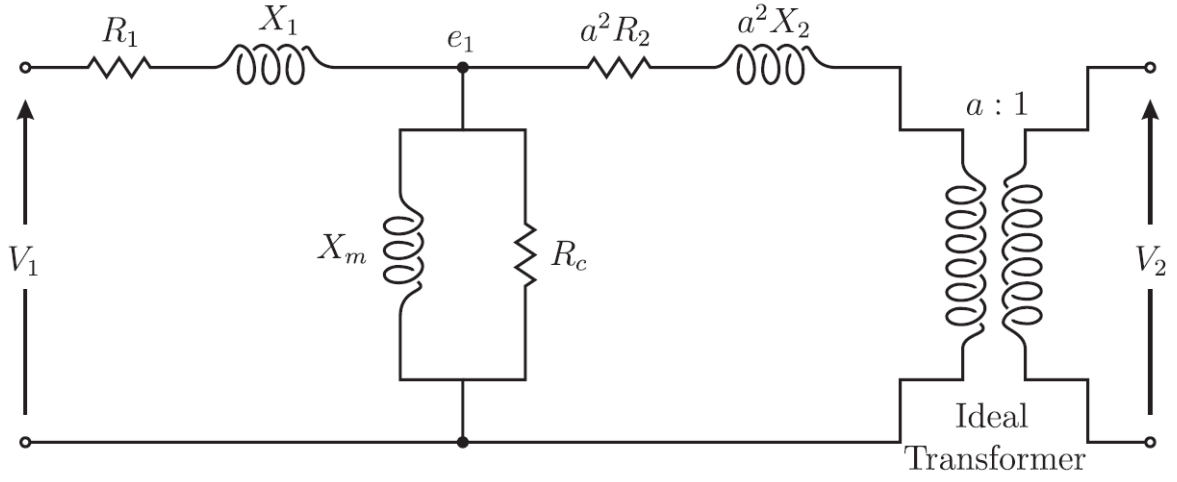

Figure 3.2: Equivalent circuit of a non-ideal transformer.

The most obvious loss is created by the current in the primary winding, even when the secondary winding is open circuited. This current has two components. The first component is the magnetizing current, which is generated by having a core of finite permeability. A significant magnetizing force is required to produce an operating flux. This is modeled as a magnetizing

reactance which is represented as a shunt reactance path (designated by X_m) on the primary side.

The second component represents two losses inside the transformer's core, which are the hysteresis and eddy current losses, such that some real power is absorbed even at no-load. These losses can be modeled by the addition of a shunt resistance (designated by R_c) on the primary side [Liew 2001].

The hysteresis real power losses P_h depend on the rotation of the domains in the ferromagnetic material. They are proportional to fB^x [Slemon and Straughen 1980] where x is the Steinmetz factor of core material, empirically derived (1.5−2.5).

However, from the transformer equation (3.8)

$$V = \frac{\omega N \phi_m}{\sqrt{2}} = 4.44 f N \phi_m$$

Or V is proportional to $f\phi$ or fB, where $\phi = BA$, and A is the cross-sectional area of the core.

Hence, P_h is proportional to $\frac{V}{f^{x-1}}$. P_h thus depends on the voltage and frequency. It is constant if both voltage and frequency are constant.

Since B can be calculated, the hysteresis losses are usually calculated from

$$P_h = k f B^x W T \tag{3.12}$$

where k is constant depending on the material, B is the maximum flux density, and WT is the weight of the core material. For induction heaters, the hysteresis losses are usually ignored, as they contribute a much smaller amount as compared to the eddy current losses.

The eddy current real power losses due to the induced currents flowing in the core material, P_e are proportional to f^2 B^2 or V^2. Thus the eddy current losses also depend on the voltage [Slemon and Straughen 1980]. The expression for eddy current losses also depends on the dimensions of the core material and whether the core is laminated. For induction heating, the eddy current losses are those heating up the workpiece. The combined hysteresis and eddy current losses are

$$P_c = P_h + P_e \tag{3.13}$$

The losses can be represented by a current i_c passing through a resistance R_c. The power losses are

$$P_c = i_c^2 R_c = \frac{V^2}{R_c} \tag{3.14}$$

The real power losses of both windings are the other significant components modelled to account for the performance of a real transformer. These can be modelled as a series resistance for each winding (R_1 and R_2 respectively). When current flows through the primary and secondary side of the transformer, some leakage flux passes through the air surrounding each winding instead of going through the core. The leakage flux links with the turns in each winding, and sets up emf's that oppose the flow of the current through each winding. Thus, the leakage flux produces the same effect as an unwanted inductance in series with each winding. The unwanted inductance is also termed the leakage inductance, which is represented by a reactance X_1 and X_2 in the primary and secondary windings respectively [Liew 2001].

3.3 TRANSFORMER EQUIVALENT CIRCUIT OF INDUCTION HEATER

If an induction heater can be considered as a special type of transformer, then a transformer equivalent circuit can be used to calculate the performance of the induction heater. The transformer equivalent circuit (TEC) method determines the parameters of the TEC using the reverse design method [Liew and Bodger 2001], [Bodger and Liew 2002]. It also calculates the performance of the induction heater. The performance of the induction heater depends on the effective eddy current resistance of the workpiece. This will depend on the material and their dimensions. For example, the length and diameter of the workpiece must be selected to optimize the performance of the heater.

An induction heater is essentially a transformer with a single shorted turn secondary winding. The transformer equivalent circuit is shown in Figure 3.3. This circuit is based on an ideal transformer, with additional circuit elements to represent the practical deviations from the ideal. It can be seen from Figure 3.3, that the ideal transformer has been eliminated and the transformer can be represented exclusively by an RL circuit referred to the primary. The TEC circuit in Figure 3.3 is relevant for low frequency modelling of induction heaters.

In this model, R_w represents the eddy current losses in the workpiece, which would normally be accounted for in the core of a transformer, R_c is the resistance of the coil, which is now the primary winding using transformer terminology (not to be confused with its former use to represent the core losses in Figure 3.2), and X_{mw} is the magnetising reactance which accounts for the current required to magnetise the core. Moreover, hysteresis losses, also normally a component of core losses in a transformer, are insignificant in induction heating. Hence the losses in the workpiece become resistance losses of the secondary winding.

The leakage reactance for each winding can be split between the coil and the workpiece as X_c

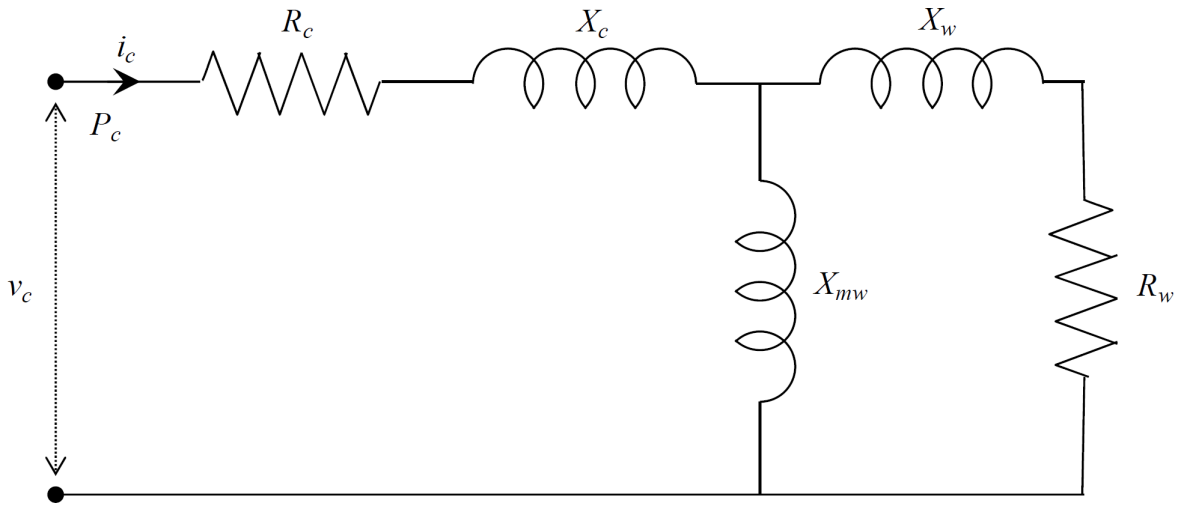

Figure 3.3: Transformer equivalent circuit of an induction heater.

and X_w. The leakage reactances account for the imperfect magnetic field coupling between the coil and the workpiece.

3.4 CALCULATION OF EQUIVALENT CIRCUIT PARAMETERS

The parameters of the equivalent circuit in Figure 3.3 are calculated using the basic dimensions and physical characteristics of materials used, as per the reverse design method [Liew and Bodger 2001], [Bodger and Liew 2002]. These are entered as known data and then the individual circuit components are calculated using magnetic and electric circuit component models.

Figure 3.4 shows a cross-sectional profile of a multi-layer coil induction heater with a tube workpiece. All the symbols represent dimensions of the materials used in the construction of the heater, including the workpiece, insulation and the coil, where LW is the length of the workpiece, DW is the diameter of the workpiece, TW is the thickness of the workpiece, IWC is the workpiece/coil insulation thickness, WC is the diameter of the coil wire, WIC is the coil interlayer insulation, and DOC is the outside diameter of the coil.

The equivalent circuit components in Figure 3.3 need to be modified as the flux path is open and not entirely constrained to be inside the core. With respect to the equivalent circuit of Figure 3.3, the winding resistance models R_c and R_w are maintained as they are not affected by the partial core configuration. Thus modifications to the calculation of reactance X_{mw} and the leakage reactance X_{cw} (the sum of X_c and X_w) are required as the core is no longer a closed loop, which affects the magnetic field characteristics of the transformer.

This is demonstrated in Figure 3.5 which shows two different open core induction heaters with

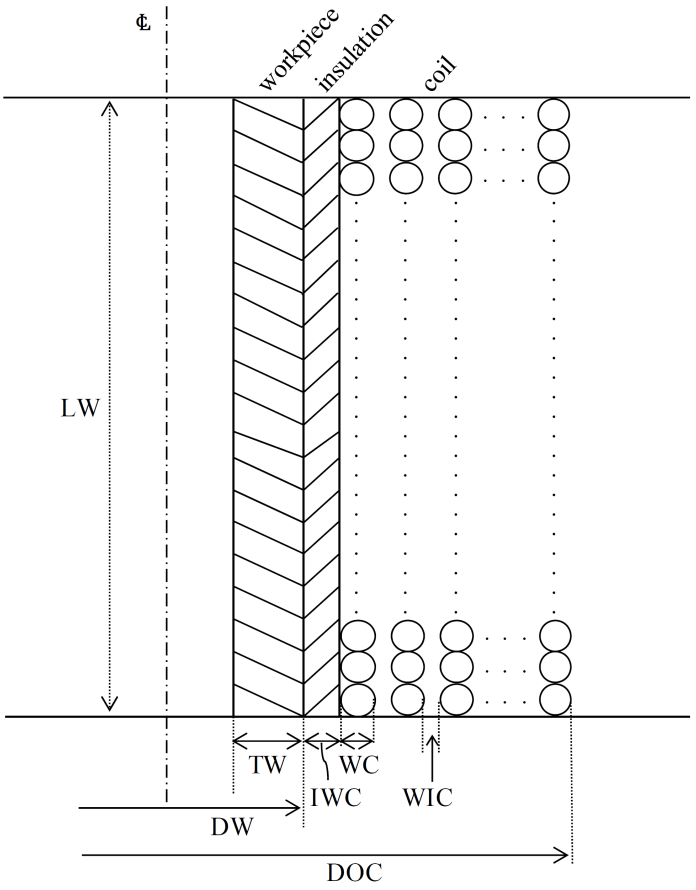

Figure 3.4: Cross-section of a multi-layer coil induction heater with a tube workpiece.

the same core length but significantly different core thicknesses. The resultant magnetic field paths are very different. These give rise to different reluctances in the air path requiring new equivalent circuit component models.

3.4.1 Coil Resistance

If l_c is the length of the coil wire and A_c is its cross-sectional area, then the primary winding or coil resistance is given by

$$R_c = \frac{\rho_c l_c}{A_c} \tag{3.15}$$

where ρ_c is the resistivity of the coil material. The value of the resistivity depends on the coil temperature as

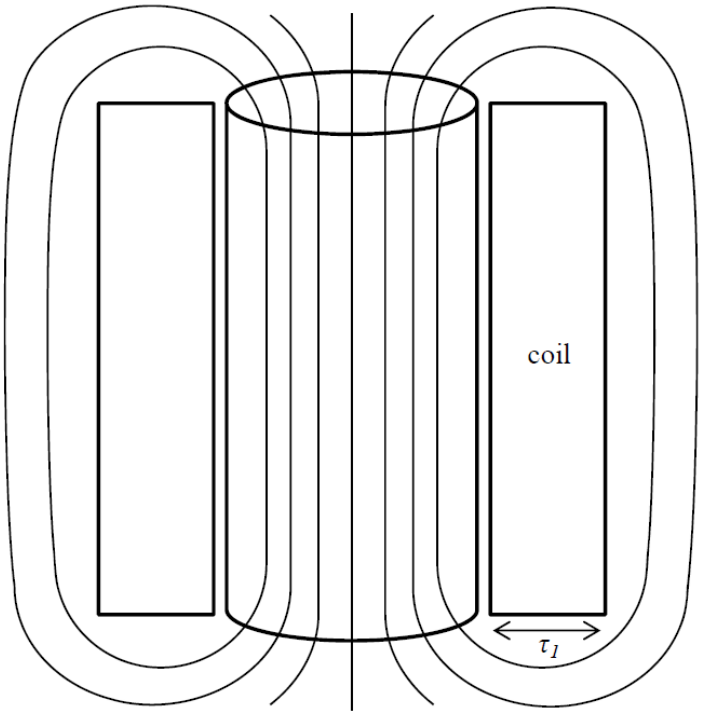

(a) Winding thickness τ_1

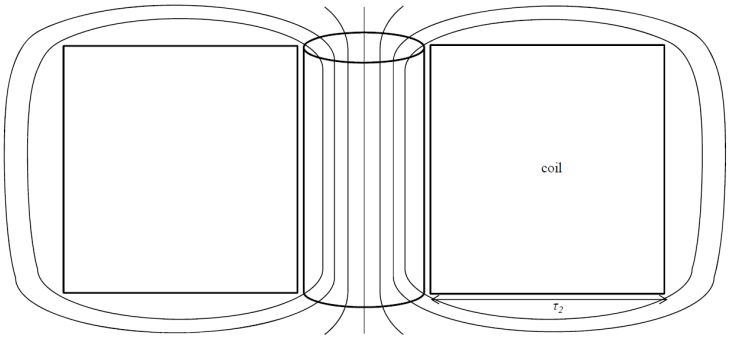

(b) Winding thickness τ_2

Figure 3.5: Flux distribution for induction heaters with different winding thicknesses.

$$\rho_c = (1 + (\Delta\rho(T_c - 20)))\rho_{20^\circ C} \tag{3.16}$$

where $\rho_{20^\circ C}$ is the resistivity at 20°C, T_c is the coil temperature, and $\Delta\rho$ is the thermal resistivity coefficient. The resistivity of all metals is considered to vary linearly with temperature. The calculation of the winding resistance R_c also takes into account the coil skin depth and its effective cross-sectional area. For the coil, the eddy current skin depth gives its effective thickness

$$\delta_c = \sqrt{\frac{2\rho_c}{\mu_0\mu_{rc}\omega}} \tag{3.17}$$

where μ_{rc} is the relative permeability of the coil, and ω is the angular frequency($2\pi f$). The coil effective cross-sectional area is calculated using the diameter of the coil and its effective thickness.

If the skin depth is greater than the radius of the coil conductor then a uniform current density can be assumed. This is set by

$$\delta_c = \frac{W_c}{2} \tag{3.18}$$

where W_c is the diameter of coil wire from Figure 3.4.

The coil effective cross-sectional area is

$$A_{ec} = \pi(W_c - \delta_c)\delta_c \tag{3.19}$$

The length of the conductor used in forming the coil, l_{ec}, is calculated from consideration of the average length per turn, multiplied by the number of turns, N_c. This needs to take into account the diameter of the workpiece, the thickness of the conductor in the radial direction, plus its insulation, and the coil inter-layer and coil/workpiece insulation thickness.

Hence, the coil resistance becomes

$$R_c = \frac{\rho_c l_{ec}}{A_{ec}} \tag{3.20}$$

3.4.2 Workpiece Magnetizing Reactance

The magnetizing reactance X_{mw} for an open core induction heater is formulated in [Liew and Bodger 2002] as

$$X_{mw} = \frac{\omega N_c^2 \mu_0 \mu_{re} A_w}{l_w} \tag{3.21}$$

where ω is the angular frequency, N_c is the number of turns on the coil, μ_0 is the permeability of free space ($4\pi \times 10^{-7}$), and μ_{re} is the effective permeability of the magnetic flux path which includes the series combination of the workpiece and the return path, usually through air. A_w is the effective cross-sectional area of the workpiece, calculated using the skin depth δ_w, and l_w is the length of the workpiece.

This formulation and calculation is a modification of the theory developed for partial core transformers [Liew and Bodger 2001]. A summary is given here for induction heaters. The magnetizing reactance of a partial core is different to that of a full core transformer, since the flux of a partial core transformer not only goes through the core, but also flows in the air around the core. This is shown in Figure 3.6.

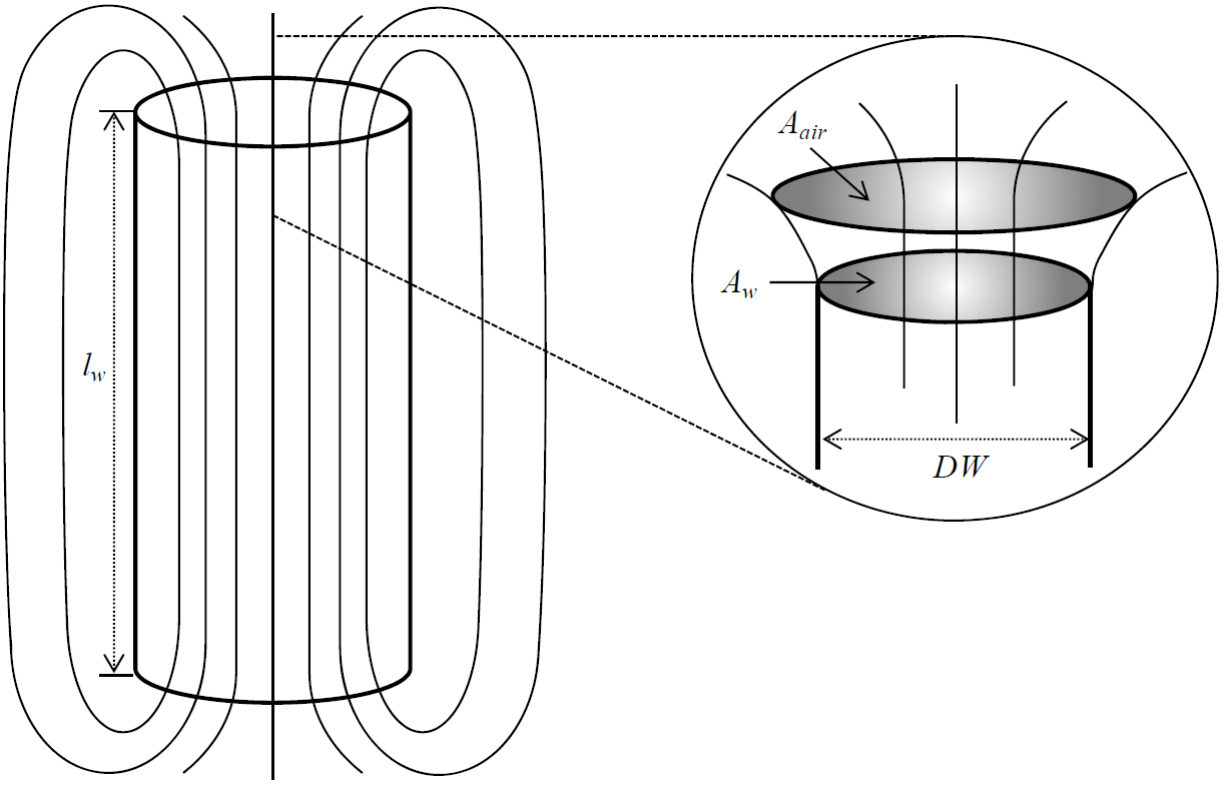

Figure 3.6: Axial view of the flux flow from a cylindrical workpiece.

The magnetic flux generated by the energised coil flows through the workpiece within a skin depth and returns via the air back to the workpiece. Hence, the reluctance of the magnetic flux path is significantly greater than if the flux was constrained to flow inside a closed core. This implies that the overall relative permeability of the induction heater should be much lower than that of the workpiece material, where it is generally of the order of $2000-10000$. Therefore, a new overall relative permeability, which takes into account the magnetic flux in the air, has to be determined.

A full derivation for the calculation of air reluctance for partial core transformers is given in [Liew and Bodger 2001]. This has been adopted for the induction heater calculations without proof, as the method involves empirical factors obtained from a range of transformers actually built. The usefulness of the calculation is ultimately supported by how well the model predicts the performance of actual built devices. Empirical factors based on a number of different as-built

induction heaters should better inform the calculation of the empirical factors.

The method assumes that the reluctance of the air is only in the regions at the ends of the core. The reluctance of the air at one end of the partial core is

$$R_{air} = 1.694 \times 10^5 \left(\frac{1}{A_w}\right)^{0.35} \left(\frac{1}{l_w}\right)^{0.31} \tag{3.22}$$

Since the workpiece flux cross-sectional area may only be a ring of skin depth thickness, a modification for the formula uses the effective radius of the ring.

$$R_{air} = 1.141 \times 10^5 \left(\frac{1}{r_w}\right)^{0.69} \left(\frac{1}{l_w}\right)^{0.31} \tag{3.23}$$

The equivalent magnetic circuit of the induction heater, that includes both the workpiece reluctance and the air reluctances, is given in Figure 3.7.

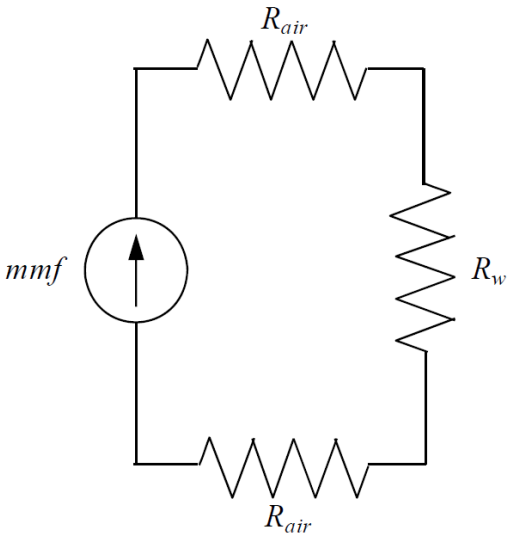

Figure 3.7: Magnetic circuit of induction heater.

The overall reluctance of the transformer is

$$R_T = R_w + 2R_{air} \tag{3.24}$$

This is equivalent to a flux path through a homogeneous medium of relative permeability μ_{rT}, hence

$$R_T = \frac{l_T}{\mu_0 \mu_{rT} A_T} \tag{3.25}$$

where l_T is the overall flux path length $= l_w + 2l_{air} \approx l_w$ as $l_{air} \ll l_w$, and A_T is the overall effective cross-sectional area of the workpiece $= A_w$

Thus

$$\mu_{rT} = \frac{l_w}{\mu_0 R_T A_w} \tag{3.26}$$

The magnetizing reactance of the induction heater is thus

$$X_{mw} = \frac{\omega N_c^2 \mu_0 \mu_{rT} A_w}{l_w} \tag{3.27}$$

3.4.3 Coil/Workpiece Leakage Reactance

The series equivalent circuit and the concept of leakage reactance for a full-core transformer stem from the difficulty in analysing the behaviour of very tightly-coupled coils in terms of self and mutual inductances. The leakage-based approach is well-suited to conventional transformers where the closed magnetic circuit leads to coupling coefficients very close to 1. This conventional approach is maintained, but modified, for the induction heater, because a closely packed multi-layered coil will act as a guide that channels the flux up the middle and around the outside, such that the almost perfect coupling between the coil and the workpiece still exists. The dimensions used in calculating the leakage flux for an induction heater are presented in Figure 3.8.

The coil and workpiece leakage reactances are calculated from the total leakage reactance which embodies the effects of both the coil and workpiece together. The total induction heater leakage reactance is [Connelly 1965]

$$X_{cw} = \frac{\omega N_c^2 \mu_0 \pi \tau_{cw}}{l_w} \tag{3.28}$$

where

$$\tau_{cw} = \left(\left(\frac{w_c d_c + w_w d_w}{3} \right) + w_{cw} \Delta d \right) \tag{3.29}$$

is the coil/workpiece thickness factor

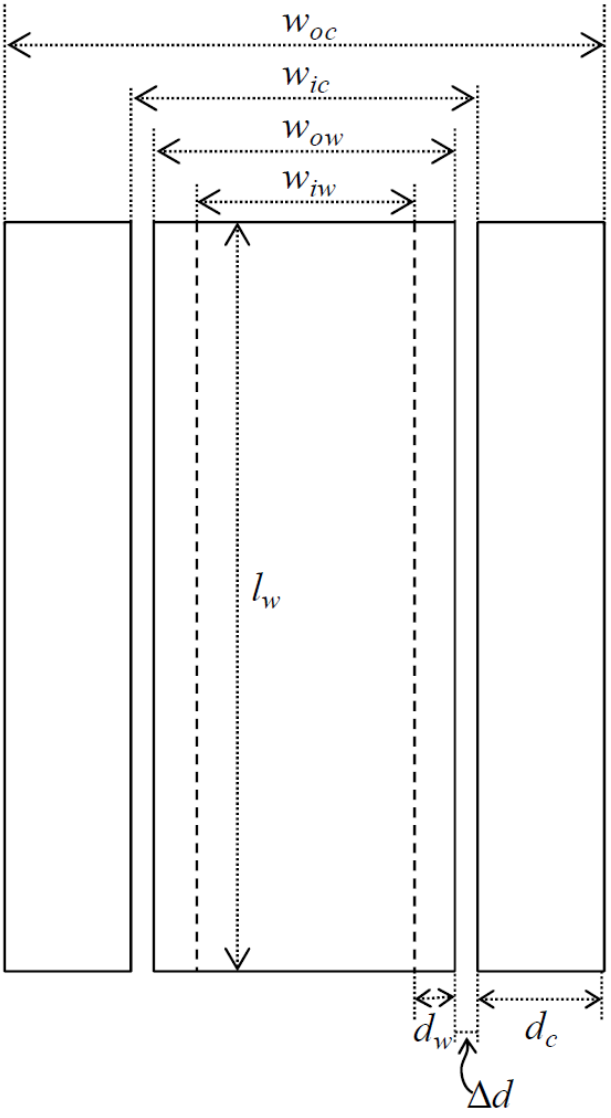

Figure 3.8: Dimensions for representing the leakage flux for an induction heater.

and

$$w_c = \left(\frac{w_{ic} + w_{oc}}{2} \right) \tag{3.30}$$

is the mean diameter of the coil

and

$$w_w = \left(\frac{w_{iw} + w_{ow}}{2} \right) \tag{3.31}$$

is the mean diameter of the workpiece

and

$$w_{cw} = \left(\frac{w_{ic} + w_{ow}}{2} \right) \tag{3.32}$$

is the mean diameter of the space between the coil and workpiece.

The calculation of X_{cw} does not separate the values of the coil and workpiece leakage reactances and they are usually assumed to be the same. Each of them is half of the total leakage reactance.

Hence

$$X_c = X_w = \frac{X_{cw}}{2} \tag{3.33}$$

3.4.4 Workpiece Eddy Current Resistance

The workpiece eddy current resistance referred to the coil is calculated using

$$R_w = \frac{\rho_w l_{we}}{A_{we}} N_c^2 \tag{3.34}$$

where ρ_w is the resistivity of the workpiece, l_{we} is the effective length of the eddy current flowing around the circumference of the workpiece, A_{we} is the effective cross-sectional area of the eddy current path, and N_c is the number of coil turns.

The effective length and cross-sectional area of the eddy current path takes into account the skin depth in the workpiece

$$\delta_w = \sqrt{\frac{2\rho_w}{\mu_0 \mu_{re} \omega}} \tag{3.35}$$

Thus

$$l_{we} = \pi(D_w - \delta_w) \tag{3.36}$$

and

$$A_{we} = l_w \delta_w \tag{3.37}$$

The losses in the workpiece consist of two major components; the hysterisis loss and the eddy current loss. The hysterisis loss is insignificant with respect to the eddy current loss and is not included in the model.

3.5 EQUIVALENT CIRCUIT PERFORMANCE

The transformer equivalent circuit in Figure 3.3 is more complicated than the series equivalent circuit presented in Chapter 2. The parallel impedance of the workpiece resistance and leakage reactance with the magnetizing reactance is

$$Z_w = \frac{jX_{mw} \times (R_w + jX_w)}{(R_w + j(X_w + X_{mw}))} \tag{3.38}$$

and the total impedance is the complex value

$$Z = (R_c + jX_c) + Z_w \tag{3.39}$$

The performance of the induction heater is then obtained by applying a voltage to the coil and calculating the current, apparent power, real power and power factor. In addition, voltage gradients, voltages per turn, current densities and the efficiency can be calculated.

3.5.1 Equivalent Circuit Performance for an Experimental Induction Heater

The TEC model is applied for the same set of induction heaters presented in Chapter 2. The dimensions of the induction heater coil and workpieces are also identical.

3.5.2 Equivalent Circuit Parameters

The calculated equivalent circuit parameters referred to the primary winding are listed in Table 3.1. These values correspond to workpiece 7.

Table 3.1: Component values for the TEC model

Circuit component	Value (Ω)
R_c	2.372
R_w	47.753
X_c	2.513
X_w	2.513
X_{mw}	31.873

The component values of the TEC model are very different from those of the SEC model presented in Chapter 2. This is because the TEC model is very different.

The coil resistance is about 10 times that previously calculated. It is a better indication of what was measured using a resistance meter applied to the coil conductor.

The workpiece resistance (referred to the coil) is also much larger (5 times) than that calculated from the SEC model. The actual resistance is very low, $4.8\mu\Omega$. Again the value should be a reasonable indication of what you could measure. The workpiece resistance is much larger than the coil resistance and hence the efficiency should be high.

For this example, the leakage reactances are relatively small, which indicates that there is good coupling between the coil and the workpiece. A relatively long coil length and small coil/workpiece interspace ensures this. Thus the TEC model gives a useful measure of this feature. The value is about the same as the air gap reactance used in the series equivalent circuit model, although here the value is used twice, for both the coil and the workpiece, as only the combined effect can be calculated. The TEC model is less dominated by the leakage (air gap) reactance.

The workpiece magnetizing reactance is much larger than the workpiece reactance used before. There is no direct correlation between this and the workpiece reactance calculated from the SEC model.

3.5.3 TEC Calculated Performance

Having calculated the parameters of the equivalent circuit, the performance of the induction heater is obtained by applying the nominal voltage to the equivalent circuit. Table 3.2 shows the calculated performances of the induction heaters at a 100V supply.

Table 3.2: Calculated performance using TEC model

Workpiece	Voltage (V)	Current (A)	Flux density (T)	Coil loss (W)	Workpiece loss (W)	Apparent power (VA)	Power factor
1	100	3.9	3.2	26.7	100.9	397.2	0.3
2	100	3.9	3.2	26.6	100.5	396.3	0.3
3	100	3.9	3.2	26.7	101.2	397.7	0.3
4	100	3.8	2.9	25.8	92.2	380.2	0.3
5	100	3.6	2.6	24.8	81.9	359.7	0.3
6	100	3.2	2.0	23.1	62.3	317.0	0.3
7	100	3.1	1.9	22.9	59.6	310.7	0.3

The calculated performances from the TEC model are significantly lower than the SEC model of Chapter 2 in terms of current, apparent power and workpiece loss. The same is not true for

the coil loss. The power factors from the TEC model are half those calculated from the SEC model. Both models yield the same flux density, but in all cases this is calculated to be a value significantly above that of the likely saturation value for mild steel. The calculated coil and workpiece losses decrease as the diameter of the workpiece increases. This is due to the longer eddy current path length and hence resistance in the workpiece. This pattern is not showed in the coil and workpiece losses calculated from the SEC model.

As a modification to the TEC model, the permeability of the workpiece is reduced until the flux density is below the saturation point. This means that the skin depth increases. The magnetizing reactance and the workpiece eddy current resistance are adjusted to account for this.

If the flux penetrates beyond the thickness of the workpiece, then part of the flux flows inside the workpiece. The parallel combination of this reluctance and that of the workpiece must be taken into account in calculating the workpiece magnetization reactance. This can be modeled as a parallel reluctance with components both in the workpiece and inside.

The workpiece reluctance is

$$R_w = \frac{l_w}{\mu_0 \mu_{rw} A_w} \tag{3.40}$$

where A_w is the cross-sectional area of the workpiece tube, and μ_{rw} is the relative permeability of the workpiece.

The inside tube reluctance is

$$R_i = \frac{l_w}{\mu_0 A_i} \tag{3.41}$$

where A_i is the cross-sectional area of the inside of the workpiece tube.

The reluctance of the parallel combination is

$$R_p = \frac{R_i \times R_w}{R_i + R_w} \tag{3.42}$$

Assuming that the flux density is within the saturation level of the material, then the effective radius of the workpiece is

$$r_e = \sqrt{\frac{A_e}{\pi}} \tag{3.43}$$

where A_e is the effective area of the flux as if it was flowing inside a solid cylinder workpiece.

$$A_e = \pi(D_w - \delta_w)\delta_w \tag{3.44}$$

The air path reluctance at one end of the workpiece is given in (3.23) as

$$R_{air} = 1.141 \times 10^5 \left(\frac{1}{r_w}\right)^{0.69} \left(\frac{1}{l_w}\right)^{0.31}$$

Thus the total reluctance for the complete flux path is

$$R_T = R_p + 2R_{air} \tag{3.45}$$

The equivalent relative permeability of the series combination of the air and the workpiece/inside tube flux path is

$$\mu_{re} = \frac{l_w}{\mu_0 A_w R_T} \tag{3.46}$$

The workpiece magnetizing reactance (referred to the coil) is

$$X_{mw} = \frac{\omega N_c^2}{R_T} \tag{3.47}$$

The equivalent relative permeability calculated using the above method for workpiece 7 is 93.5 which is much lower than the nominal workpiece value of 750. At 93.5, the flux density in the workpiece is 1.7T, and the skin depth in the workpiece has now increased from 1.1 to 2.9mm. Table 3.3 shows the calculated performance of the induction heater for operation at the saturation point set at a realistic 1.7T. The workpiece losses are higher than those given in Table 3.2 but still significantly lower than those calculated using the SEC model. The power factors have, in general, increased.

3.6 SUMMARY

In this chapter, the equivalent circuits model of ideal and non-ideal transformer were presented. These were transformed into a circuit to model an induction heater.

The low frequency modelling of induction heaters using the TEC model has been presented. The performances of the induction heaters from this model are compared to the SEC model

Table 3.3: Calculated performance using TEC model below the saturation point

Workpiece	Voltage (V)	Current (A)	Flux density (T)	Coil loss (W)	Workpiece loss (W)	Apparent power (VA)	Power factor
1	100	4.3	1.7	30.8	190.9	427.1	0.5
2	100	4.3	1.7	30.6	189.2	425.1	0.5
3	100	4.3	1.7	30.9	191.9	428.1	0.5
4	100	3.9	1.7	27.6	159.5	393.5	0.5
5	100	3.6	1.7	24.9	126.5	360.3	0.4
6	100	3.1	1.7	22.3	73.6	311.7	0.3
7	100	3.1	1.7	22.3	67.4	306.3	0.3

calculated performances of an experimental heater for a variety of sizes of mild steel workpieces presented in Chapter 2.

The calculated performances of the TEC model shows significantly lower values in terms of the current and workpiece losses compared to the SEC model. The power factors calculated from the TEC model are higher than those calculated from the SEC model.

Chapter 4

FINITE ELEMENT ANALYSIS AND MEASURED PERFORMANCE OF EXPERIMETAL INDUCTION HEATER

4.1 INTRODUCTION

The finite element method is a numerical technique which gives an approximate solution to a complicated problem. Finite element analysis offers the best approach to determine the flux pattern inside the heater. This chapter presents the computational results obtained using finite element analysis (FEA) for a two dimensional model of the experimental induction heater. These results correspond to a 100V supply to the coil. At this supply voltage, solutions are computed and performances of the heater are calculated.

Also in this chapter, the measured performances of the experimental heater are assessed. The experimental set-up and method of measurements performed are discussed. Measurement results include current, real power, apparent power and power factor. In addition, eddy current losses and winding losses of the mild steel workpiece are calculated from the measurements. These measured results are compared to the results obtained using FEA, and the SEC, and TEC models.

4.2 FINITE ELEMENT METHOD

The finite element method has proved to be the most powerful tool in the CAD design of electrical machines. It can allow accurate calculation of the flux distribution, flux density, winding inductance, EMF forces and torques, even under conditions of iron saturation. The method can also be applied to the structural and thermal analysis of a machine design.

The finite element method is well documented in the literature [Lowther and Silvester 1986], [Hamdi 1994]. In this method, the field problem is subdivided into a number of *finite elements* or a *mesh*. The magnetic potential distribution of the field within each element is approximated by a polynomial with unknown coefficients. A numerical solution to the field problem is then

obtained with respect to some optimal criterion [Hamdi 1994]. The finite element analysis is the solution of the set of equations for the unknown coefficients. Principal element types in two-dimensional analysis are triangle or quadrilateral, while tetrahedron elements are used in three-dimensional analysis. Element types are defined in terms of the element shape and the order of the polynomial interpolation. An element contains a number of *nodes*, where the number is related to the type of the element.

In 2D, the problem is subdivided into triangles defined by three vertices (nodes), taking care that the sides of the triangles coincide with material boundaries. The accuracy of the solution depends upon the nature of the field and the size of the mesh elements. In regions where the direction or magnitude of the field is changing rapidly, high accuracy requires small elements or high polynomial orders (or a combination of both). After the solution has been obtained, the flux density can be extracted, and eddy current losses in the workpiece and winding are calculated. The Maxwell stress method is used in this analysis. The magnetic field analysis in this thesis has been performed using the commercial MagNet software package [MagNet7.4 2014].

To reduce computational time, a two dimensional (2D) model of the heater was created instead of a three dimensional (3D) model.

4.2.1 FEA Study of the Experimental Induction Heater

The FEA study was applied for the set of induction heaters presented in Chapter 2. The design of the heaters has been modelled with triangular elements. Figures 4.1 and 4.2 show a half-model of the cross-section of workpiece 1, and the finite element mesh of the heater of workpiece 1. The mesh is refined in the region where the flux-density is expected to be high; where there is rapid spatial variation of the field. In this model, the area of most importance is the workpiece, and as such, it is important that meshing refinements be made in this to ensure that there are enough small elements to model the skin depth properly.

In this model, the mesh also extends outside the workpiece, to include any fringing fields that leak outside when the workpiece is heavily saturated. The coil is represented by a simple geometrical rectangular shape, that represents the exact cross-section of the coil. The total flux-linkage is the sum of the flux-linkages of all the individual loops of wire.

Each coil was modelled as a block of solid copper that covers all turns of that coil. The insulation between the coil and the workpiece was modelled as air.

The mild steel workpiece was modelled as a single block of isotropic linear material with a relative permeability of 750 and a resistivity of 16 Ωm $\times$ 10^{-8}. These values were used in Chapters 2 and 3.

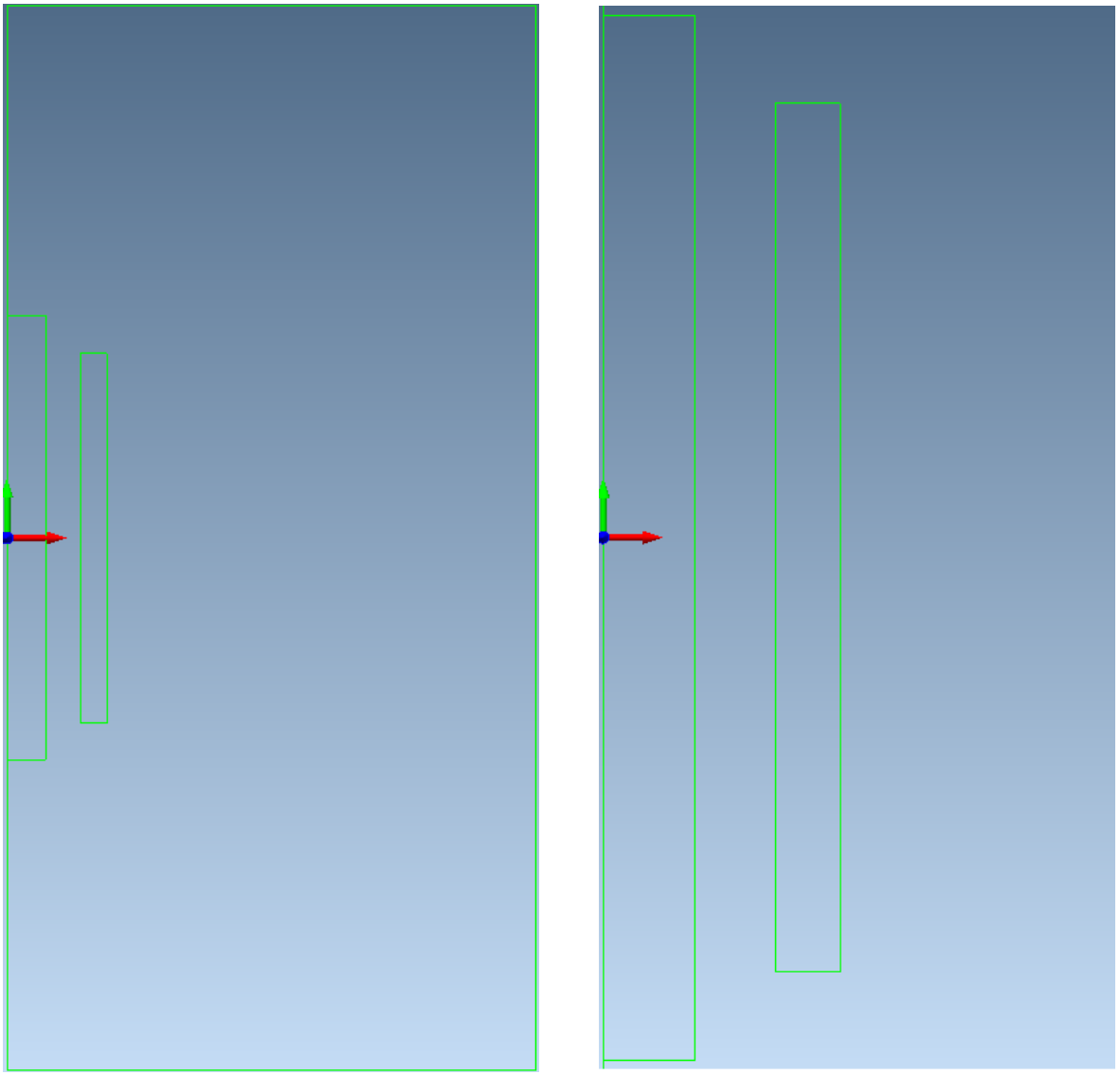

(a) General view (b) Enlarged view

Figure 4.1: Cross-section of workpiece 1.

A MagNet model was made from the geometry to which the materials, boundary conditions and excitations were assigned. The B-H curve data of the core material to be used was created in MagNet for this analysis using the material data sheet. The first task in creating a model is to draw the geometry of the designed heater. After this, the components of the heater can be made from the geometry and the material properties (including magnetic permeability, electric conductivity and mass density) created from the material information. The coil is created and then its properties are assigned. These properties include the number of turns, supply voltage and type of coil used, solid or stranded coils. The next step is to add a boundary condition that surrounds the model to take into account the fringing fields. This is followed by customisation of the mesh elements. The model is then solved by choosing the solver and adaption options. The

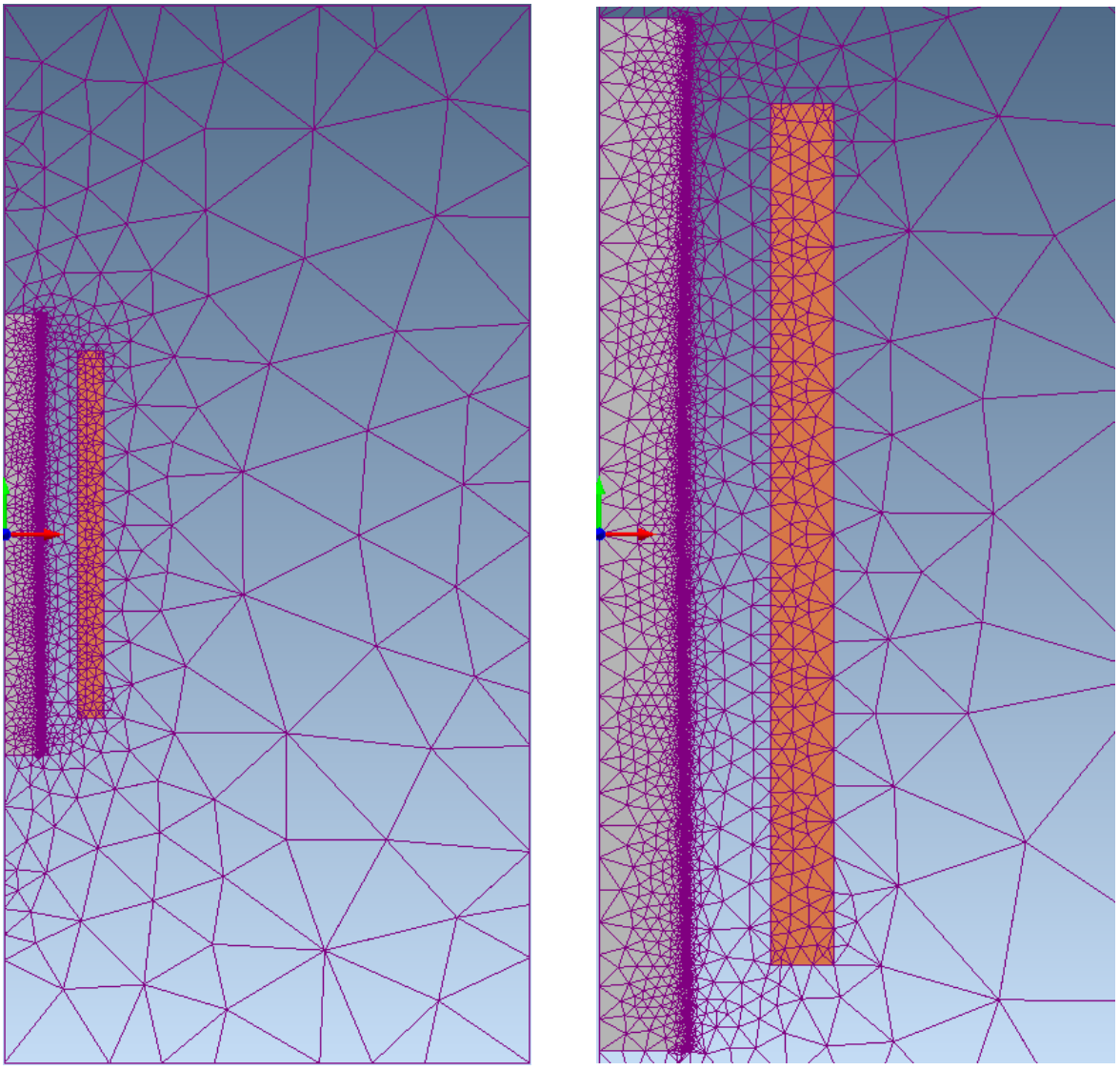

(a) General view (b) Enlarged view

Figure 4.2: Finite element mesh of experimental induction heater of workpiece 1.

solver used for this analysis is *Time-harmonic* as the source current is a sinusoidal alternating quantity. Once the model is solved, the field solutions, field animations and graph of global quantities can be viewed.

4.2.2 Flux Plot of the Experimental Induction Heater

Having created the dimensions and properties of the workpiece and coil in MagNet, the field plots and numerical results of the heater are then obtained using FEA. The resulting workpiece and coil dimensions formed the starting point in the design evaluation. The final design is achieved through the iterative process of performance calculations using the finite element analysis. The

material properties of the mild steel workpiece used for the experimental heater depicted in Chapter 2 are repeated here in Table 4.1. The dimensions of the workpieces are given in Chapter 2. They all have the same lengths, but different diameters and thicknesses. These experimental workpieces were used with the same induction coil presented in Chapter 2.

Table 4.1: Physical properties of copper and mild steel

Material	Copper	Mild steel
Resistivity (Ωm $\times$ 10^{-8})	1.72	16
Relative permeability	1	750
Skin depth at 50Hz (mm)	9.3	1.0

A half-model of the flux plot of the heater of experiment 1 is shown in Figure 4.3. The coil is energized with 100V supply. The maximum flux density in the workpiece is 1.7T. A small amount of fringing can be seen at both ends of the workpiece. Most of the flux lines pass through about 1mm at the surface of the workpiece, i.e., the skin depth for mild steel is about 1mm. Saturation is mainly in the skin depth of the workpiece.

4.2.3 FEA Performance Calculation

Table 4.2 shows the performance of the experimental heater at 100V supply, calculated using FEA. All the maximum flux densities are at the assumed knee point of the B-H curve. The coil current and coil losses are, in general lower than those calculated using the SEC and TEC models in Chapters 2 and 3 respectively. The workpiece losses and power factors are also lower than those calculated from the SEC and TEC models. The calculated coil losses and workpiece losses decrease as the diameter of the workpiece increases. This pattern shows up in the TEC model calculations, but not so with the coil and workpiece losses in the SEC model.

Table 4.2: Calculated performance using FEA model

Workpiece	Voltage (V)	Current (A)	Flux density (T)	Coil loss (W)	Workpiece loss (W)	Apparent power (VA)	Power factor
1	100	2.3	1.7	8.6	55.5	230	0.3
2	100	2.3	1.7	8.4	55.4	230	0.3
3	100	2.3	1.7	8.6	55.9	230	0.3
4	100	2.1	1.7	7.1	49.4	210	0.3
5	100	1.9	1.7	6.1	42.0	190	0.3
6	100	1.5	1.7	3.9	28.0	150	0.3
7	100	1.5	1.7	3.5	26.2	150	0.3

The FEA has been used to determine the workpiece losses, and winding losses and can, therefore, be used to predict the performance of the experimental heater more precisely. The FEA has

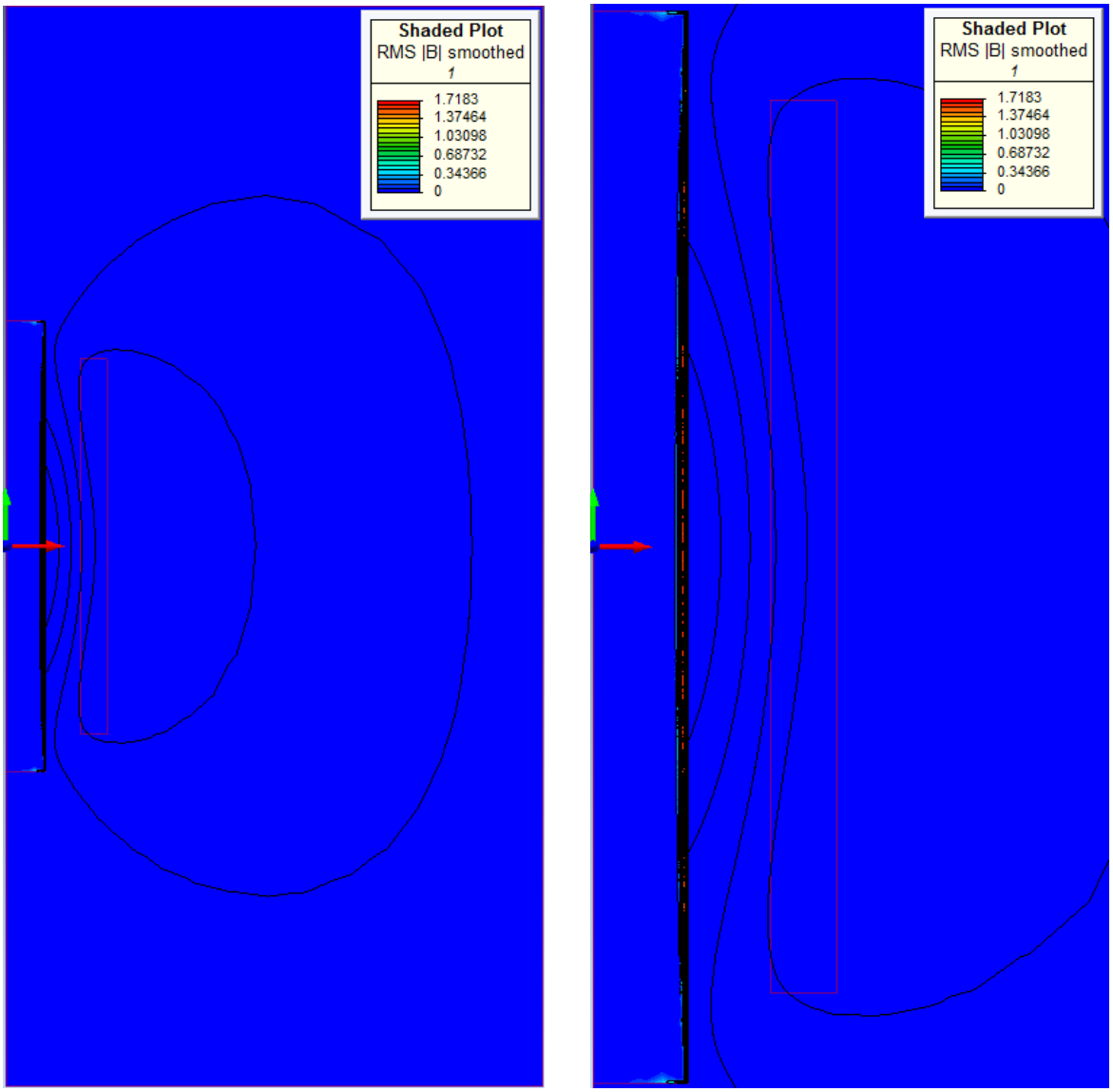

(a) General view (b) Enlarged view

Figure 4.3: Flux plot of experimental induction heater of workpiece 1.

shown that the experimental heater performs as expected, however, it is now needed to compare the performance of the real heater to check the actual performance.

4.3 MEASURED PERFORMANCE OF EXPERIMENTAL INDUCTION HEATER

In this section, the measured performances of the experimental induction heater are presented.

The test set-up consisted of a variac, power meter, current clamp and a multimeter, with a thermocouple to monitor the temperature of the workpiece. The variac was increased from 50V to 100V in steps of 10V while the measurements were taken. Measured results included current,

real power, apparent power and power factor.

The measured performances of the experimental induction heater are given in Table 4.3. The ambient temperature during the test was between 20°C to 25°C.

Table 4.3: Measured performance of experimental induction heater

Workpiece	Voltage (V)	Current (A)	Coil loss (W)	Workpiece loss (W)	Apparent power (VA)	Power factor
1	100	1.9	7.8	84.2	199	0.5
2	100	1.6	5.5	62.5	167	0.4
3	100	1.6	5.5	62.5	170	0.4
4	100	1.9	7.8	91.2	196	0.5
5	100	1.7	6.2	81.8	174	0.5
6	100	1.1	2.6	48.4	117	0.4
7	100	1.0	2.2	46.9	109	0.5

The flux density cannot be measured. The coil loss is calculated using the measured coil resistance and the measured current. The workpiece loss is then calculated by subtracting the coil loss from the measured real power.

The measured currents are lower than those calculated by any of the three models. The measured coil losses are close to those calculated from the FEA and SEC models, but quite dissimilar to those from the TEC model because of the current differences.

The workpiece losses are between those calculated using the FEA and TEC models, and much less than those calculated by the SEC model. This is due to the higher curent calculated from the SEC model. A maximum deviation of -72.5% for workpiece 1 and workpiece 4 was observed whereas for workpiece 7, the deviation increases to -84.6% as a higher current was measured.

The power factors are close to those from the FEA and TEC models and slightly less than those from the SEC model. However, both the SEC and TEC models yield performance measures significantly different from those measured and need refinement to improve their performance predictions.

With respect to the FEA model, the ratios of the measured power of the mild steel workpiece and the measured coil resistance that were calculated using the FEA is determined. These results are given in Table 4.4 for different workpieces.

A constant factor of 1.3 is observed for the coil ratio and about 2.4 for the workpiece, for all the mild steel workpiece experiments. The constant factor of 1.3 was expected as the coil has the same cross-sectional area for the experiments and the FEA. The 2.4 constant factor varied between 2.1 and 2.5 for all the workpieces as they all have different diameters and thicknesses.

Table 4.4: Ratio of coil and workpiece loss

Workpiece	Measured coil loss/ FEA coil loss	Measured workpiece loss/ FEA workpiece loss
1	1.3	2.3
2	1.3	2.5
3	1.3	2.5
4	1.3	2.3
5	1.3	2.6
6	1.3	2.2
7	1.3	2.1

The calculation of resistance in MagNet assumes that the stranded area is the coil components cross-sectional area divided by its number of strands, i.e. a space factor of about 100%. The coil cross-sectional area is modelled as a rectangular block in FEA as compared to it being a circle in the experimental model. The ratio of the area is

$$\begin{aligned} Ratio &= \frac{c^2}{\pi(c^2/4)} \\ &= 1.27 \\ &\approx 1.3 \end{aligned} \tag{4.1}$$

where c is the diameter and length of the rectangular block respectively. Thus the factor of 1.3 reflects this ratio of cross-sectional areas or a space factor of 0.79.

4.3.1 Analysis

The Finite Element Analysis yields results much closer to those measured than either the SEC or TEC models and is preferred, at least for the case presented. However, such modelling relies on proprietary software which may be more difficult to access, making it less amenable for teaching purposes.

The SEC and TEC models give very disparate results for this design. The SEC model does not accommodate workpiece saturation, while the TEC model can allow for this. Even so, the TEC model results, while much closer to the measured values for the workpieces tested, are still significantly higher than the measured values.

These differences may be explained in part by the materials having different physical characteristics than the generic values chosen, but also the applicability of using lumped circuit equivalents

of open core devices.

The SEC and TEC models are seen to be useful closed form analytical expressions which can easily be programmed using readily available advanced calculators or spreadsheet software. However, their accuracies are such that they yield design guides only, rather than definitive performance results. The TEC model is refined in Chapter 5 to improve its performance predictions.

4.4 SUMMARY

This chapter discussed the FEA of a 2D model of the experimental induction heater. The FEA has been used to determine the flux pattern, workpiece losses, and winding losses and can, therefore, be used to predict the performance of the experimental heater more precisely. A maximum flux density of 1.7T in the workpiece is saturating the core.

The measured performances for seven experimental induction heater workpieces are also discussed. The measured performances were used to validate the results obtained from the FEA, SEC and TEC models. The measured performances correlated well with the FEA only after using correction factors 1.3 and 2.4 for coil and workpiece losses respectively. Using a corrected FEA model, the design FEA model would give values close to the experimental results.

Chapter 5

TRANSFORMER AND TRANSDUCTION HEATING

5.1 INTRODUCTION

In Chapter 3, an induction heater was modelled as a special type of transformer, where the coil surrounded the workpiece to be heated. The workpiece acted as the core of the transformer and got hot because of the eddy currents flowing through it. In this chapter, an equivalent circuit to model the performance of a transformer heater is presented. It is then converted to an equivalent circuit to model the performance of transduction heaters, a combination of transformer and induction heaters. Transduction heaters have not been (and cannot be) modelled using the SEC approach.

Finite element analysis was also used in conjunction with the TEC model to simulate a set of transduction heating experiments and the results are compared. Analysis of the TEC calculated results suggested modification of three parameters: the secondary resistance, the core tube eddy current resistance and the core tube magnetizing reactance. The improved TEC model was then used to design, build and test a 6kW transduction heater. The measured results are compared with calculated results from the TEC and FEA models.

5.2 TRANSFORMER HEATER

It is possible to design a transformer directly as a heater. This is often used to provide hot fluids. The typical arrangement is to have a primary winding that does not produce much heat, a laminated core that also does not produce much heat, but a shorted secondary winding that produces most of the heat. The arrangement is shown in Figure 5.1, where the secondary winding is outside the primary. This allows for ease of access to the fluid.

By making the secondary conductor hollow, or by adding a fluid channel to the back of its conductor as is done to cool induction heater coils, the real power losses in the secondary can be transferred by convection to the fluid, thus heating it up. The secondary tube requires fluid inlet

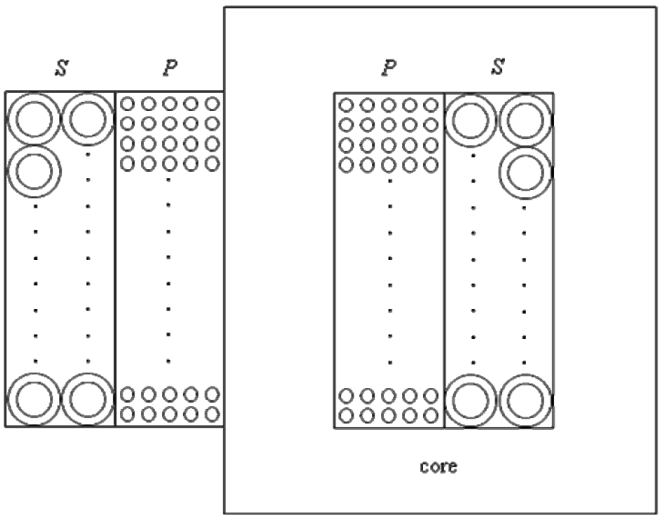

Figure 5.1: Transformer heater physical arrangement.

and outlet connections, and a plug to separate the inlet and outlet fluid but provide electrical conductivity between the two. The coupled electrical circuit of Figure 5.2 shows a shorted secondary winding.

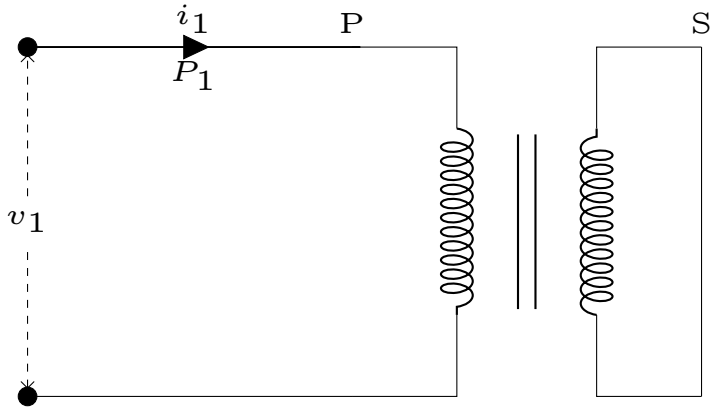

Figure 5.2: Coupled circuit representation.

5.3 EQUIVALENT CIRCUIT OF TRANSFORMER HEATER

The equivalent circuit of a shorted turn transformer heater is shown in Figure 5.3. This is the same model as that presented for the transformer model of an induction heater in Chapter 3. However, because the transformer heater has a full core, some of the parameters represent different components of the heater.

The primary winding resistance is R_1 and the secondary winding resistance is R_2. The latter is an

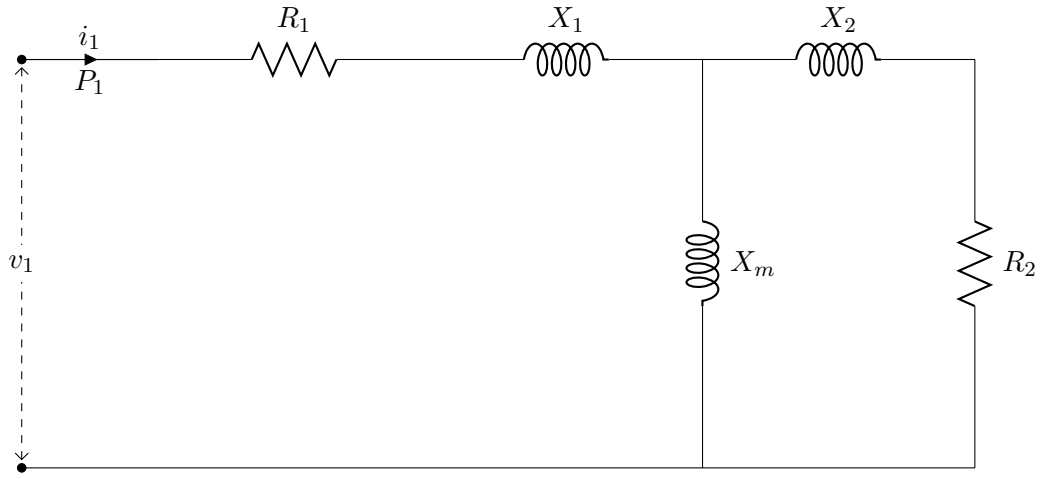

Figure 5.3: Transformer heater equivalent circuit.

average value as the tube temperature will vary, linearly, along its length as the fluid temperature increases from inlet to outlet. X_m represents the magnetizing reactance. The leakage reactance, representing the leakage flux of each winding, can be split between the primary and secondary as X_1 and X_2.

With respect to the core, the eddy current and hysteresis losses would normally be accounted for in a transformer within a resistance R_c across X_m. However, for a transformer heater, where the secondary losses dominate, these losses can be considered insignificant and may be ignored unless more accurate modeling is considered necessary. Hence the core loss resistance R_c is not explicitly included in the model.

The parameters making up the model can be calculated using the basic dimensions and characteristics of the materials used, as per the reverse design method. These are entered as know data and then the individual components calculated using magnetic and electric circuit component models.

A cross-sectional profile of a multi-layer winding transformer with a full core is shown in Figure 5.4. All the symbols represent dimensions of the materials used in the construction of the transformer heater, including the core, insulation and the windings.

5.3.1 Winding Resistances

The primary winding resistance is

$$R_1 = \frac{\rho_{1w} l_{1w}}{A_{1w}} \tag{5.1}$$

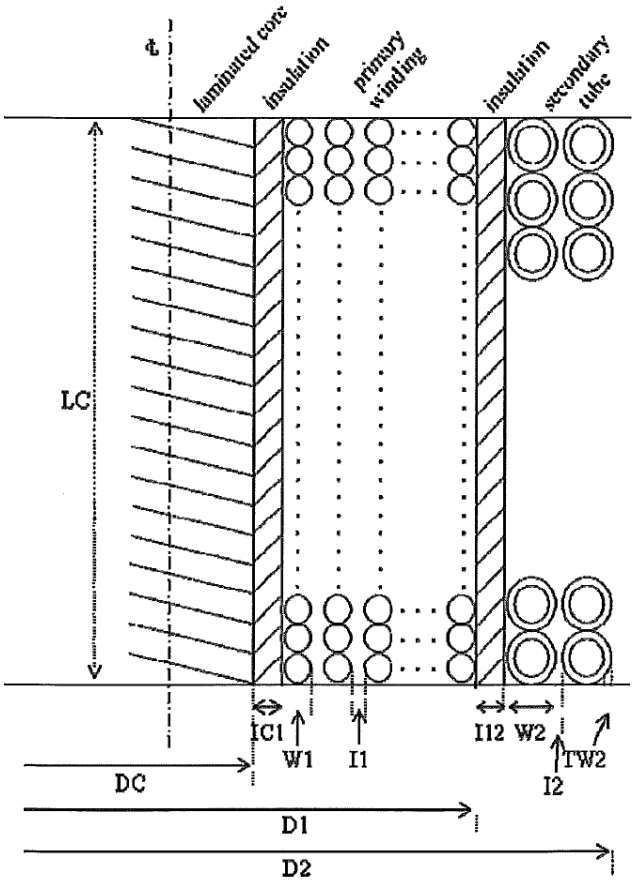

Figure 5.4: Cross-section of a multi-layer winding transformer heater with a full core.

where ρ_{1w} is the resistivity of the primary winding conductor, l_{1w} is the length of the primary winding conductor and A_{1w} is the cross-sectional area of the primary winding conductor.

The secondary winding resistance referred to the primary winding is

$$R_2 = \frac{\rho_{2w} l_{2w}}{A_{2w}} a^2 \tag{5.2}$$

where ρ_{2w} is the resistivity of the secondary winding conductor or tube, l_{2w} is the length of the secondary winding conductor or tube, A_{2w} is the cross-sectional area of the secondary winding conductor and a is the primary to secondary turns ratio.

5.3.2 Magnetizing Reactance

For a full-core transformer, where the magnetic flux flows around a closed core, the magnetizing current reactance is

$$X_m = \frac{\omega N_1^2 \mu_0 \mu_{rc} A_c}{l_c} \tag{5.3}$$

where ω is the angular frequency, N_1 is the number of turns on the primary coil, μ_0 is the permeability of free space, and μ_{rc} is the coil permeability of the magnetic flux path. A_c is the effective cross-sectional area of the coil, calculated using the skin depth δ_c, and l_c is the coil length.

5.3.3 Leakage Reactance

The primary and secondary winding leakage reactances of a transformer are calculated from the total leakage reactance which embodies the effects of both windings together. The leakage reactances X_1 and X_2 are calculated from

$$X_1 = X_2 = \frac{\omega \mu_0 N_1^2 \pi \tau_{12}}{2 l_c} \tag{5.4}$$

where τ_{12} is the winding thickness factor, as described in Chapter 3: Transformer Model of Induction Heater, with subscripts 1 and 2 substituted for c and w.

Having obtained the component values, the equivalent circuit can be solved to calculate the performance of the device.

5.4 TRANSDUCTION HEATING

Transformer heater can be combined with an induction heater to form a transduction heater. In this section, the development of transduction heating concepts from the basic induction heating and transformer heating concepts is presented. The performance of the transduction heater is modeled using the improved TEC model. A 6kW transduction heater is designed and verified using the improved TEC and FEA models is also presented in this section.

5.4.1 Basic Heating Concepts

Heating fluid using induction heating can be achieved by passing the fluid through a hollow ferromagnetic workpiece as shown in Figure 5.5.

The removal of the centre of a workpiece in Figure 5.5 has little effect on the magnetics and hence the current drawn from the supply, as long as the thickness of the tube is greater than the skin depth of the magnetic field and hence the steel is not in saturation.

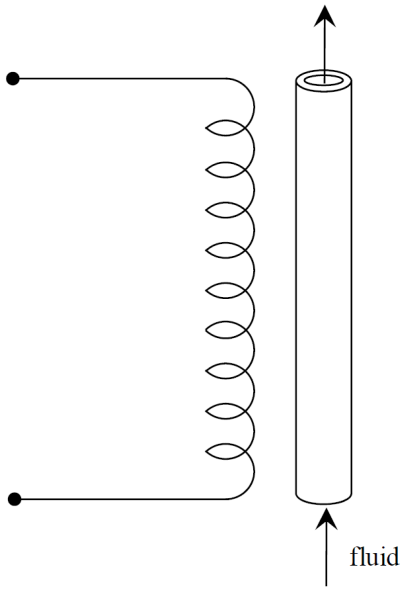

Figure 5.5: Conceptual arrangement of induction fluid heater.

Alternatively, the heating can be achieved by passing the fluid over the workpiece, on the outside, or between two tubes of different diameters such that they form a jacket through which the fluid flows.

An alternative to induction heating of fluids is transformer heating, as shown in Figure 5.6. The fluid gains heat as it passes through the hollow tube of the shorted secondary, or through a cooling channel adhered to the back of a solid conductor.

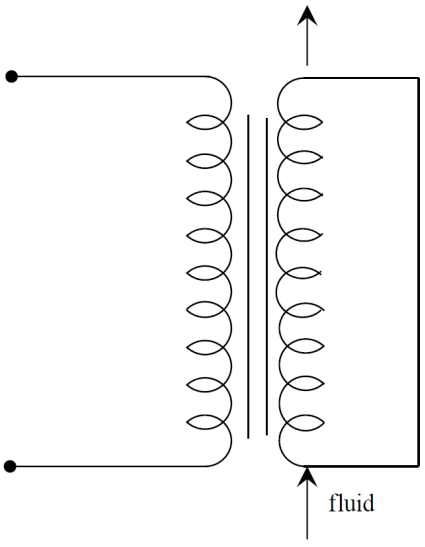

Figure 5.6: Conceptual arrangement of transformer fluid heater.

The technologies of a transformer heater and an induction heater can be combined as illustrated in Figure 5.7.

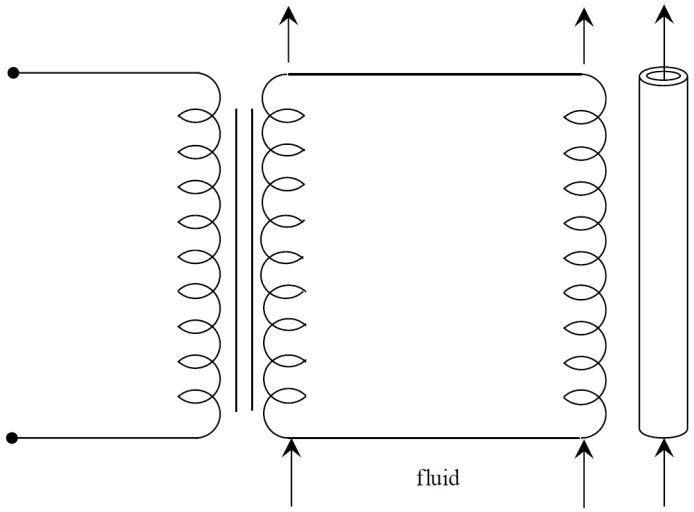

Figure 5.7: Conceptual arrangement of combined transformer heater and induction fluid heater.

This shows the coil of the induction heater is connected to the secondary winding of the transformer. Depending on the physical design and voltage and current ratings, the secondary, coil and the workpiece can all be used to heat the fluid.

An alternative concept is to combine these technologies to form a single device, the transduction fluid heater as shown in Figure 5.8. The conceptual arrangement is a modification of an early commercial manifestation of such a device, the "Transflux" heater [Bodger *et al.* 1996].

The arrangement has a primary winding that does not produce much heat, a core tube that produces heat, and a shorted secondary winding that produces most of the heat. By making the secondary conductor hollow, or by adding a fluid channel to the back of its conductor, the real power losses in the secondary tube can be transferred by convection to the fluid, thus heating it up.

5.5 TRANSDUCTION HEATER

A manifestation of the conceptual design of Figure 5.8 can be achieved by placing a highly conductive tube (such as copper or aluminium) on the outside of the core tube and passing the fluid through the core tube. If a suitable size tube is not available, such a conductor can be rolled from sheet metal and bonded to the core tube. In this case the secondary is effectively a short circuited single turn. This does not alter the characteristics of the heater and the same equivalent circuit can be used to evaluate the performance of the heater.

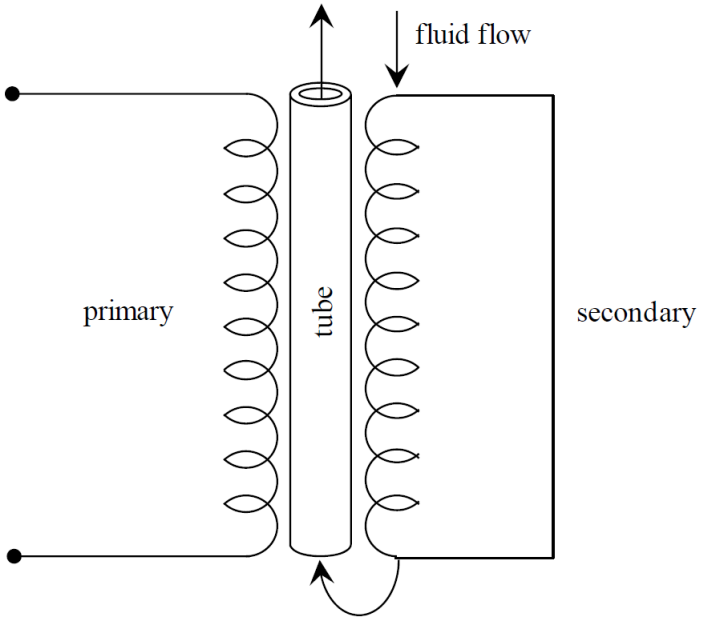

Figure 5.8: Conceptual arrangement of transduction fluid heater.

One option is for the fluid to make a single pass up through the centre of the workpiece. Thus the heat from the secondary and the workpiece tubes conducts radially inwards to the fluid. However, since the primary winding is electrically and hence thermally insulated from the core and the secondary tubes, not much of the heat generated in the primary winding is captured by the fluid. Most of this heat is radiated and convected outwards to ambient surroundings.

Alternatively, the fluid can be passed between the core and secondary tubes, and the primary winding former. This helps capture some of the primary winding heat. However, again some heat goes to the ambient surroundings. Thus the transduction fluid heater is less than 100% efficient. While the natural cooling of the primary winding by the ambient surroundings may be sufficient for continuous operation, some form of forced cooling may be required if higher temperatures are involved.

A cut-away image of the transduction heater, where the fluid passes between the bonded secondary and core tubes and the primary winding former, is shown in Figure 5.9.

Stainless steel liners inside the primary winding former and outside (or instead of) the secondary winding, allow heating of corrosive fluids, or fluids where non-contamination is critical, without significantly affecting the electrical to thermal performance of the device. This is because the relative permeability of stainless steel is effectively unity and the depth of penetration of the magnetic field is large allowing the magnetic fields essentially to pass straight through and into the ferromagnetic workpiece.

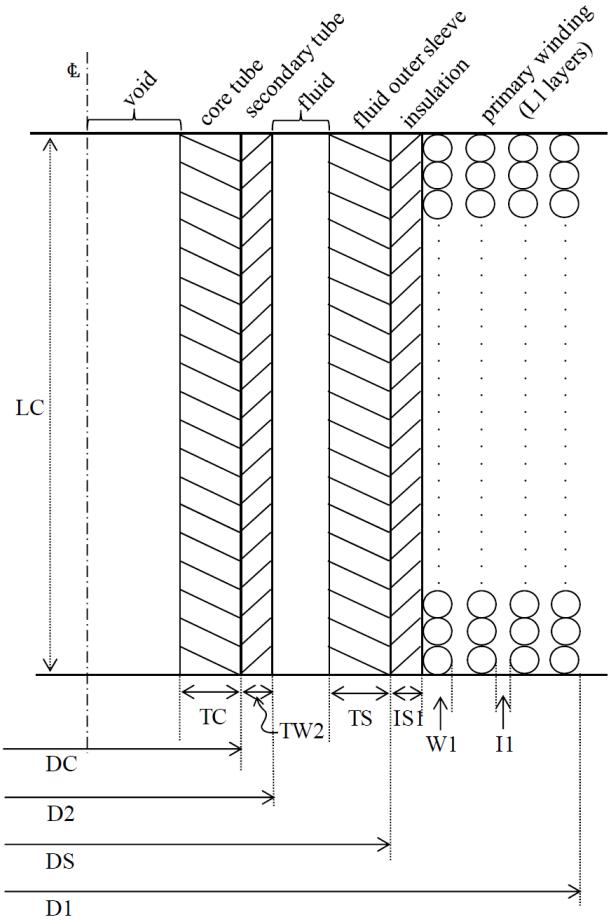

Figure 5.9: Cut-away image of transduction fluid heater.

Because of the strength of the materials involved and the robustness of the manufacture, with this technology, relatively high fluid pressures and temperatures can be achieved.

Laminated steel placed inside the core tube improves the power factor of this device if the core tube steel is in saturation. This can also help counter the decreased power factor due to the increased spacing between the primary and the secondary windings, because of the stainless steel insertions and the fluid channel.

5.6 MEASURED PERFORMANCE OF EXPERIMENTAL TRANSDUCTION HEATER

A coil of a small transduction heater was constructed with the following parameter dimensions as shown in Table 5.1. This is the same coil that was used for the induction heating experiments in Chapters 2, 3 and 4 respectively.

A number of mild steel, stainless steel, aluminium, and copper tubes of various diameters and thicknesses were cut to provide workpieces and secondary tubes that fitted inside the coil. The

Table 5.1: Coil dimensions

Material	Copper	Units
Resistivity	1.72×10^{-8}	Ωm
Length	208	mm
Outside diameter	114	mm
Inside diameter	83	mm
Wire diameter	1.7	mm
Wire area	2.27	mm^2
Number of layers	9	-
Turns per layer	111	-
Number of turns	999	-
Length of wire	309	m
Calculated resistance	2.34	Ω
Measured resistance (50Hz)	2.15	Ω

dimensions of these are listed in Table 5.2.

Table 5.2: Workpiece and secondary tube dimensions

Workpiece	Material	Length (mm)	Diameter (mm)	Thickness (mm)
1	Mild steel	250	44.3	solid
2	Mild steel	250	44.5	12.6
3	Mild steel	250	44.2	6.3
4	Stainless steel	250	50.8	1.2
5	Aluminium	250	50.8	1.3
6	Copper	250	62.0	0.8
7	Mild steel	250	70.0	2.0
8	Mild steel	250	73.0	solid
9	Aluminium	250	76.0	1.25

Various combinations of the tubes were assembled inside the coil. Figure 5.10 shows a photograph of the transduction heater with a combination of tubes (2+5) inside the coil.

The test set-up and measurement method is the same as presented for the induction heating experiments in Chapter 4. By applying a 100V supply to the coil, the performances of different tube combinations are given in Table 5.3. These values were used as a benchmark to compare calculated performance values against.

5.7 EQUIVALENT CIRCUIT OF TRANSDUCTION HEATER

The transduction heater can be modelled as a transformer with a single shorted turn secondary winding, and the core tube as a partial core of a transformer [Liew and Bodger 2001]. The core tube has the function of acting like the core of a transformer, but it is incomplete in that the

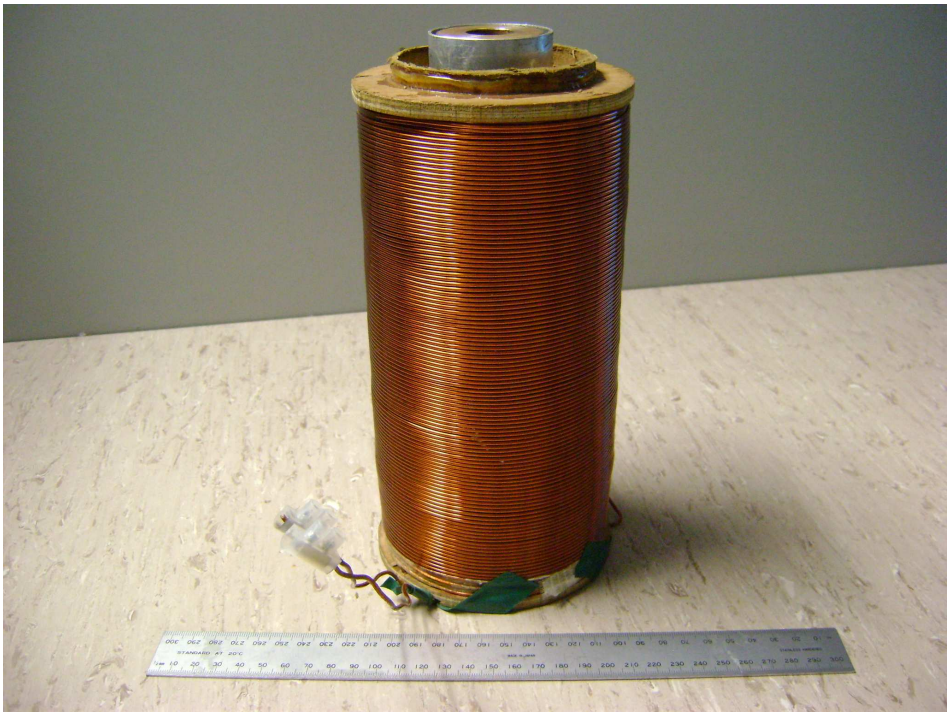

Figure 5.10: Transduction heater with combination of tubes (2+5).

Table 5.3: Measured performance at 100V supply

Workpiece label	Voltage (V)	Current (A)	Real power (W)	Apparent power (VA)	Power factor
1 +4	100	2.4	110	239	0.46
2 + 5	100	5.1	370	470	0.78
3 + 6	100	5.2	410	490	0.82
3 + 9	100	4.0	320	380	0.83
7 + 9	100	3.8	320	370	0.87
8 + 9	100	3.8	320	370	0.88

return path of the magnetic flux is through the ambient medium. The equivalent circuit that is used to model the transduction heater is shown in Figure 5.11.

where R_1, R_2 are the primary and secondary resistances, X_{mc}, is the core tube magnetizing reactance, R_{ce} is the core tube eddy current resistance, and X_1, X_2 are the primary and secondary leakage reactances. Hysteresis losses, usually the dominant part of core losses in a transformer, are ignored in this model as they are insignificant compared to the eddy current losses.

The parameters of the equivalent circuit in Figure 5.11 are calculated using the basic dimensions and physical characteristics of materials used, as per the reverse design method [Liew and Bodger 2001], [Bodger and Liew 2002]. These are entered as known data and then the individual circuit components are calculated using magnetic and electric circuit component models.

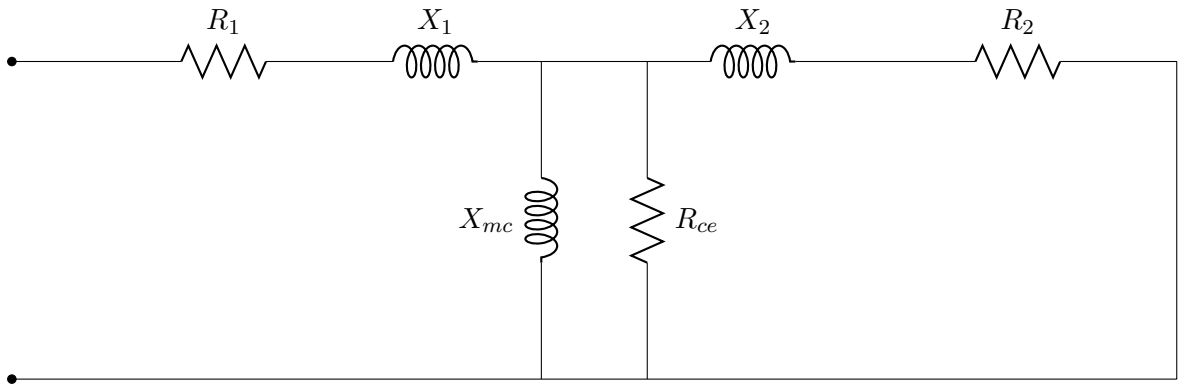

Figure 5.11: Equivalent circuit of transduction heater.

5.7.1 Winding Resistance

The primary winding resistance is given by

$$R_1 = \frac{\rho_{1w} l_{1w}}{A_{1w}} \tag{5.5}$$

where ρ_{1w} is the resistivity of the primary winding conductor, l_{1w} is the length and A_{1w} is the cross-sectional area of the primary winding conductor.

The secondary winding resistance referred to the primary winding is

$$R_2 = \frac{\rho_{2w} l_{2w}}{A_{2w}} a^2 \tag{5.6}$$

where ρ_{2w} is the resistivity of the secondary winding conductor or tube, l_{2w} is the length of the secondary tube, A_{2w} is the cross-sectional area of the secondary winding conductor and a is the primary to secondary turns ratio.

The variation of resistivity with temperature of the conductor materials are accounted for. In general, the operating resistivity of a material is

$$\rho_c = (1 + (\Delta\rho(T_c - 20)))\rho_{20^\circ C} \tag{5.7}$$

where $\rho_{20^\circ C}$ is the resistivity at 20°C, T_c is the material temperature, and $\Delta\rho$ is the thermal resistivity coefficient.

5.7.2 Magnetizing Reactance

The magnetizing current reactance is

$$X_{mc} = \frac{\omega N_1^2 \mu_0 \mu_{rce} A_c}{l_c} \tag{5.8}$$

where, N_1 is the number of turns on the primary coil, A_c is the effective cross-sectional area of the core tube, calculated using the depth of penetration, δ_c, and l_c is the flux path length. Also, μ_{rce} is the effective value based on the composite air/iron magnetic flux path, as for the transformer model of an induction heater [Takau and Bodger 2013].

If the magnetic flux density in the core tube exceeds the saturation value, the relative permeability reduces, forcing the flux skin depth to increase and the density to reduce. If the calculated skin depth is greater than the thickness of the core tube, then the flux flows through both the core tube metal and inside fluid space. This is also modelled as for the transformer model of an induction heater [Takau and Bodger 2013].

5.7.3 Core Tube Eddy Current Resistance

In this model the eddy current losses in the core tube are accounted for by the resistance R_{ce} across X_{mc}. Thus R_{ce} is calculated from

$$R_{ce} = \frac{N_1^2 \rho_c l_{ce}}{A_{ce}} \tag{5.9}$$

where ρ_c is the core tube resistivity, l_{ce} is the length of the eddy current path around the core tube, and A_{ce} is the cross-sectional area of the eddy current path, the product of l_c and δ_c. Again, the variation of resistivity with temperature of the conductor material is accounted for.

5.7.4 Leakage Reactance

The primary and secondary leakage reactances of a transformer are calculated from the total leakage reactance which embodies the effects of both windings together. The leakage reactances X_1 and X_2 are calculated from

$$X_1 = X_2 = \frac{\omega \mu_0 N_1^2 \pi \tau_{12}}{2 l_c} \tag{5.10}$$

where τ_{12} is the winding thickness factor, related to the thickness of the primary winding and the secondary tube [Takau and Bodger 2013].

5.8 EQUIVALENT CIRCUIT PERFORMANCE

The equivalent circuit of the transduction heater can be solved to calculate the performance of the device. The physical characteristics of the copper, stainless steel, aluminium and mild steel tubes were taken as given in Table 5.4.

Table 5.4: Physical properties

Material	Copper	Mild steel	Stainless steel	Aluminium
Resistivity (Ωm $\times$ 10^{-8})	1.72	16	70	2.65
Relative permeability	1	750	1	1
Skin depth at 50Hz(mm)	9.3	2.5	60	11.6
Density (kg/m^3)	8960	7870	8000	2700

The same combinations of tubes as assembled for the measurements were used and the parameters of the equivalent circuits calculated from their material characteristics and dimensions. The performance of the heater was calculated by solving the equivalent circuit equations and determining the current, power and power factor for a given applied voltage. The equivalent circuit also allowed separation of the real power losses into individual component values. In addition, as required, efficiencies, voltage gradients, voltages per turn and current densities can be calculated. The calculated results are given in Table 5.5.

Table 5.5: Calculated performance using TEC model for a 100V supply

Workpiece	Voltage (V)	Current (A)	Primary loss (W)	Secondary loss (W)	Core loss (W)	Real power (W)	Apparent power (VA)	Power factor
1 + 4	100	3.9	36.7	18.1	165.3	220.1	398.0	0.55
2 + 5	100	7.6	135.2	313.1	109.2	557.5	765.0	0.73
3 + 6	100	7.2	118.8	308.9	133.8	561.5	717.0	0.78
3 + 9	100	6.9	111.1	310.3	157.3	578.7	693.0	0.83
7 + 9	100	5.8	77.4	337.9	64.2	479.5	579.0	0.83
8 + 9	100	5.7	75.8	339.4	59.1	474.3	573.0	0.83

In general, the calculated real powers are significantly higher than those measured. This is reflected in the higher current values and apparent power. This suggested that the overall calculated impedance was low compared to the measured value. However, the power factors were similar.

Within the detail of the calculated results, one specific anomaly is that the losses in the core tube are significantly higher than those in the secondary tube for the (1+4) combination. However

for the rest of the combinations, the losses in the secondary tube are significantly higher than those in the core tube. Also, the primary winding losses are significantly lower compared to the secondary tube losses for all the combinations except for (1+4). This anomaly may be due to an incorrect assumed resistivity of the stainless steel.

Analysis of the TEC calculated results in comparison to the measured values suggested empirical modification of the parameters to bring the equivalent circuit into alignment. The inclusion of scaling factors has been successfully applied in similar related work [Lapthorn and Bodger 2009], [Bell and Bodger 2007].

The secondary resistance R_2, the core tube eddy current resistance R_{ce}, and the core tube magnetizing reactance X_{mc} were all scaled by a factor of 1.8. The secondary resistance R_2 is modified as the magnetic coupling between the primary and the secondary is not perfect and the actual value is not replicated by using the turns ratio. Similarly, the core tube resistance R_{ce} is modified. The magnetizing reactance X_{mc} is modified because the calculation used for partial cores assumes a laminated core and not a core tube. More accurate models based on fundamental relationships are not available at this time. The remaining parameters R_1, X_1, and X_2 are left unchanged. The calculated value of the primary resistance R_1 was close to the measured value so it was not modified. The leakage reactances X_1, and X_2 are left unchanged as the magnetic flux is through the ambient medium and therefore not affected by the core tube.

Table 5.6 lists the calculated performances using the TEC model with the scale factor applied. The current, primary winding loss, secondary winding loss, core loss, and apparent power are significantly lower than those in Table 5.5. The power factors have, slightly, increased.

Table 5.6: Calculated performance using TEC model at 100V supply with scale factor applied

Workpiece	Voltage (V)	Current (A)	Primary loss (W)	Secondary loss (W)	Core loss (W)	Real power (W)	Apparent power (VA)	Power factor
1 + 4	100	2.4	13.7	12.1	101.1	135.9	243.0	0.56
2 + 5	100	5.1	59.6	266.0	86.5	412.1	507.0	0.81
3 + 6	100	4.5	47.6	232.0	98.0	377.6	454.0	0.83
3 + 9	100	4.3	41.7	213.0	107.0	361.7	425.0	0.85
7 + 9	100	3.5	27.9	225.0	42.4	295.3	348.0	0.85
8 + 9	100	3.4	27.3	225.0	39.0	291.3	344.0	0.85

The calculated results are now much closer to the measured values of Table 5.3.

5.9 FEA PERFORMANCE CALCULATION

MagNet software was used to create a 2D FEA model of the actual heater. Figures 5.12 and 5.13 show examples of the flux plots for the workpiece combinations of (1+4) and (2+5). The

coil is energised with a 100V supply. The maximum flux density in the workpiece is 1.7T. A small amount of fringing can be seen at both ends of the workpiece for the combination of (2+5). Most of the flux is confined to the region near the surface of the mild steel workpiece. There is very little field in the interior of the workpiece as the radius is several times greater than the skin depth of the workpiece.

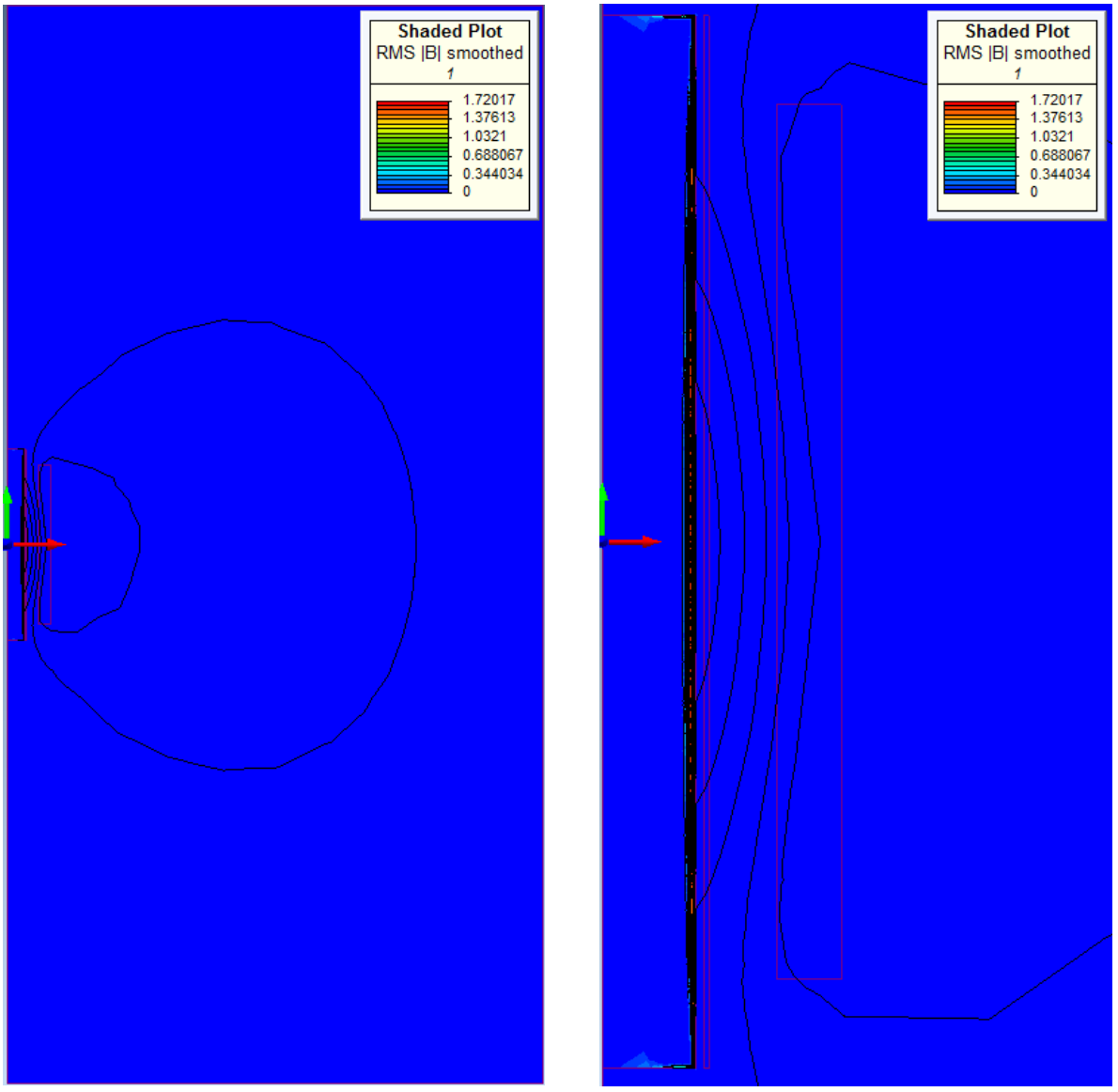

(a) General view (b) Enlarged view

Figure 5.12: Flux plot of workpiece combination (1+4).

Table 5.7 shows the performance of the experimental heater at a 100V supply voltage, calculated using FEA. All the workpiece maximum flux densities are at the assumed knee point of the B-H curve. The primary losses are, in general, lower than those given in Table 5.6 except for the (3+6) combination. The coil current and power factors are close to those given in Table 5.6.

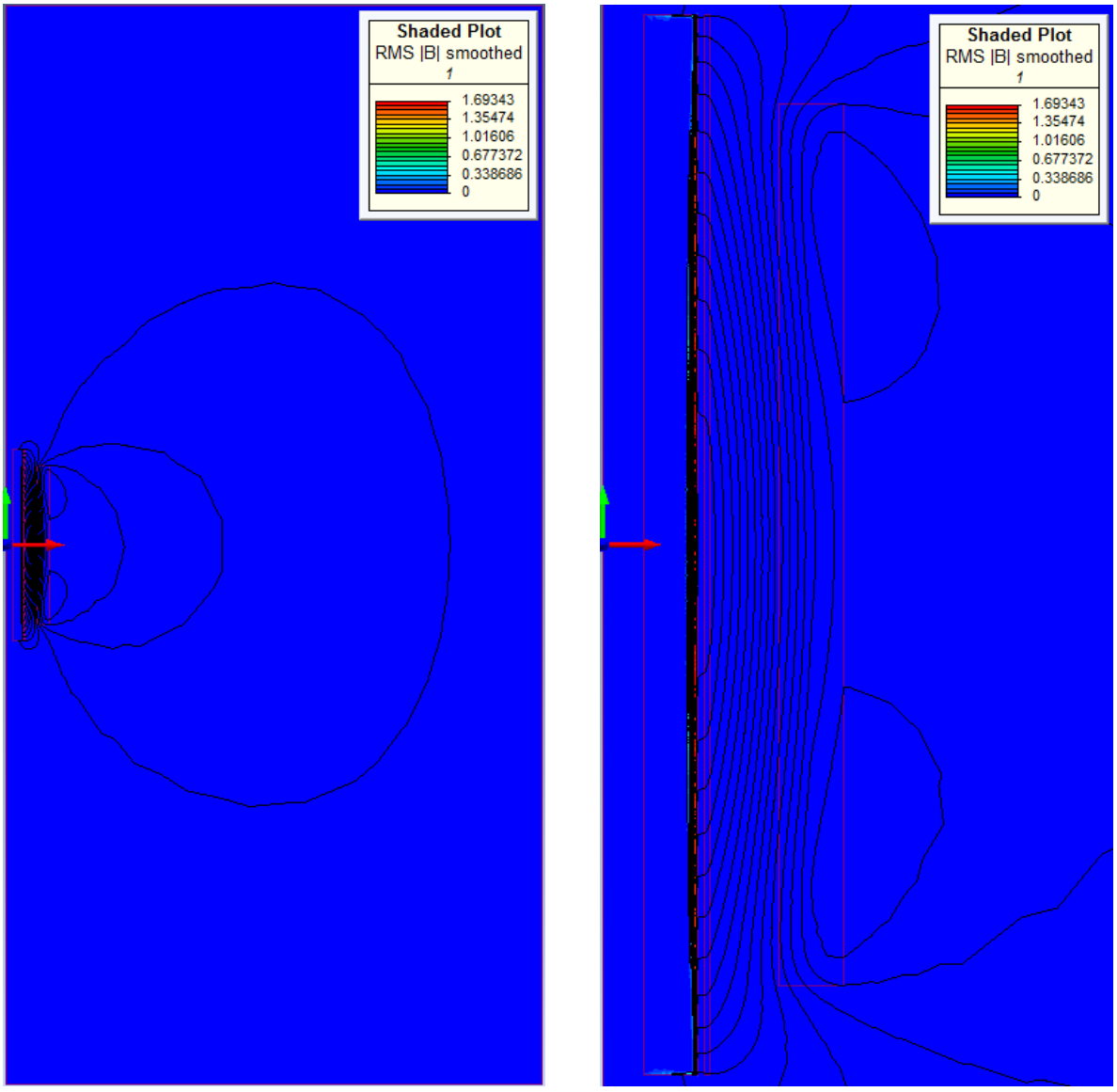

(a) General view (b) Enlarged view

Figure 5.13: Flux plot of workpiece combination (2+5).

Table 5.7: Calculated performance using FEA at a 100V supply

Workpiece	Voltage (V)	Current (A)	Primary loss (W)	Secondary loss (W)	Core loss (W)	Real power (W)	Apparent power (VA)	Power factor
1 + 4	100	2.3	8.6	19.9	55.0	83.5	230.0	0.36
2 + 5	100	5.1	43.1	303.8	36.3	383.2	510.0	0.75
3 + 6	100	5.7	53.8	362.3	36.5	452.6	570.0	0.79
3 + 9	100	3.9	25.8	241.3	48.1	315.2	390.0	0.81
7 + 9	100	3.5	20.7	262.4	23.4	306.5	350.0	0.88
8 + 9	100	3.5	20.3	264.6	22.1	307.0	350.0	0.88

The FEA model yields results significantly higher than those measured for workpiece combinations of (2+5) and (3+6) and lower for the rest of the combinations in terms of the power losses. The TEC model yields results significantly higher than those measured for the workpiece combinations of (1+4), (2+5) and (3+9). However, the rest of the combinations are close to the measured values.

5.10 DESIGN OF A 6KW TRANSDUCTION HEATER

The improved performance prediction of the TEC model was used to design a 6kW transduction heater. The calculated performance of the designed heater was compared with FEA calculations and experimental results. The coil and workpiece dimensions of the designed heater are given in Tables 5.8 and 5.9. The measured resistance of the coil is very close to the calculated value from the TEC model as shown in Table 5.8.

Table 5.8: Coil dimensions

Material	Copper	Units
Resistivity	1.72×10^{-8}	Ωm
Length	420	mm
Outside diameter	114	mm
Inside diameter	83	mm
Wire diameter	3.4	mm
Wire area	9.08	mm^2
Number of layers	7	-
Turns per layer	140	-
Number of turns	980	-
Length of wire	289	m
Calculated resistance	0.55	Ω
Measured resistance (50Hz)	0.54	Ω

Table 5.9: Workpiece dimensions

Workpiece	Length (mm)	Diameter (mm)	Thickness (mm)
Mild steel core tube	500	60.0	4.6
Secondary copper tube	500	62.6	1.3

Figure 5.14 shows the designed heater with the mild steel and secondary copper tubes inside the coil. The physical properties of the mild steel and copper tubes are given in Table 5.9.

The various components of the TEC circuit are given in Table 5.10. The equivalent circuit parameters show that the primary winding resistance is lower compared to the secondary resistance, and there are lower leakage reactances, since the primary winding and secondary tube thickness is smaller.

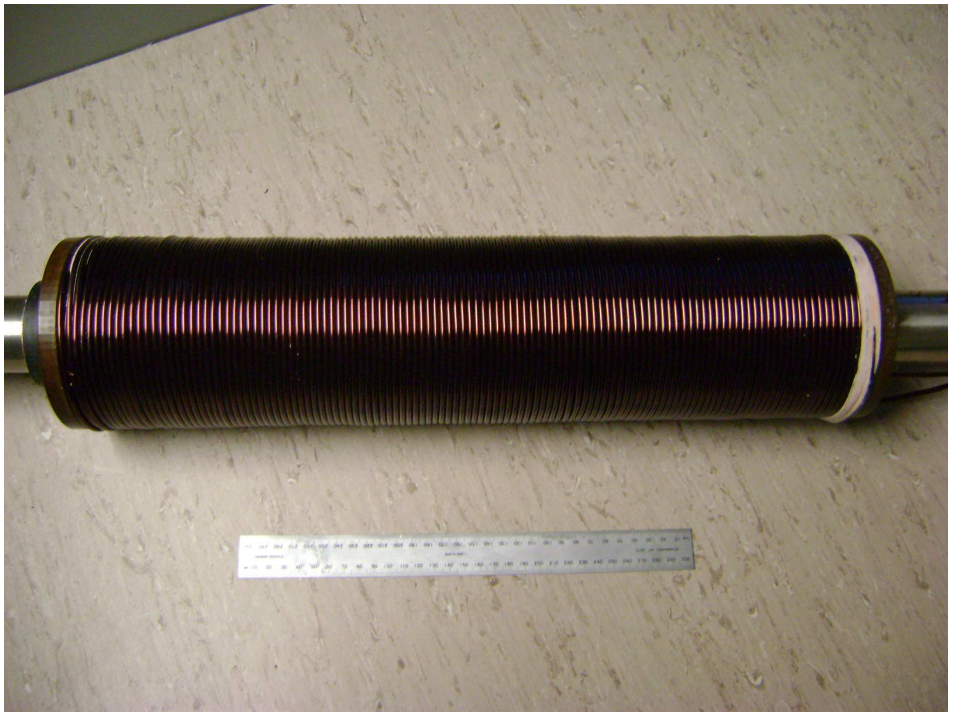

Figure 5.14: 6kW transduction fluid heater.

Table 5.10: Component values for the TEC model

Circuit component	Value (Ω)
R_1	0.55
R_2	8.74
X_1	1.24
X_2	1.24
X_{mc}	35.8
R_{ce}	27.8

The calculated results of the transduction heater using the TEC and FEA models are given in Table 5.11, along with the measured performance.

Table 5.11: Calculated and measured results of the designed transduction heater

	TEC	FEA	Measured
Voltage (V)	230	230	230
Current (A)	30.9	43.9	31.0
Apparent power (kVA)	7.13	10.1	7.13
Real power (kW)	6.5	8.4	6.3
Power factor	0.91	0.83	0.91

The calculated results from the TEC match the measured results well, reinforcing the usefulness of the TEC model to predict the performance of transduction heaters. The calculated results from the FEA model show significantly higher values in terms of the current, apparent power,

and real power compared to the results from the TEC. However, the power factor is significantly lower than the TEC and measured results. Because of the higher current calculated from FEA, the rest of the measured parameters are all affected as well. This may be due to how FEA calculates the resistance from the geometry of the coil and inductance from Maxwell's equations and also the material properties created in MagNet for the calculation.

Other performance measures can be determined by calculation from the TEC program but cannot be measured on an actual transduction heater. These are given in Table 5.12.

Table 5.12: TEC calculated performance

Parameter	Value
VT1-primary voltage/turn	0.23V
V2-secondary eddy voltage	0.20V
VA-primary/secondary voltage ratio	1123.7
VE-core tube eddy voltage	0.20V
A1-primary winding current area	$9.08\times10^{-6}\text{m}^2$
J1-primary winding current density	3.41A/mm^2
I2-secondary tube current	22.3kA
A2-secondary tube current area	$6.5\times10^{-4}\text{m}^2$
J2-secondary tube current density	34.3A/mm^2
ICE-core tube eddy current	7.1kA
ACE-core tube eddy current area	$1.75\times10^{-3}\text{m}^2$

The voltage per turn on the primary is very low and no extra insulation is required. The currents in the secondary and core tubes are very large in comparison to the primary current, but they can be directly cooled by the water or the liquid that is going to be heated, so their current densities are acceptable. The primary current density is 3.41A/mm^2 which is at a level that natural cooling of the coil (primary winding) would be sufficient. The tolerable current density J1 in a conductor depends mainly on its cooling. For no forced or artificial cooling, J1 = $1-4\text{A/mm}^2$, varying from large to small conductors respectively.

5.11 SUMMARY

This chapter presented the modelling of transduction heaters using TEC and FEA models. The performances of the transduction heaters from these models were compared to the measured performances of an experimental heater for a variety of sizes of mild steel, copper, aluminium and stainless steel tubes. The calculated performances of the TEC model showed significantly lower values in terms of the current and workpiece losses compared to the FEA model. The TEC model was improved by applying an empirically derived scale factor to selected components to give much closer values to those measured.

The improved TEC model was then used to design a new transduction heater. The calculated

and measured performances were very close. The TEC model gave a better prediction than the FEA model, suggesting that the TEC model can be a useful tool to design transduction heaters.

The research will now move to the design of an industrially useful device, which will be presented in Chapter 6.

Chapter 6

DESIGN OF AN INDUSTRIAL TRANSDUCTION FLUID HEATER

6.1 INTRODUCTION

This chapter presents the design and construction of a three phase 40kW transduction fluid heater. The three phase heater is obtained by connecting three single phase units in an appropriate star configuration, with the fluid tubes connected in series.

A generic definition of transduction heating is explained, as derived from the co-joining of transformer and induction heating. The transduction heater design description and considerations such as winding dimensions and layout are then discussed. Details of the construction of the transduction fluid heater are also given. This includes discussion of the core tube and secondary tube design, thermal insulation, inter-layer insulation, the primary winding construction, and also the cooling method used.

The chapter concludes with details of the physical specifications used in the design program and the equivalent circuit parameters given as an output of the TEC program. The magnetic field patterns of the designed transduction fluid heater are determined using FEA. The calculated results obtained from these two models are discussed and compared.

6.2 TRANSFORMERS

A single phase power transformer is a device which has a primary and a secondary winding wound about a core. When a voltage is applied to the primary winding of a transformer, a magnetic field is generated in the core. This couples to and produces an emf in the secondary winding. Power, and hence energy, is transferred from an ac system of one voltage connected to the primary winding, to an ac voltage of another system connected to the secondary winding.

The power transformer is normally designed for high efficiency (of the order of $98-99\%$). The windings are usually made of copper, an inexpensive, low resistivity material, to give low power

losses, although other materials are used. The power losses are approximately equal in the primary and secondary windings. A ferromagnetic core is used, again achieving low losses.

The core material is usually laminated into high resistance paths to reduce eddy current power losses and to provide a uniform flux density. The material is chosen to have little hysteresis heating. Its high permeability implies very little magnetization current.

6.3 INDUCTION HEATERS

An induction heater can be viewed as a special type of transformer where the primary winding is placed about the material to be heated. The power losses, and hence heating, due to eddy currents induced in the material, are encouraged. The core material, referred to as the workpiece or billet, is usually solid. The efficiency of an induction heater is usually not as high as that for a transformer heater.

The extent of the heating is determined by the material resistivity, its magnetic permeability and the frequency of the excitation source. These factors are combined into a depth of penetration or skin depth of the flux and current in the material. Significant heating in the billet or workpiece is usually found in the first $1.5-2$ skin depths. For copper at 50Hz, the skin depth is approximately 10mm. For mild steel it is about 2.5mm. Material inside the skin depth relies on conduction heat flow from this region.

6.4 TRANSDUCTION HEATER DESIGN

Transduction heating is a combination of transformer and induction heating. It is an induction heater that includes a secondary winding to boost performance. Both induction and transformer heaters use the fundamental principles of magnetic fields as the power transfer medium from the supply to the material to be heated. Thus, there is an electric-magnetic-electric-heat series of energy conversion.

The easiest way to design the transduction fluid heater is by the selection of the sizes and shapes of the components that can be procured and which start with the core tube and work outwards. The material characteristics are thus estimated and dimensions measured, and entered as known data. Individual circuit components are then calculated using magnetic circuit and electric circuit component models and assembled into an equivalent circuit. The performance of the heater is calculated from this equivalent circuit and is therefore a result of the design. This is called the reverse design method [Liew and Bodger 2001], [Bodger and Liew 2002]. This design method takes into account the physical characteristics, such as material resistivities, permeabilities, and

the dimensions of the windings and the core as specifications. By altering these specifications, the performance of the device can be optimized and a suitable design obtained.

6.5 DESIGN DESCRIPTION

The TEC model accurately predicted the performance of the 6kW transduction heater designed in [Takau and Bodger 2014]. The research is now moved to the design of an industrially useful device, that is, the design of a nominal 40kW transduction fluid heater that can be used to heat fluids (water or food). For example, in the pasteurization of milk, the milk has to be heated up to 85°C from 4°C and then is cooled to 4°C again. The response rate of the heater must be very fast in order to ensure proper treatment of the milk. In the case of long life milk, it is necessary to heat the milk to a temperature of 140°C and then cool it again [MilkFacts 2014], [ScientificAmerican 2014]. The heater of this thesis has been designed with such requirements in mind.

6.5.1 Design Consideration

The performance of the 6kW transduction heater designed in [Takau and Bodger 2014] was predicted well using both the TEC model and the FEA software. The new design includes some of the design materials used in this original heater. These include the composite tubes for the core tube and the secondary tube. The new materials that are added include grooved fiberglass sheets for insulation between the layers of the primary winding, vegetable oil for cooling the primary winding, a stainless steel baffle outside the primary winding, to allow heat from the winding to flow to a heat exchanger outside the baffle with flowing water, and a stainless steel tube for the housing. The size and length of the primary winding conductor was also changed for the new design.

A detailed cross-section of the new transduction fluid heater is shown in Figure 6.1. To measure the thermal performance of the heater, thermocouples are placed at different locations to monitor the temperature rise of the primary winding, the oil, and the cooling water and fluid inlets and outlets. The new design can be used as a water heater or as a fluid heater for other than water, depending on the applications.

To use the device as a water heater, the water outlet can be connected to the product inlet using a pipe or a hose. In this variation, the heat generated in the primary, core tube and the secondary tube could all be used to heat the water. Hence, a higher efficiency is expected in this design. For other than water, the efficiency is less than 100%, as the heat generated in the primary will be lost to the cooling water. However, by careful design, these winding losses can

be minimized sufficiently to provide high overall device efficiency. In addition, the heated water could be used in some secondary process.

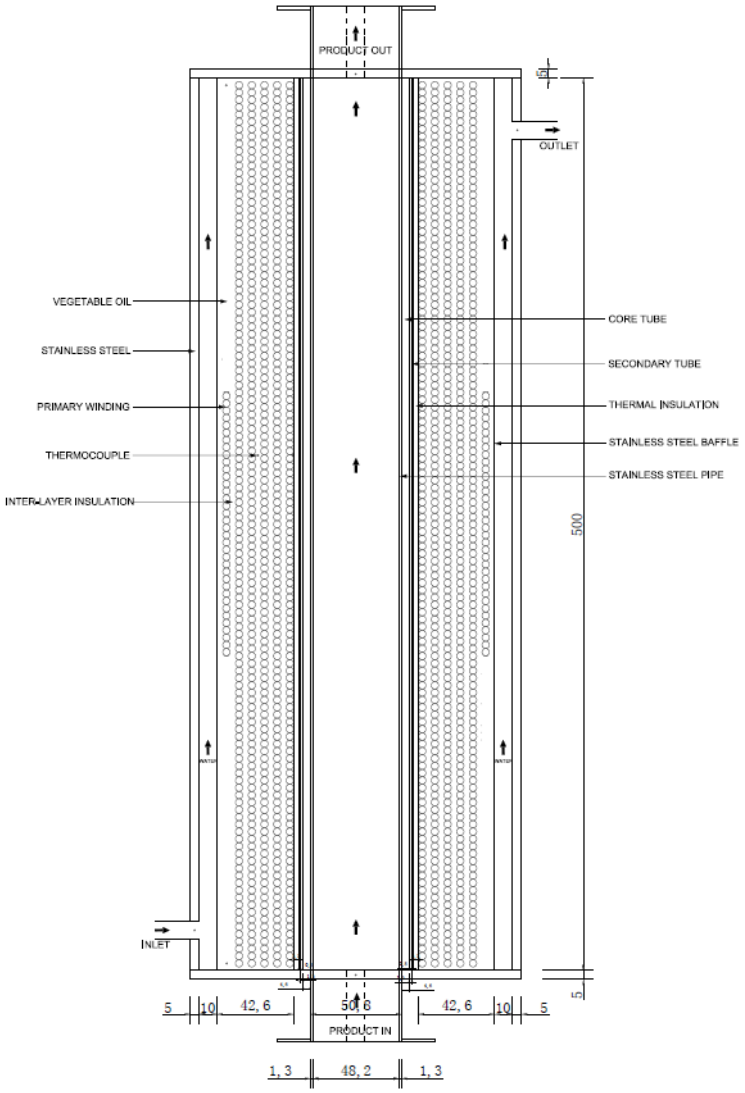

Figure 6.1: Cross-section details of transduction fluid heater.

6.6 CONSTRUCTION DETAILS

The construction of the designed heater used some of the same design components as for the 6kW transduction heater [Takau and Bodger 2014].

6.6.1 Core Tube

The core tube is a sleeve of ferromagnetic mild steel inside the secondary tube. The core tube has the function of acting like the core of a transformer. However, it is incomplete in that the return path of the magnetic flux is through the ambient medium. The core tube also acts as a billet of an induction heater and gets hot due to eddy current flow inside it.

The fluid which is desired to be heated passes inside a stainless steel tube that is inside the core tube. This stainless steel tube is essentially the workpiece in induction heating terminology, however, there are no eddy currents induced in this stainless steel tube as the magnetic flux does not penetrate into it. Thus, it is not part of the transduction heater, but rather a material to be heated indirectly by heat transfer from the transduction heater.

The stainless steel tube pipe selected such that there is a good physical contact between the workpiece and the core tube, so that heat generated in the transduction heater is conducted to the workpiece. Any fluid flowing in the stainless steel tube will make surface contact so that the heat generated is transferred by convection into the fluid.

The length and diameter of the workpiece are selected as what is required. For the core tube, the length is generally set to the same length as the workpiece to give uniform heat transfer to the workpiece. The thickness of the core tube is selected so that it is about 2 skin depths. Thus there is no significant magnetic field penetration inside this tube and hence into the workpiece. The dimensions of the core tube are listed in Table 6.1. The thickness of the core tube was that readily available from a manufacturer.

Table 6.1: Core tube dimensions

Parameter	Dimension	Units
Core length	500	mm
Outside diameter	60	mm
Thickness	4.6	mm
Resistivity	1.72×10^{-8}	Ωm
Relative permeability	750	-
Skin depth at 50Hz	1.0	mm
Material density	7870	kg/m^3

6.6.2 Secondary Tube

On the outside of the core tube is the secondary tube. This is selected (or machined) to fit neatly over the core tube so that they are also in physical contact. Significant heat is generated in the secondary tube. This heat is conducted through the core tube and transferred to the workpiece. The thickness of the secondary tube is much less than the depth of penetration of the magnetic

field in the material at mains frequency. Thus a uniform current density in the secondary tube can be assumed. Also most of the magnetic field penetrates through to the core tube.

The length of the secondary tube is again most likely to be equal to the length of the core tube, for uniform heat transfer to the core tube. The designer specifies the length, thickness, permeability and resistivity of the secondary tube.

The secondary tube is constructed from a non-ferromagnetic copper tube. The dimensions of the secondary tube are listed in Table 6.2. Figure 6.2 shows a photograph of the core tube and secondary tube outside the stainless steel pipe.

Table 6.2: Secondary tube dimensions

Parameter	Dimension	Units
Secondary tube length	500	mm
Outside diameter	62.6	mm
Thickness	1.3	mm
Resistivity	1.72×10^{-8}	Ωm
Relative permeability	1	-
Skin depth at 50Hz	9.3	mm
Material density	8960	kg/m^3

Figure 6.2: The core and secondary tubes over the workpiece.

6.6.3 Thermal Insulation

To restrict the heat going outwards, it is necessary to thermally insulate the composite of the secondary and core tubes. The quality and thickness of the thermal insulation (or former) between the secondary tube and the primary winding is selected based on thermal considerations. This space has neither electric nor magnetic field effects but the thickness does affect the coupling and hence the leakage flux, and the calculation of parameters associated with the metallic components of the device.

The thermal insulation composite tube in this project is made with 50/50 cross weave fiberglass. It is recommended that the thermal insulation can withstand the glow-wire and needle flame tests of IEC 60695-2-11. The glow-wire test is not carried out on parts of thermal insulation classified as having a flammability index of 850°C. The thermal insulation also acts as reinforced insulation between the primary winding and the secondary tube. The dimensions of the thermal insulation are given in Table 6.3 and a photograph is shown in Figure 6.3.

Table 6.3: Thermal insulation dimensions

Parameter	Dimension	Units
Length	500	mm
Outside diameter	72.9	mm
Thickness	4.6	mm
Material density	1181	kg/m^3

Figure 6.3: Thermal insulation composite tube.

6.6.4 Primary Winding

For the primary winding, its length is typically the same length as the secondary and the core tube. A conductor diameter, its insulation, and the number of layers are selected. The material will have relative permeability and resistivity properties.

A primary winding was constructed with the parameters and dimensions shown in Table 6.4. The 5.3 layers were wound over the former (or thermal insulation) with the last half layer wound on the center as shown in Figure 6.1. This ensured symmetrical flux distribution along the heater.

Relative to the 6kW transduction heater, the number of turns in the primary winding has changed, and the wire length is slightly greater as the former for the winding is a larger diameter than the core tube on which it was previously wound.

Table 6.4: Primary winding dimensions

Material	Copper	Units
Length	500	mm
Outside diameter	152.1	mm
Inside diameter	72.9	mm
Wire diameter	4.0	mm
Wire area	12.6	mm^2
Number of layers	5.3	-
Turns per layer	121	-
Number of turns	641	-
Length of wire	216.6	m
Resistivity	$1.72\times\ 10^{-8}$	Ωm
Calculated resistance	0.297	Ω

6.6.5 Inter-Layer Insulation

To ensure that the heat is dissipated evenly between the layers of windings, an alternative insulation introduced in [Lapthorn *et al.* 2013b] was used. Figure 6.4 shows a photograph of the interlayer insulation design. The insulation consists of 3mm thick, g10 fibreglass. The fibreglass sheets have 3mm wide vertical slots machined into the material every 3mm using a computer aided manufacturing machine. This allows the oil to flow freely between the windings of each layer. The depth of the cuts was 2mm leaving 1mm of the fibresheet. In addition to this, 85mm long slots were cut into the vertical channels with slots on adjacent channels offset, as shown in Figure 6.4. The first layer of winding is wound directly onto the former (thermal insulation) as shown in Figure 6.5(a). Then the second layer of winding is wound on top of the inter-layer insulation and so forth as shown in Figure 6.5(b).

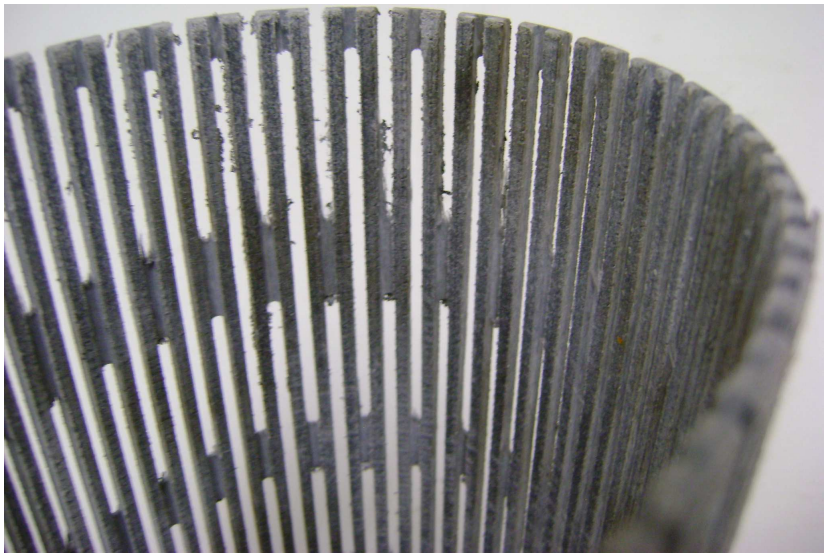

Figure 6.4: Inter-layer insulation.

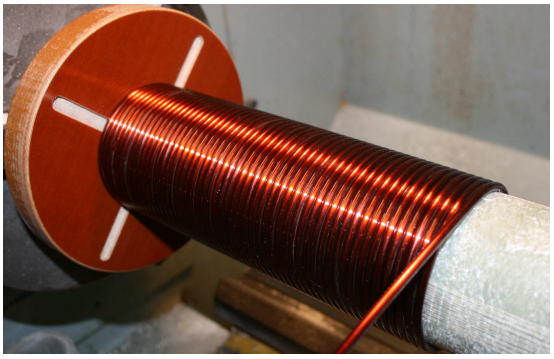

(a) First layer of winding.

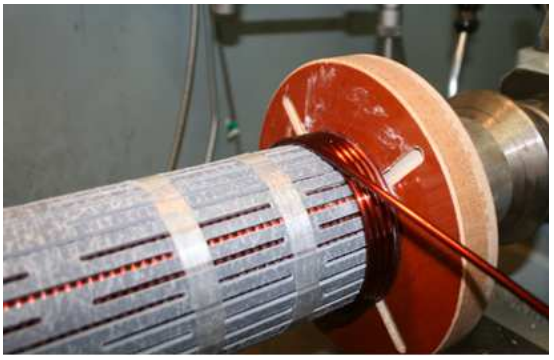

(b) Second layer of winding.

Figure 6.5: Winding layout of 40kW transduction heater.

6.6.6 Baffle

The outside layer of the primary winding has an insulation layer around it. A stainless steel baffle is placed around this to contain the oil and prevent it from leaking to the cooling water. The stainless steel baffle will add some weight to the heater but it will not have much effect magnetically as its relative permeability is unity and its skin depth is very large. The magnetic field will penetrate right through it to the outside of the baffle. There will be some small additional eddy current losses due to induction heating in the stainless steel baffle but since it is water cooled, any heat generated will be captured. The dimensions of the stainless steel baffle are listed in Table 6.5. A photograph of the assembled winding prior to installation of the outer insulation layer is shown in Figure 6.6.

Table 6.5: Stainless steel baffle dimensions

Parameter	Dimension	Units
Length	500	mm
Outside diameter	162.2	mm
Thickness	2.05	mm
Material density	8000	kg/m^3

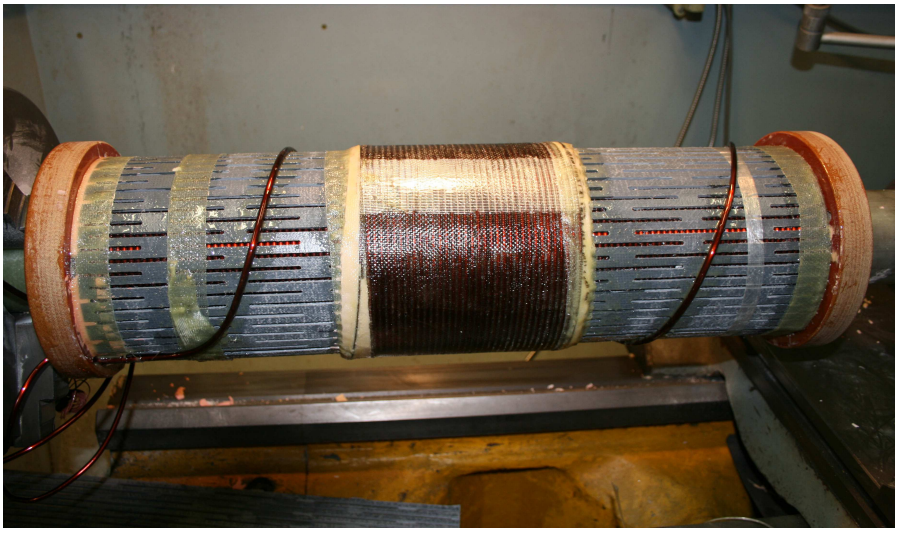

Figure 6.6: Assembled winding without outside insulation baffle.

6.6.7 Transduction Heater Cooling

Continuous operation of the transduction heater would not be possible without significant forced cooling. There are four cooling methods generally used for cooling oil-immersed transformers. They are oil natural air natural (ONAN), oil natural air forced (ONAF), oil directed air forced (ODAF), and oil forced air forced (OFAF). In this design, ODWF or oil directed water forced cooling is used. It is just like ODAF with the difference that the hot oil is cooled by means of forced water instead of air. Both of these transformer cooling methods are called forced directed oil cooling of a transformer. Water is used as it is a better heat exchange medium than air. From Figure 6.1, the water is circulated between the water inlet and the outlet to cool the oil.

In this project, the cooling oil is BIOTEMP transformer oil which is made from renewable and biodegradable vegetable-based oil. In the unlikely event of containment failure and contamination of the fluid (e.g. food stuff) to be heated by this oil, the fluid is contaminated by a biodegradable product. This is better than using mineral oil. This oil also acts as part of the supplementary insulation of the primary winding. BIOTEMP exhibits excellent dielectric characteristics with high temperature stability, and flash and fire resistance of 330°C and 360°C, respectively, compared with 145°C and 160°C for mineral oil. The viscosity (which de-

scribes the oils resistance to flow) for BIOTEMP transformer oil is 10 at 100°C and 40 at 45°C [Biotemp 2014].

6.6.8 Transduction Heater Housing

The transduction heater housing is constructed from a stainless steel tube with thickness of 2.05mm. Inside the internal tube of the water jacket is the stainless steel baffle that prevents the oil from leaking into the cooling water. The cooling water is contained between the internal and external walls of the water jacket. This external stainless steel tube will also add some weight but it will not have much effect magnetically as its relative permeability is unity and its skin depth is very large. Again, the magnetic field will penetrate right through it to the outside of the tube. There will be some additional eddy current losses due to induction heating in the stainless steel tube but since it is water cooled, any heat generated will be captured. A non-metallic enclosure could also be used and would not give any losses, however, a stainless steel enclosure is preferable in food areas.

A photograph of the water jacket used for the housing is shown in Figure 6.7(a). The oil and water inlets can be seen on the left. The fully assembled coil is then inserted inside the water jacket as shown in Figure 6.7(b).

(a) Water jacket. (b) Assembled winding inside water jacket.

Figure 6.7: Transduction heater housing.

6.7 EQUIVALENT CIRCUIT

The equivalent circuit that is used to model the transduction fluid heater is shown in Figure 6.8.

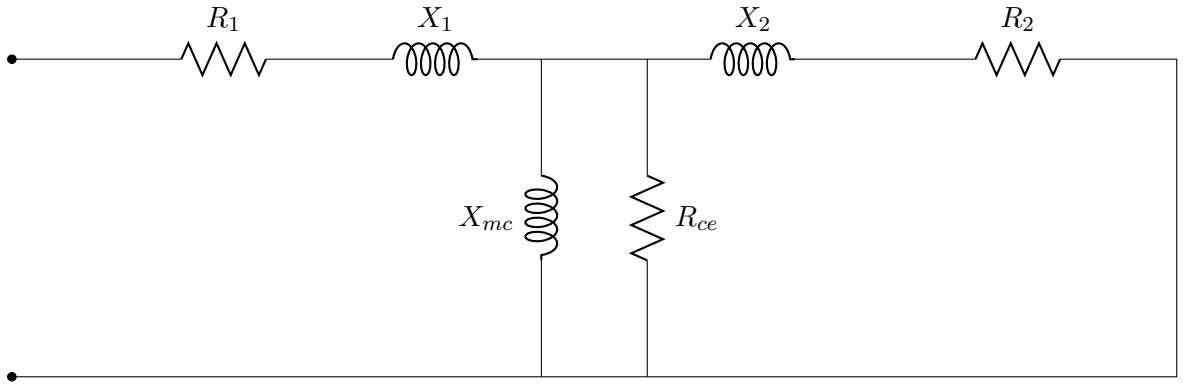

Figure 6.8: Equivalent circuit of transduction heater.

where R_1, R_2 are the primary winding and secondary tube resistances, X_{mc}, is the core tube magnetizing reactance, R_{ce} is the core tube eddy current resistance, and X_1, X_2 are the primary and secondary leakage reactances. Hysteresis losses, usually the dominant part of core losses in a transformer, are ignored in this model as they are insignificant compared to the eddy current losses. The variation of resistivity with temperature of all metal materials should be accounted for, as this may be a high temperature device.

All the equivalent circuit components are calculated using the same formulae as presented in Chapter 5. Also for this design, the fluid is constrained to flow inside the centre of the core tube.

6.7.1 Equivalent Circuit Performance

The physical dimensions and materials used in the design of the heater are given in Tables 6.1, 6.2, 6.3, 6.4. The parameters from these tables were entered into a computer program written using the modeling methods in [Liew and Bodger 2001], [Bodger and Liew 2002]. The program was able to determine the equivalent circuit parameters and performance for the designed heater.

6.7.2 Calculated Performance

The equivalent circuit parameters are listed in Table 6.6. The higher temperatures of the secondary and core tube components in particular have significantly increased the resistances of these components. The magnetizing component has a larger value due to the higher equivalent relative permeability. A mild steel core tube with low relative permeability aids in reducing the

magnetizing reactance and improving the power factor. The leakage reactances are both lower due to the smaller primary winding and secondary tube thickness.

Table 6.6: Equivalent circuit parameters

Circuit component	Value (Ω)
R_1	0.297
R_2	3.772
X_1	0.949
X_2	0.949
X_{mc}	10.622
R_{ce}	8.963

Having calculated the parameters of the equivalent circuit, the performance of the transduction fluid heater is obtained by applying the nominal voltage to the equivalent circuit. The calculated values of the TEC model are given in Table 6.7.

Table 6.7: Equivalent circuit performance

Parameter	Value
V-voltage	230V
I-current	70.1A
S-volt-amperes	16.1kVA
P-real power	12.9kW
PF-power factor	0.80
EFF-efficiency	88.7

The proportion of real power dissipated in the secondary and core tubes is much higher than real power dissipated in the primary and hence the efficiency is high. The real power in the primary winding is about 1.5kW. This is dissipated into the oil and then to the cooling water. The net amount of real power for this design has comes from the secondary tube and the core tube together. Most of the apparent power is real which gives a reasonable power factor of 0.84, much better than that for an induction water heater.

For comparison, without the copper secondary tube, the device is an induction heater. This is essentially an open circuit of the device. At 230V, the supply current was about 27.6A and the power factor was about 0.74.

Without the core tube, the device is a coreless transformer. In this case the magnetizing reactance and the power factor would be very low.

The primary current was 70.1A which gave a current density of 5.6A/mm^2, which was marginal for a multi-layer winding with forced water cooling. These figures would decrease as the temperatures and hence the resistances of the tubes increase.

Other performance measures can be determined by calculation from the TEC program but

cannot be measured on an actual transduction fluid heater. These are given in Table 6.8.

Table 6.8: TEC calculated performance

Parameter	Value
VT1-primary voltage turn	0.36V
V2-secondary eddy voltage	0.28A
VA-primary/secondary voltage ratio	827.45
A1-primary winding current area	1.26×10^{-5} m^2
J1-primary winding current density	5.58A/mm^2
I2-secondary tube current	29.39kA
A2-secondary tube current area	6.50×10^{-4}m^2
J2-secondary tube current density	45.74A/mm^2
ICE-core tube eddy current	12.79kA
ACE-core tube eddy current area	2.3×10^{-3}m^2
JCE-core tube eddy current density	5.54A/mm^2

The currents in the secondary and core tubes are very large in comparison to the primary current, but they are directly cooled by the water, so their current densities are acceptable. This will heat the workpiece as required.

Three of these units would give a total power of 39kW.

6.8 FEA RESULTS

The dimensions in Tables 6.1 and 6.2 have been used to draw the transduction heater in MagNet to create its geometry. The coils are also created and its properties assigned. A boundary condition was added to surround the model to take into account the fringing fields. This is followed by customization of the mesh elements. The model is then solved using the time harmonic solver and the field solutions and performance can then be viewed. Figure 6.9(a) shows a half model of the coil and the workpiece of the designed heater. An enlarged view of the computer generated flux plot, together with the shaded plot of the flux density magnitude, is shown in Figure 6.9(b). The values are represented by colours ranging from blue for minimum to red for maximum.

The computer results in Figure 6.9(b) show that the flux density varies from 1.2T in the middle of the mild steel core tube to 1.9T on the surface of the core tube. A flux density of 1.9T on the surface of core tube of the heater is saturating the core material. The flux plot also shows that the magnetic field does penetrate through the secondary tube to the core tube as expected. The performance of the heater from FEA is listed in Table 6.9.

The calculated results from FEA model show significantly higher values in terms of the current, apparent power, and real power compared to the results from the TEC model shown in Table

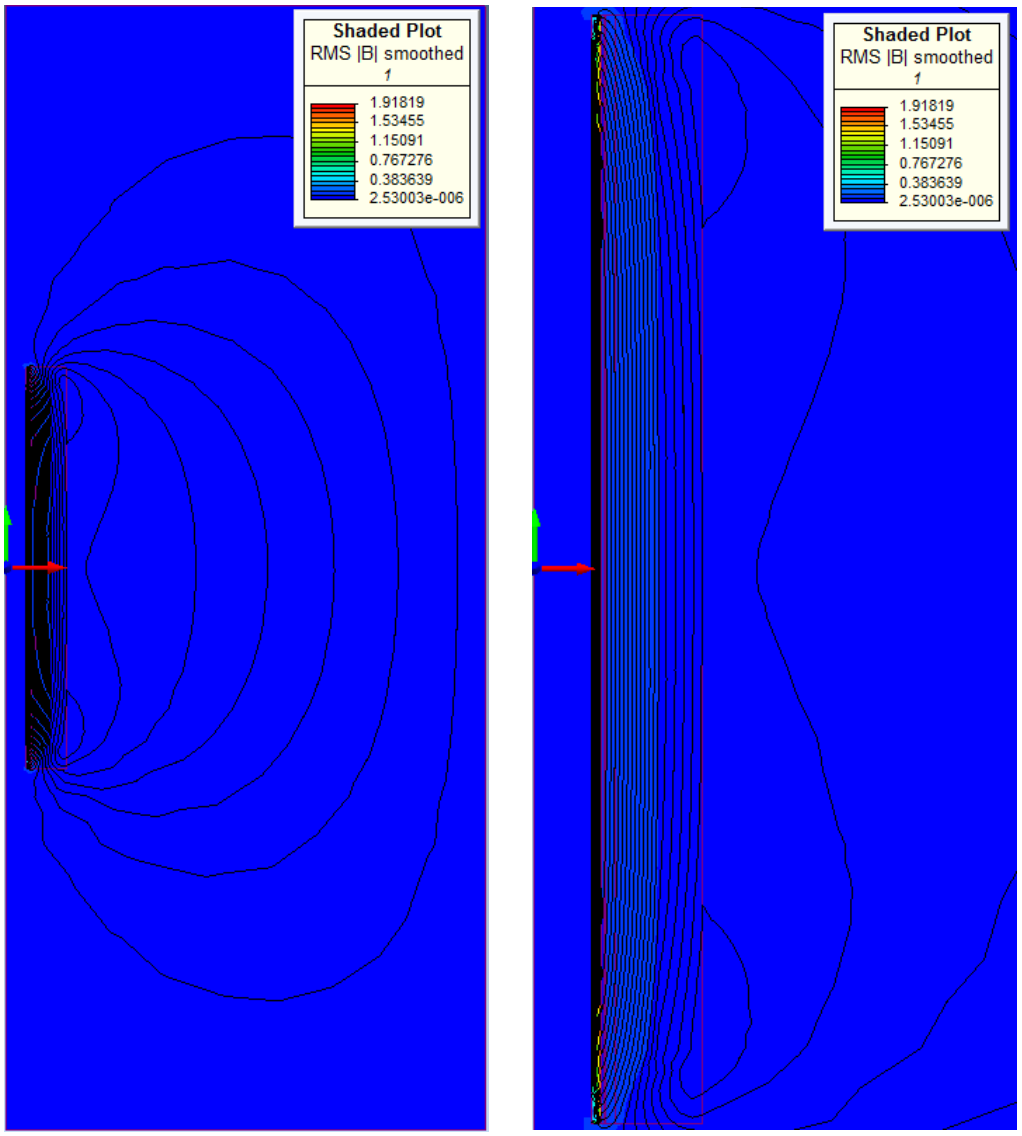

(a) General view (b) Enlarged view

Figure 6.9: Flux plot of designed heater.

Table 6.9: FEA transduction heater performance

Parameter	Value
V-voltage	230V
I-current	96.1A
S-volt-amperes	22.1kVA
P-real power	15.4kW
PF-power factor	0.70

6.7. However, the power factor is significantly lower than the TEC value. Measured results from the constructed device are needed to determine which model is most accurate.

6.9 SUMMARY

In this chapter, the design of a nominal 40kW transduction fluid heater has been presented. The transduction fluid heater was designed using a computer program written in MATLAB and is based on the reverse design method described in [Liew and Bodger 2001], [Bodger and Liew 2002].

The design of the transduction fluid heater used aspects of the 6kW prototype [Takau and Bodger 2014]. The new design used the same material dimensions for the core tube and the secondary tube. Other aspects of the design that were added to the original design were inter-layer insulation, cooling for the primary winding, and the length of the primary winding was adjusted to be the same as the secondary and core tubes. Construction materials and dimensions of the designed heater were also given. This included the primary winding, thermal insulation, secondary tube, core tube, inter-layer insulation, and also the cooling system for the winding.

The TEC model used the reverse design method to determine the circuit parameters and then calculate the performance of the heater.

An alternative to the TEC model, the FEA model, was also used to predict the performance of the heater. A two dimensional finite element analysis of the heater was used to show the magnetic field distribution of the heater.

The calculated results of the TEC model shows significantly lower values in terms of the current, apparent power, and real power compared to those calculated from the FEA. The power factor was greater. The calculated results from the FEA model were slightly different due to the higher current. Again, the same differences were obtained from the 6kW design presented in Chapter 5.

Chapter 7

EXPERIMENTAL RESULTS

7.1 INTRODUCTION

This chapter presents the performance tests on the three phase 40kW transduction fluid heater designed and constructed in Chapter 6. These tests include winding resistance, insulation resistance, power input, heating, ac withstand voltage, and glow-wire flammability. Where applicable, the tests were undertaken according to the International Standards, IEC 60335-1:2010 and IEC 60335-2-35:2012.

The chapter begins with an overview of the experimental setup used throughout the testing, with a discussion of the equipment used during the testing. Also the methods used in taking electrical measurements are examined. The results of the testing are presented and the test results are then compared with the modeling from Chapter 6.

7.2 EXPERIMENTAL SETUP

The testing of the 40kW transduction fluid heater was conducted in the High Voltage Laboratory. This facility has a controllable three phase supply capable of delivering up to 600A at 400V. In addition, the laboratory is fitted with water mains that can be used to supply the heater.

7.2.1 Test Equipment

The test set-up for the 40kW transduction heater is shown in Figures 7.1 and 7.2. The arrangement of the three phase units were in-line rather than in parallel. This is to allow a single fluid tube that can be easily cleaned, rather than having a more complicated manifold. The arrangement can be oriented either horizontally and vertically during the tests. The test set-up consists of a variable 70A variac, 50Hz, ac supply connected in series with the heater and the controller. The power meters are connected to monitor the voltage, current, power factor and

power input for each phase of the heater. A data logger and a laptop were also connected to the heater to monitor the thermal performance of the winding and oil during normal operation. The water flow rate was measured using a calibrated stop watch with a 9L bucket.

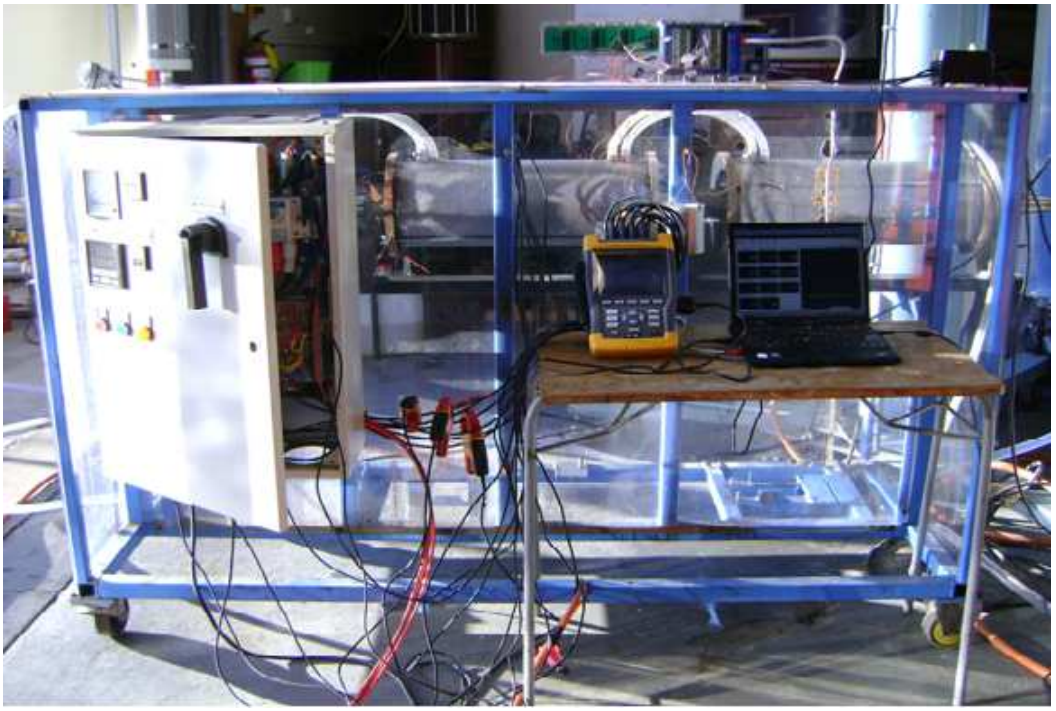

Figure 7.1: Test setup (front view).

Other measurement equipment used in the testing included a Digital Micro-Ohmmeter from Megabras used for dc resistance measurements, a S1-5005 insulation tester from Megger for insulation resistance measurements and a 500VA 7452 electrical safety analyzer from Extech Electronics for the ac withstand voltage test.

Figure 7.2 shows that the water and oil inlets are both located on the same side of the heater. This is slightly different from the design details in Chapter 6. This was made for ease of connections only.

7.2.2 Taking Measurements

An important aspect of taking measurements is making sure the measuring equipments are used correctly and also their functions are used within their calibrated range. In addition, the general conditions for the tests were also applied as applicable from the standards. For example, a water temperature of 15°C ± 5°C was used for the tests. Also, the tests were carried out at an ambient temperature of 20°C ± 5°C.

Figure 7.2: Test setup (rear view).

7.3 TRANSDUCTION HEATER PERFORMANCE

The main performance indicator for a transduction heater is the efficiency of the power transfer or the distribution of the losses. The tests for instantaneous water heater are outlined in the IEC 60335-1 and IEC 60335-2-35 standards. These standards were used as a guide in conducting the relevant tests as the designed heater was for industrial purposes.

This section presents the tests and measurements undertaken to determine the performance of the heater. These measurements are examined and used to validate the calculated results from the TEC and FEA models.

The tests were arranged and performed from ensuring the device was electrically safe to energise, to some of the tests, such as the AC withstand voltage test, being performed later as they were considered potentially damaging to the heater. The glow-wire flammability test was performed on a separate sample of the non-metallic part of the heater.

7.3.1 Winding Resistance and Insulation Resistance Tests

The dc resistance test was performed before the final connection of the heater was completed. This was measured using a MPK254 Digital Micro-Ohmmeter from Megabras. The test results

are listed in Table 7.1, and are compared to calculated values in section 4.1

Table 7.1: Measured winding resistance

Parameter	Measured (Ω)
L1 winding	0.304
L2 winding	0.294
L3 winding	0.297

The second test performed was an insulation resistance test. This was performed with a S1-5005 insulation tester from Megger. The insulation was tested between each phase terminals and the stainless steel tank enclosure and between each phase terminals in turn. The test voltage was 500Vd.c. and was applied for 60 seconds. The test results for the insulation test are given in Table 7.2.

Table 7.2: Insulation resistance test

Applied between:	Insulation resistance
Between each phase terminals and the stainless steel enclosure	>10GΩ
Between each phase terminals in turn	>1TΩ

The measured values of the insulation are in the TΩ and GΩ range which shows that there is no insulation breakdown or short-circuit between the phase terminals and the stainless steel enclosure or between phase terminals.

7.3.2 Power Input Test

The transduction heater was operated at 230V/400V and the electrical parameters were measured for each phase. The test was performed in horizontal and vertical mounting positions of the heater. Two sets of five measurements from both horizontal and vertical mounting positions were averaged and used for the results. The measured electrical parameters from both tests at switch-on (i.e. units at ambient temperature) are given in Tables 7.3 and 7.4. Both tests show that the measured electrical performances are very close despite their mounting positions during the test. The measured parameters of L2 from both tests are slightly less compared to L1 and L3. This shows that L2 may be out of balance due to the asymmetry of the center phase.

7.3.3 Heating Test

The heating test determines the thermal characteristics of the heater during normal operation. This test was performed in the vertical mounting position of the heater as any thermo cycling

Table 7.3: Measured power input at rated voltage(horizontal mounting)

Parameter	L1	L2	L3	Total
kW	13.5	13.1	14.0	40.7
kVA	16.0	15.0	16.6	47.6
kVAR	8.4	7.2	8.9	24.6
PF	0.85	0.88	0.84	0.86
Current (A)	69.2	65.1	71.4	-
Voltage (V)	230.9	230.3	232.7	-

Table 7.4: Measured power input at rated voltage(vertical mounting)

Parameter	L1	L2	L3	Total
kW	13.5	13.3	13.8	40.6
kVA	15.9	15.2	16.3	47.4
kVAR	8.4	7.3	8.6	24.4
PF	0.85	0.88	0.84	0.86
Current (A)	68.8	66.1	70.7	-
Voltage (V)	230.5	230.1	231.1	-

of oil is most effective in this direction. The supply to the heater was slowly increased from 0V to the rated voltage with the current monitored in steps of 10A increments. The winding temperatures recorded were too high at 30A or 116V, the half power of the heater, and the experiment was terminated. The maximum absolute temperatures recorded are given in Table 7.5. The measured winding temperatures show that the water cooling of the outer jacket was working up to the third layer of the winding, with a maximum of 96°C. However, this value is still high for the winding temperatures especially since the heater was at half power. The first winding layer maximum temperature after one hour of testing was 138°C which was also too high for normal operation. This shows that forced water cooling alone was not enough to cool the winding temperatures, at least for this configuration. The ambient temperature during the test was below the requirements of the standards.

A plot of temperatures over time during the heating test is given in Figure 7.3. The mark line shows when the experiment was terminated.

Efficiency

The efficiency of the heater was calculated at the tested voltage during the heating test in Section 7.3.3. The water flow rate was fixed at 19.7l/m and the water outlet temperature was stabilized at 17°C. Using the water inlet, flow rate, water temperature, and the specific heat of water (4187J/kg°C), the calculated power was 7.7kW.

The efficiency was then obtained by the ratio of the calculated output power and the measured

Table 7.5: Heating test

Measured part	Measured temperature (°C)
Initial ambient temperature	5.8
Final ambient temperature	8.3
Water inlet	11.4
Water outlet	17.0
L1 oil temperature (top)	116.2
L1 oil temperature (bottom)	30.9
L2 oil temperature (top)	102.8
L2 oil temperature (bottom)	31.7
L3 oil temperature (bottom)	22.6
L1 winding (third layer)	97.8
L2 winding (third layer)	85.4
L3 winding (third layer)	98.5
L2 winding (first layer)	137.6
L3 winding (first layer)	132.5
Test power input	7.8(kW)
Test voltage	116(V)

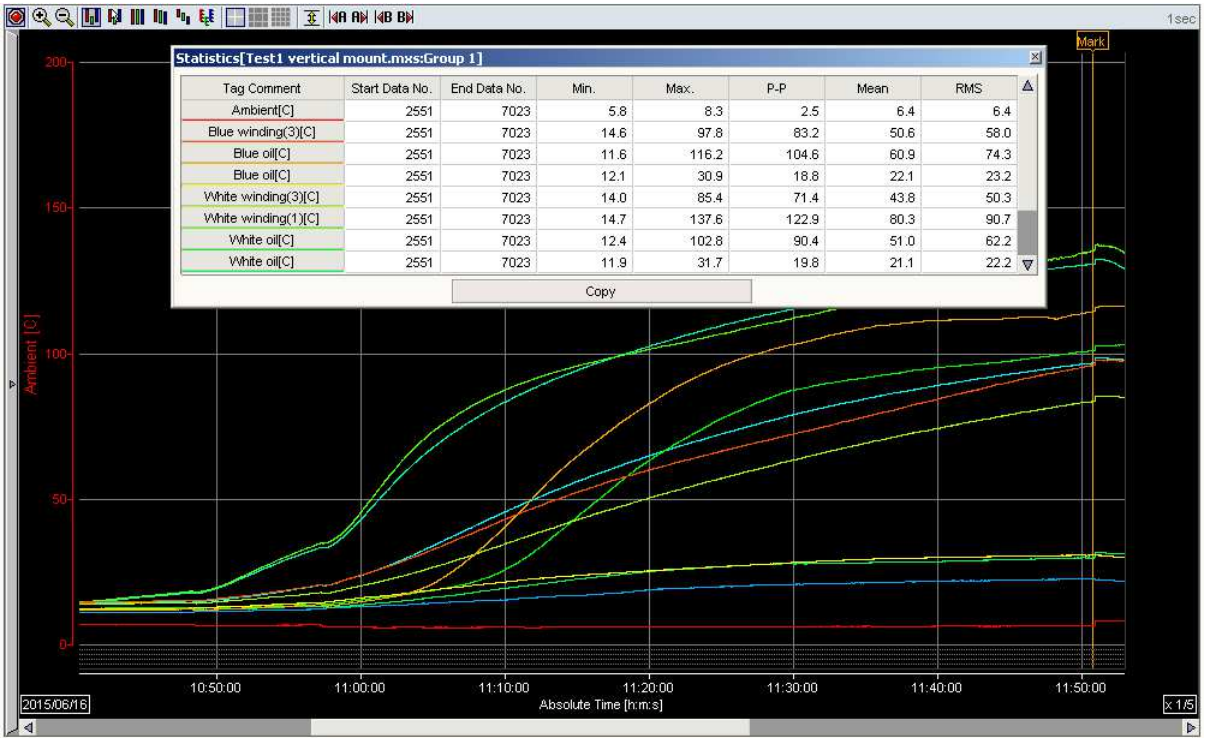

Figure 7.3: Temperatures over time during heating test.

input power during the heating test from Table 7.5. The efficiency of the heater at half power was calculated to be 98.7%. The 1.3% loss was due to the heat dissipated at both ends of the secondary and mild steel tubes.

To operate the heater at steady state, the winding temperatures must be less than 100°C at full load during normal operation. This applies for winding with insulation classes A(105), (E)120, and (B)130. The forced oil cooling method was another option to apply in addition to the forced water cooling. However, the current design has too much restriction on the oil circulation and therefore this cooling method was not applied.

Another configuration for the current design was to remove the water inlet that was used to cool the oil and link it directly with the oil in the winding compartment. This creates a barrier between the windings and the cooling jacket and increases the volume of oil to better cycle and cool the winding. In this configuration, the forced water cooling is removed and the device relies on natural air convection to cool the oil. The water inlet in this configuration was now straight through the product in, product out tube according to the design details of Figure 6.1. This configuration was only applied to coil L2 the white phase (center phase). The other two phases were connected as the first configuration for comparison. The heater was then operated by slowly increasing the supply from 0V and with the current monitored in steps of 10A increments. The maximum absolute temperatures recorded from this configuration are given in Table 7.6.

Table 7.6: Heating test

Measured part	Measured temperature (°C)
Initial ambient temperature	20.9
Final ambient temperature	21.8
L1 oil temperature (top)	93.9
L1 oil temperature (bottom)	26.7
L2 oil temperature (top)	118.8
L2 oil temperature (bottom)	56.1
L3 oil temperature (bottom)	21.9
L1 winding (third layer)	83.3
L2 winding (third layer)	91.1
L3 winding (third layer)	90.2
L2 winding (first layer)	105.1
L3 winding (first layer)	120.2
L3 water jacket enclosure	16.6
L2 water jacket enclosure	70.0
L1 water jacket enclosure	17.8
Test power input	6.6(kW)
Test voltage	98.6(V)

The measured results show the winding temperature for the first layer of the center phase (L2) was 15°C lower than that for L3 phase. At lower voltages the margin of difference was small, but this increased as the voltage was increased. The measured oil temperature was 118.8°C and the enclosure was measured at 70.0°C. By comparison, the measured temperatures for the blue and red phase enclosures were 17.8°C and 16.6°C respectively. These are low compared to the center phase due to the forced water cooling. The measured results from this configuration

have shown some improvement in terms of L2 winding temperature and certainly a pointer in the right direction to improve the cooling of the windings. Other recommendations to solve the cooling are given in the next Chapter under future work. The efficiency of this configuration dropped to 86% due to more losses dissipated in the oil and to ambient air. The measured flow rate in this test was 27l/m with a 3°C change of temperature.

A plot of temperatures over time for this configuration is given in Figure 7.4. The first and second mark lines show when the current was increased in steps of 10A increments whereas the last mark line shows when the experiment was stopped.

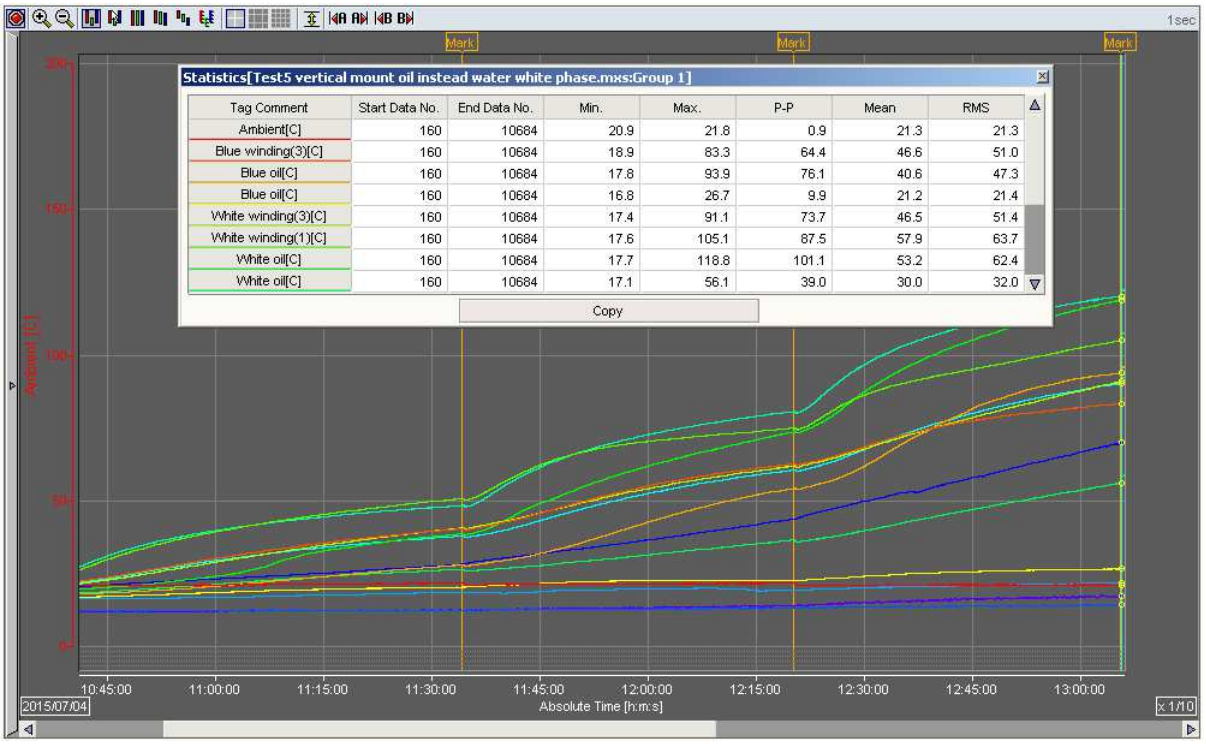

Figure 7.4: Temperatures over time during heating test.

7.4 OTHER EXPERIMENTAL RESULTS

The following tests were conducted on the 40kW transduction heater in addition to those mentioned in Section 7.3.

7.4.1 AC Withstand Voltage Test

This test was performed in accordance with IEC 60335.1. The equipment used the 500VA, 7452 electrical safety analyzer from Extech Electronics and was capable of supplying short circuit cur-

rent between the output terminals after the output voltage had been adjusted to the appropriate test voltage. The test voltages were 1750V and 3000V, and the test duration was 60 seconds. This test was performed last as this was considered potentially damaging to the heater. Test results from the AC withstand voltage test are given in Table 7.7.

Table 7.7: AC Withstand voltage test

Test voltage applied between:	Test voltage (V)	Breakdown
Parts separated by supplementary insulation (Phase + neutral → Cable sheath)	1750	No
Parts separated by reinforced insulation (Phase + neutral → Stainless steel enclosure)	3000	No

The measured test results showed that the heater withstood the required test voltage with no insulation breakdown.

7.4.2 Glow-wire Test

Glow-wire testing was conducted in accordance with IEC 60695-2-11. The test specimens were arranged so that the surface in contact with the tip of the glow-wire was vertical and the glow wire tip applied to the surface of the specimen likely to be subjected to thermal stresses in normal use. A layer of white pineboard and wrapping tissue was placed beneath the specimen and the glow wire tip. The test was performed on non-metallic material supporting live parts and thermoplastic material providing supplementary or reinforced insulation. Separate samples of the inter-layer insulation, thermal insulation, and non-metallic cover piece were used for the test. Figure 7.5 shows the test set-up for the glow-wire test. This test was performed at UL test lab. The glow-wire test results are given in Appendix A.

The standard requires that unattended appliance with non-metallic parts that are within 3mm of current carrying parts of more than 0.2A must comply with the glow-wire test at 750°C and 850°C. The non-metallic part is allowed to ignite during the 750°C glow-wire test provided it does not drip and burn the wrapping tissue. In this case, a further consequential needle flame test is required. The glow-wire test was applied for 30 seconds. None of the non-metallic parts produced any ignition or flame during the 750°C glow-wire test. At 850°C, the thermal insulation produced a flame, but did not drip or burn the wrapping tissue. All the non-metallic parts were deemed to comply with the requirements of the standards.

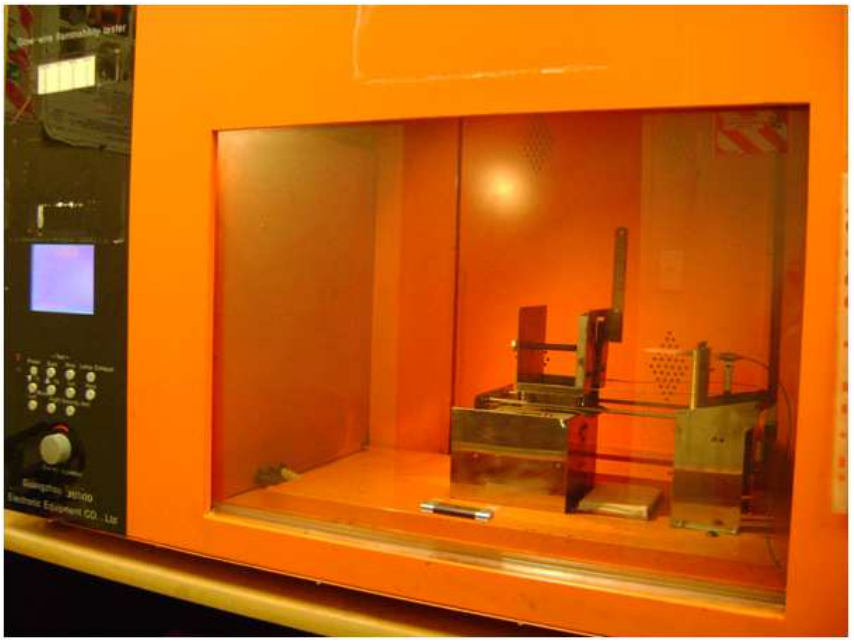

Figure 7.5: Glow-wire test setup.

7.5 COMPARISON WITH TEC AND FEA MODELS

The measured performance test results were compared to the TEC and FEA modeling given in Chapter 6. Only calculated results that can be measured were used for comparisons. These comparisons are presented in Tables 7.8 and 7.9.

7.5.1 Winding Resistance Test Results

The measured and calculated winding resistances from the TEC and FEA models are given in Table 7.8. The measured resistances show good agreement with those calculated from the TEC model compared to the FEA model. The calculated resistance from FEA is significantly lower than the measured and TEC values. The winding resistance in FEA was calculated using the coil loss and the coil current.

Table 7.8: Measured winding resistance results

Parameter	Measured	TEC	FEA
L1 winding (Ω)	0.304	0.297	0.127
L2 winding (Ω)	0.294	0.297	0.127
L3 winding (Ω)	0.297	0.297	0.127

The measured winding resistances are expected to be the same for the three coils, however the measured winding resistance for L1 may be slightly different compared to L2 and L3 due to

the construction of the last layer of the winding. Despite the difference, the measured winding resistance L1 is still close to the calculated value from the TEC model.

7.5.2 Electrical Performance

The measured and calculated performances of the heater from the TEC and FEA models are given in Table 7.9. In this table, only the measured electrical performance from the vertical mounting was used for comparison as both calculated results are very close to each other. The measured results show good agreement with the TEC calculated results compared to those calculated from FEA. Both measured and TEC results are significantly less than those calculated from FEA except for the power factor. The measured power factor was close to the calculated value from TEC but significantly higher than that calculated from FEA. The FEA calculated results are significantly higher than those measured and calculated from the TEC because of the higher current. The higher current did affect the rest of the calculated parameters as it was noted from the 6kW design presented in Chapter 5.

Table 7.9: Measured and calculated performance

Parameter	Measured	Measured	Measured	TEC	FEA
-	L1	L2	L3	-	-
kW	13.5	13.1	13.8	12.9	15.4
kVA	15.9	15.2	16.3	16.1	22.1
kVAR	8.4	7.3	8.6	-	-
PF	0.85	0.88	0.84	0.80	0.70
Current (A)	68.8	66.1	70.7	70.1	96
Voltage (V)	230.5	230.1	231.1	230	230

7.6 SUMMARY

This chapter presented the experimental setup and testing of the 40kW transduction fluid heater. Details of the experimental test procedures and the equipment used during the testing were given.

The 40kW transduction heater was extensively tested to ascertain its electrical performance. The performance tests included power input and heating. Additional tests included winding resistance and insulation resistance, ac withstand voltage and glow-wire flammability. The separate source ac withstand voltage test proved that the dielectric strength of the insulation system was sufficient for the rated voltage. In addition, the glow-wire flammability test showed that the inter-layer insulation, thermal insulation, and non-metallic cover piece were all heat retardant.

The measured results were compared to the modelling from Chapter 6. There was good agreement between measured and calculated electrical performance results from the TEC model compared to the FEA model. The various components of the modelling results were discussed with reference to the measured electrical performance, and limitation of the current design was examined in terms of cooling.

Chapter 8

CONCLUSIONS AND FUTURE WORK

8.1 CONCLUSIONS

This thesis started by introducing the basic principle of induction heating. Applications of induction heating from the 19th century were discussed. The conventional approach to model the performance of induction heaters known as the series equivalent circuit (SEC) model was presented. This was used to calculate the performance of a set of experimental induction heaters.

An alternative approach to the SEC model was then developed. This was known as the transformer equivalent circuit (TEC) model. This modelled the induction heater as a shorted secondary transformer. Equivalent circuits, which are often used in modelling ideal and non-ideal transformers, have been presented. These include the core loss components, the primary winding components and the secondary winding components. These equivalent circuits were transformed into a circuit to model the performance of induction heaters. A simulation program was written using a reverse design approach to calculate the circuit components of the TEC model. The TEC model was then used to calculate the performance of a set of experimental induction heaters.

Finite element analysis (FEA) was also presented. This was used to calculate the performance of the set of experimental induction heaters used for the SEC and TEC models. The set of experimental induction heaters were constructed and tested. The measured results were used to compare with calculated results from the FEA, TEC and SEC models. The FEA calculated results correlated well with the measured results followed by the TEC and then the SEC model. The coil losses and workpiece losses decreased as the diameter of the workpiece increased. This pattern showed up in the TEC and FEA models but not so with the coil and workpiece losses in the SEC model. The calculated results from the TEC model showed the usefulness of the transformer model to predict the performance of induction heaters.

The research was then extended to transduction heating, an induction heater with a secondary winding to boost performance. The TEC and FEA models only were used to calculate the performance of a set of transduction heating experiments. There is no equivalent SEC model

for such heaters. The measured results from the transduction heating experiments showed modifications were required to the equivalent circuit parameters of the TEC model to improve its performance prediction. The circuit components that were modified included the magnetizing reactance and the leakage reactances. The modified TEC model was verified with a 6kW experimental transduction heater design. The measured results showed good agreement with those calculated from the TEC model compared to FEA.

A new simulation program was written that used the developed model to calculate the performance of transduction heaters. The program was then used to design a 40kW transduction heater. The new design had several aspects in common with the 6kW heater. The 40kW design used a new version of the inter-layer insulation for cooling purposes.

The 40kW heater was then built and a series of electrical tests were performed to determine its performance characteristics. The tests were based, where applicable, on international instantaneous water heater standards. The measured electrical performance showed good agreement with the TEC calculated results. The measured power factor was greater than that predicted by the TEC but still close compared to the calculated value from FEA. The design heater was found to be 98.7% efficient at half power. At half power, the winding temperatures were over 100°C. The initial design with forced water cooling did not seem to cool the winding up to the first layer of winding. An investigation into the winding temperature overheating led to the conclusion that insufficient cooling in terms of the thermo cycling of oil was the main contributing factor. An alternative configuration for cooling was then tested together with the forced water cooling. This alternative configuration was applied for the center phase or L2 only. Some improvement in terms of the winding temperature was measured. The measured winding temperature for L2 was 15°C lower than that for the Red phase (L3). The margin of difference was small at lower voltages but increased as the supply voltage was increased. The measured results pointed in the direction of the need for a baffle between the winding and the water jacket, with more volume of circulating oil to cool the oil.

An additional test included a separate source ac withstand voltage test, which proved the dielectric strength of the insulation material was sufficient for the rated voltage. The measured test results showed that the heater was able to withstand the short circuit forces without damaging the windings. A final test included a glow-wire flammability test which showed that all the non-metallic parts were resistant to heat and fire.

The research contained in this thesis demonstrates that the performance of transduction heaters can be successfully modeled using a TEC model. It enables the design of transduction heaters based on available materials and using dimensions as design parameters rather than determining these from voltages and power ratings as used in traditional transformer design methods.

Transduction fluid heaters have the potential to become widespread as benefits of high efficiency,

reduced size, simplified construction and even heating will see them become a more cost effective solution over traditional water heater designs. From the measured performance test results, there is only one factor that is currently preventing the commercial viability of the transduction fluid heaters, and that is the cooling of the primary winding.

8.2 FUTURE WORK

The test results of the designed 40kW transduction heater presented one major limitation while it was being tested and evaluated, as presented in Chapter 7. This section presents the future work that can be performed to improve the thermal design and performance of transduction heaters.

8.2.1 Heater Design

The design of transduction heaters has to be a compromise between electrical and thermal aspects. The major limitation of the current design is the inability to cool the first layer of the primary winding. The measured test results from the different L2 configuration have shown some improvement in terms of reducing the L2 winding temperature. It is suggested that a baffle is required to promote better circulation of the oil with a water jacket outside the baffle to cool the oil. Figure 8.1 shows a half sketch of the transduction heater with the baffle. A more rigorous exercise to model the thermal characteristics of the heater should lead to a practical solution to the winding heating problem.

The following recommendations are considered minor that can be incorporated into the design to encourage better oil circulation.

Thermal insulation

The thermal insulation can be re-designed so that the oil can access the inner side of the first layer of the winding. The thickness of the thermal insulation used in the current design was 4.6mm. It is recommended that a series of 1mm grooves be machined into the outside surface of the thermal insulation. These grooves should be aligned with the slots in the non-metallic cover-piece, to allow oil to flow in the grooves.

Non-metallic cover piece

The non-metallic cover piece that encloses the winding from both ends may need to be re-designed as well. The current design has four slots as shown in Figure 8.2. It is suggested that

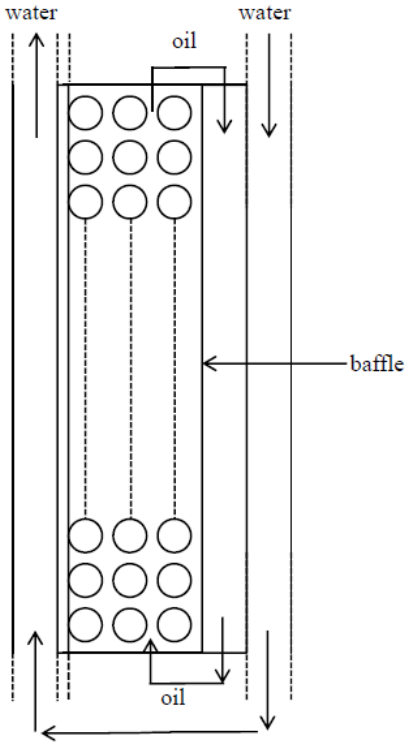

Figure 8.1: Transduction heater with baffle.

more slots are required or be re-designed to align with the grooves in the thermal insulation. This will promote better circulation.

Inlet and outlet

For future prototypes, the inlet and outlet for the oil must be located at the bottom and top of the heater. This will allow oil circulation if forced oil cooling is required. The current design had both oil inlet and oil outlet on the same side of the heater. This restricts the flow of oil when forced oil cooling was required to apply for comparisons.

8.2.2 Improve Performance

There were some aspects of the measured performance presented in Chapter 6 that could be improved upon. This includes the power factor. To improve the performance of the heater, the power factor can be improved further by reducing the thickness of the inter-layer insulation from 3mm to 2mm. This will reduce the leakage flux between the winding and the secondary tube and hence increase the power factor and the performance of the heater. The 40kW heater

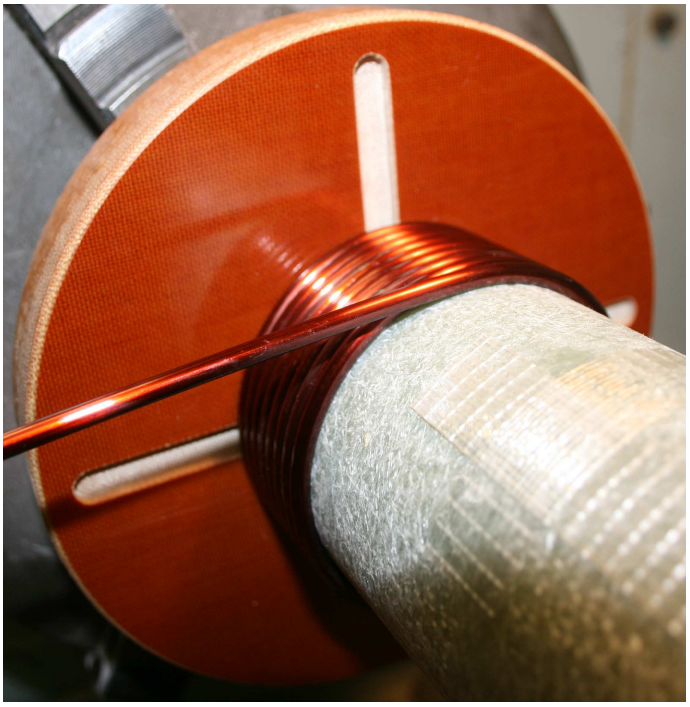

Figure 8.2: Non-metallic cover piece with four slots.

was originally designed with a 2mm inter-layer insulation but only 3mm was available from the manufacturer.

The other circuit parameter that will be affected when the inter-layer insulation is reduced to 2mm thickness is the resistance of the winding. The outside diameter of the winding will decrease as a results of reducing the thickness. This will reduce the length of the wire and hence the resistance. The efficiency of the heater will increase as the resistance of the winding becomes smaller compared to the resistance of the secondary tubes.

The thickness of the thermal insulation (or the former) can be reduced from 4.6mm to 3.2mm. This will minimise the coupling between the primary and the secondary and hence the leakage flux. The 40kW heater was designed with a 3.2mm thickness but only 4.6mm was available.

In addition, the three phase units can be arranged in an equilateral triangular configuration. In this arrangement, the magnetic flux from each unit would return through the remaining two core tubes reducing the magnetic reluctance. This arrangement will give improved performance but can complicate cleaning the secondary tubes.

REFERENCES

Baker, R.M. (1957), 'Design and calculation of induction-heating coils', *American Institute of Electrical Engineers, Part II: Applications and Industry, Transactions of the*, Vol. 76, No. 1, March, pp. 31–40.

Bara, N.P. (2013), 'Finite element analysis of induction furnace for optimum heat transfer', *International Journal of Innovative Research in Science, Engineering and Technology*, Vol. 2, No. 5, pp. 1313–1319.

Barber, H. (1983), *Electroheat*, Granada Publishing, Great Britain.

Bell, S.C. (2004), 'An investigation into the magnetic performance of a three-phase partial-core transformer', Third Professional Year Project, University of Canterbury, Christchurch.

Bell, S.C. (2008), *High-voltage partial-core resonant transformers*, PhD thesis, University of Canterbury, Christchurch, New Zealand.

Bell, S.C. and Bodger, P.S. (2007), 'Power transformer design using magnetic circuit theory and finite element analysis - a comparison of techniques', In *Power Engineering Conference, 2007. AUPEC 2007. Australasian Universities*, Dec, pp. 607–612.

Biotemp (2014), 'Biodegradable dielectric insulating fluid', Website. http://www.nttworldwide.com/docs/BIOTEMP-ABB.

Bodger, P.S. and Liew, M.C. (2002), 'Reverse as-built transformer design method', *Int. J. Elect. Enging. Educ*, Vol. 39, No. 1, pp. 42–53.

Bodger, P.S., Walker, R.J.H. and McInnes, I. (1996), 'Significant technology improvements in fluid heating', *BNCE/UIE XIII Congress on Eletricity Applications*, June.

Burca, A., Trip, N.D. and Leuca, T. (2014), 'Considerations on the design of a low power induction heating system', In *Fundamentals of Electrical Engineering (ISFEE), 2014 International Symposium on*, Nov, pp. 1–4.

Chuwan, S. (2012), 'Partial core eco power transformer', Third Professional Year Project, University of Canterbury, Christchurch.

Clain, S., Rappaz, J., Swierkosz, M. and Touzani, R. (1993), 'Numerical modeling of induction heating for two-dimensional geometries', *Mathematical Models and Methods in Applied Sciences*, Vol. 03, No. 06, pp. 805–822.

Connelly, F.C. (1965), *Transformers: Their Principles and Design for Light Electrical Engineers*, Sir Isaac Pitman and Sons Ltd, London.

Davies, E.J. (1990), *Conduction and Induction Heating*, IEE power engineering series, P. Peregrinus Limited.

Davies, J. and Simpson, P. (1979), *Induction Heating Handbook*, McGraw-Hill Book Company(UK) Ltd, 1st ed.

Dodd, C.V. and Deeds, W.E. (1968), 'Analytical solutions to eddy-current probe-coil problems', *Journal of Applied Physics*, Vol. 39, No. 6, May, pp. 2829–2838.

Dodd, C.V., Cheng, C.C. and Deeds, W.E. (1974), 'Induction coils coaxial with an arbitrary number of cylindrical conductors', *Journal of Applied Physics*, Vol. 45, No. 2, Feb, pp. 638–647.

Edwards, J.D. (2004), 'Course in electromechanics', Infolytica Corporation, Montreal, September.

Egan, L.R. and Furlani, E.P. (1991), 'A computer simulation of an induction heating system', *Magnetics, IEEE Transactions on*, Vol. 27, No. 5, Sep, pp. 4343–4354.

Erickson, C.J. (1995), *Handbook of Electrical Heating for Industry*, IEEE Press, New York.

Fisk, M. (2008), *Simulation of Induction Heating in Manufacturing*, PhD thesis, Lulea University of Technology.

Hamdi, E.S. (1994), *Design of Small Electrical Machines*, John Wiley and Sons Inc., New York, USA.

Herman, S.L. (2011), *Electrical Transformers and Rotating Machines*, Delmar, Cengage Learning.

Huo, X.T. (2009), *New Model of Eddy Current Loss Calculation and Application for Partial Core Transformers*, Master's thesis, University of Canterbury, Christchurch, New Zealand.

Hurley, W. and Kassakian, J.G. (1979), 'Induction heating of circular ferromagnetic plates', *Magnetics, IEEE Transactions on*, Vol. 15, No. 4, Jul, pp. 1174–1181.

Hussein, A.M. and Biringer, P.P. (1992), 'Closed-form solution for the induction heating problem with rotational symmetry', *Journal of Applied Physics*, Vol. 72, No. 1, Jul, pp. 265–269.

IEC60335-1: (2010), 'Household and similar electrical appliances - safety - part 1: General requirements'.

IEC60335-2-35: (2012), 'Household and similar electrical appliances - safety - part 2-35: Particular requirements for instantaneous water heaters'.

IEC60695-2-11: (2014), 'Fire hazard testing - part 2-11: Glowing/hot-wire based test methods - glow-wire flammability test method for end-products (gwept)'.

Jang, S.M., Cho, S.K., Lee, S.H., Cho, H.W. and Park, H.C. (2003), 'Thermal analysis of induction heating roll with heat pipes', *Magnetics, IEEE Transactions on*, Vol. 39, No. 5, Sept, pp. 3244–3246.

Labridis, D. and Dokopoulos, P. (1989), 'Calculation of eddy current losses in nonlinear ferromagnetic materials', *Magnetics, IEEE Transactions on*, Vol. 25, No. 3, May, pp. 2665–2669.

Lapthorn, A. (2013), *High Temperature Superconducting Partial Core Transformers*, PhD thesis, University of Canterbury, Christchurch, New Zealand.

Lapthorn, A. and Bodger, P. (2009), 'A comparison between the circuit theory model and finite element model reactive components', In *Power Engineering Conference, 2009. AUPEC 2009. Australasian Universities*, Sept, pp. 1–6.

Lapthorn, A., Bodger, P. and Enright, W. (2013a), 'A 15-kva high-temperature superconducting partial-core transformer 2014;part i: Transformer modeling', *Power Delivery, IEEE Transactions on*, Vol. 28, No. 1, Jan, pp. 245–252.

Lapthorn, A., Bodger, P. and Enright, W. (2013b), 'A 15-kva high-temperature superconducting partial-core transformer 2014;part ii: Construction details and experimental testing', *Power Delivery, IEEE Transactions on*, Vol. 28, No. 1, Jan, pp. 253–260.

Laurent, J.C. and Malhame, R.P. (1994), 'A physically-based computer model of aggregate electric water heating loads', *Power Systems, IEEE Transactions on*, Vol. 9, No. 3, Aug, pp. 1209–1217.

Liew, M.C. (2001), *Reverse Design Transformer Modeling Technique with Particular Application to Partial Core Transformers*, PhD thesis, University of Canterbury, Christchurch, New Zealand.

Liew, M.C. and Bodger, P.S. (2001), 'Partial-core transformer design using reverse modelling techniques', *IEE Proceedings - Electric Power Applications*, Vol. 148(6), pp. 513–519.

Liew, M.C. and Bodger, P.S. (2002), 'Applying a reverse design modelling technique to partial core transformers', *J. Electrical and Electronics Engineering, Australia*, Vol. 22, No. 1, pp. 85–92.

Lowther, D.A. and Silvester, P.P. (1986), *Computer-Aided Design in Magnetics*, Springer-Verlag, Berlin.

Lucia, O., Maussion, P., Dede, E. and Burdio, J. (2014), 'Induction heating technology and its applications: Past developments, current technology, and future challenges', *Industrial Electronics, IEEE Transactions on*, Vol. 61, No. 5, May, pp. 2509–2520.

MagNet7.4 (2014), *MagNet 7.4 finite-element package for electromagnetic analysis, Infolytica Corporation, Montreal*.

Metaxas, A.C. (1996), *Foundations of Electroheat: A Unified Approach*, John Wiley and Sons Inc., 605 Third Avenue, New York, NY-10158-0012, USA.

MilkFacts (2014), 'Milk facts info', Website. http://www.milkfacts.info/milk/processing/heat/treatments/.

Mok, J. (2012), 'Transduction heater', Third Professional Year Project, University of Canterbury, Christchurch.

Namjoshi, K.V. and Biringer, P.P. (1993), 'Current distribution in exciting coil conductors in cross-field heating systems', *Magnetics, IEEE Transactions on*, Vol. 29, No. 2, Mar, pp. 1570–1573.

Namjoshi, K.V., Lavers, J.D. and Jain, P.K. (2001), 'Vector potential due to a circular loop in a toroidal cavity in a high-permeability core', *Magnetics, IEEE Transactions on*, Vol. 37, No. 6, Nov, pp. 3900–3906.

Perry, M.P. (1985), *Low Frequency Electromagnetic Design*, Electrical and Computer Engineering, Marcel Dekker, Inc., 270 Madison Avenue, New York.

Qianzhe, Z., Yibing, L., Yanping, L. and Weisong, Z. (2010), 'Numerical simulations for the induction heating process of non-linear ferromagnetic billets', In *Advanced Technology of Design and Manufacture (ATDM 2010), International Conference on*, Nov, pp. 99–103.

Recktenwald, G.W. (2000), *Numerical Methods with MATLAB : Implementations and Applications*, Prentice Hall, Upper Saddle River, New Jersey 07458.

ScientificAmerican (2014), 'Scientific american', Website. http://www.scientificamerican.com/article/experts-organic-milk-lasts-longer.

Simpson, P.G. (1960), *Induction Heating: Coil and System Design*, McGraw-Hill Book Company, Inc., United States.

Slemon, G.R. and Straughen, A. (1980), *Electric machines*, Addison-Wesley Pub. Co.

Stansel, N.R. (1949), *Induction Heating*, McGraw-Hill Book Co., 1221 Avenue of the Americas, New York, NY 10020, United States.

Takau, L. and Bodger, P. (2013), 'Low frequency modelling of induction heaters using series equivalent circuit, transformer equivalent circuit and finite element analysis', In *Power Engineering Conference (AUPEC), 2013 Australasian Universities*, Sept, pp. 3244–3246.

Takau, L. and Bodger, P. (2014), 'Modelling of transduction heaters using transformer equivalent circuit and finite element analysis', *Journal of Energy and Power Engineering*, June, pp. 1085–1092.

Tham, H.J., Chen, X., Young, B.R. and Duffy, G.G. (2009), 'Ohmic heating of dairy fluids-effects of local electric field on temperature distribution', *Asia-pacific Journal of Chemical Engineering*, Vol. 4, pp. 751–758.

Tudbury, C.A. (1959), 'Electric and magnetic conditions inside an induction-heated work-piece', *American Institute of Electrical Engineers, Part II: Applications and Industry, Transactions of the*, Vol. 78, No. 2, May, pp. 79–83.

Tudbury, C.A. (1960), *Basics of Induction Heating*, A Rider publication, J. F. Rider Publisher, Inc., New York.

Yafei, S., Jing, S. and Dongjie, N. (2009), 'Numerical simulation of induction heating of steel bar with nonlinear material properties', In *Automation and Logistics, 2009. ICAL '09. IEEE International Conference on*, Aug, pp. 450–454.

Zhong, M. (2012), *Partial Core Power Transformer*, Master's thesis, University of Canterbury, Christchurch, New Zealand.

Zinn, S. and Semiatin, S.L. (1988), *Elements of Induction Heating*, ASM International, Metals Park, Ohio, United States.

Appendix A

GLOW-WIRE FLAMMABILITY TEST RESULTS

SPECIMEN NUMBER	1	2	3	4
SPECIMEN DESCRIPTION	Inter-layer insulation	Inter-layer insulation	Inter-layer insulation	Inter-layer insulation
Material	Fibreglass	Fibreglass	Fibreglass	Fibreglass
Colour	Grey	Grey	Red	Red
Test specimen	SC	SC	SC	SC
Glow wire tip temperature (°C)	750	850	750	850
Duration of glow wire application (t_a) (s)	30	30	30	30
OBSERVATIONS				
Duration from beginning of glow-wire tip application to ignition of specimen or layer (t_i) (s)	NI	NI	NI	NI
Duration from beginning of glow-wire tip application to when flames extinguish (t_e) (s)	NI	NI	NI	NI
Maximum height of flames after initial 1s (to nearest 5 mm) (mm)	NA	NA	NA	NA
Flame impingement on other parts	NA	NA	NA	NA
Degree of tip penetration	WPNI	WPNI	WPNI	WPNI
Degree of specimen distortion	SMD	SMD	SMD	SMD
Scorching of pinewood board	NO	NO	NO	NO
EVALUATION CRITERIA				
Visible flame or sustained glowing	NO	NO	NO	NO
Duration of flaming or glowing after tip removal (max. allowable 30 s) (s)	NA	NA	NA	NA
Surrounding parts burned away completely (not permitted)	NA	NA	NA	NA
Ignition of wrapping tissue layer (not permitted)	NO	NO	NO	NO
RESULTS	PASS	PASS	PASS	PASS

LEGEND:

CE	Complete Equipment	SA	Sub Assembly	SE	Self Extinguished
EBD	Emitted Burning Droplets	SBD	Specimen Burned and Distorted	SMD	Specimen Melted and Distorted
ME	Manually Extinguished	SC	Separate Component	SS	Specimen Scorched
NA	Not Applicable	SCC	Specimen Completely Consumed	WPNI	Wall Penetrated but no Ignition
NI	No Ignition	X	Flame Appeared for an Instant		

SPECIMEN NUMBER	5	6	7	8
SPECIMEN DESCRIPTION	Thermal insulation	Thermal insulation	Non-metallic cover piece	Non-metallic cover piece
Material	Fibreglass	Fibreglass	Tufnol	Tufnol
Colour	Green	Green	Brown	Brown
Test specimen	SC	SC	SC	SC
Glow wire tip temperature (°C)	750	850	750	850
Duration of glow wire application (t_a) (s)	30	30	30	30
OBSERVATIONS				
Duration from beginning of glow-wire tip application to ignition of specimen or layer (t_i) (s)	NI	1	NI	NI
Duration from beginning of glow-wire tip application to when flames extinguish (t_e) (s)	NI	34	NI	NI
Maximum height of flames after initial 1s (to nearest 5 mm) (mm)	NA	20	NA	NA
Flame impingement on other parts	NA	NO	NA	NA
Degree of tip penetration	WPNI	SE	WPNI	WPNI
Degree of specimen distortion	SMD	SE	SMD	SMD
Scorching of pinewood board	NO	NO	NO	NO
EVALUATION CRITERIA				
Visible flame or sustained glowing	NO	YES	NO	NO
Duration of flaming or glowing after tip removal (max. allowable 30 s) (s)	NA	4	NA	NA
Surrounding parts burned away completely (not permitted)	NA	NO	NA	NA
Ignition of wrapping tissue layer (not permitted)	NO	NO	NO	NO
RESULTS	PASS	PASS	PASS	PASS

LEGEND:

CE	Complete Equipment	SA	Sub Assembly	SE	Self Extinguished
EBD	Emitted Burning Droplets	SBD	Specimen Burned and Distorted	SMD	Specimen Melted and Distorted
ME	Manually Extinguished	SC	Separate Component	SS	Specimen Scorched
NA	Not Applicable	SCC	Specimen Completely Consumed	WPNI	Wall Penetrated but no Ignition
NI	No Ignition	X	Flame Appeared for an Instant		

Appendix B

LIST OF PUBLICATIONS

B.1 CONFERENCE PAPERS

TAKAU, L. AND BODGER, P. (2013), 'Low Frequency Modelling of Induction Heaters Using Series Equivalent Circuit, Transformer Equivalent Circuit and Finite Element Analysis', In *Australasian Universities Power Engineering Conference (AUPEC)*, Hobart, Tasmania, Australia, September, pp. 3244-3246.

B.2 JOURNAL PAPERS

TAKAU, L. AND BODGER, P. (2014), 'Modelling of Transduction Heaters Using Transformer Equivalent Circuit and Finite Element Analysis', *Journal of Energy and Power Engineering*, June, pp.1085-1092.

TAKAU, L. AND BODGER, P. (2015), 'A 40kW Transduction Fluid Heater - Part I: Design and Construction', *IET Electric Power Applications*, To be submitted.

TAKAU, L. AND BODGER, P. (2015), 'A 40kW Transduction Fluid Heater - Part II: Experimental Results', *IET Electric Power Applications*, To be submitted.